REPORT DOCUMENTATION PAGE		Form Approved OMB No. 0704-0188

Public reporting burden for this collection of information is estimated to average 1 hour per response, including the time for reviewing instructions, searching existing data sources, gathering and maintaining the data needed, and completing and reviewing this collection of information. Send comments regarding this burden estimate or any other aspect of this collection of information, including suggestions for reducing this burden to Department of Defense, Washington Headquarters Services, Directorate for Information Operations and Reports (0704-0188), 1215 Jefferson Davis Highway, Suite 1204, Arlington, VA 22202-4302. Respondents should be aware that notwithstanding any other provision of law, no person shall be subject to any penalty for failing to comply with a collection of information if it does not display a currently valid OMB control number. **PLEASE DO NOT RETURN YOUR FORM TO THE ABOVE ADDRESS.**

1. REPORT DATE *(DD-MM-YYYY)*	**2. REPORT TYPE**	**3. DATES COVERED** *(From - To)*
05-07-2007	Final Report	3/1/04 - 3/31/07

4. TITLE AND SUBTITLE

1 FLOW CONTROL OVER SHARP-EDGED WINGS

5a. CONTRACT NUMBER

5b. GRANT NUMBER

FA9550-04-1-0144

5c. PROGRAM ELEMENT NUMBER

6. AUTHOR(S)

Jose Rullan[1], Pavlos P. Vlachos[2] and Demetri P. Telionis[1]

[1] Engineering Science & Mechanics, [2] Mechanical Engineering
Virginia Polytechnic Institute and State University

5d. PROJECT NUMBER

5e. TASK NUMBER

5f. WORK UNIT NUMBER

7. PERFORMING ORGANIZATION NAME(S) AND ADDRESS(ES)

Virginia Tech
Dept. of Engineering Science and Mechanics
Blacksburg, VA 24061

8. PERFORMING ORGANIZATION REPORT NUMBER

9. SPONSORING / MONITORING AGENCY NAME(S) AND ADDRESS(ES)

Rhett Jefferies, Lt Col, USAF, Program
AFOSR/NA
875 North Randolph Street
Suite 325, Room 3112
Arlington, VA 22203-1768

10. SPONSOR/MONITOR'S ACRONYM(S)

11. SPONSOR/MONITOR'S REPORT NUMBER(S)

AFRL-SR-AR-TR-08-0113

12. DISTRIBUTION / AVAILABILITY STATEMENT

Approved for public release;
distribution unlimited

13. SUPPLEMENTARY NOTES

14. ABSTRACT **Wings swept by 30 to 40 degrees with sharp leading edges are today very common on fighter aircraft. There is very little work devoted to the understanding of the aerodynamics of such wings. The problem is that such wings may be able to sustain attached flow, even if their tip vortices are broken down, or stall like two-dimensional wings. The aerodynamics of such wings were studied and investigated experimentally. Pressure distributions and velocity fields were obtained in a wind tunnel and a water tunnel. The effectiveness of leading-edge control of the flow over such wings was explored. Oscillating mini-flaps and pulsed jets along the leading edge were employed. The results indicate that two-D-like vortices are periodically generated and shed. It was also discovered that an underline feature of the flow, a streamwise vortex is periodically activated, penetrating the separated flow, eventually emerging downstream of the trailing edge of the wing. The results indicate that significant increases in lift can be achieved in the average, by managing the development of streamwise and spanwise vortices. The technique is effective in the range of angles of attack of 10 to 20 degrees, for which the uncontrolled flow is stalled.**

15. SUBJECT TERMS					
16. SECURITY CLASSIFICATION OF: Unclassified			17. LIMITATION OF ABSTRACT	18. NUMBER	19a. NAME OF RESPONSIBLE PERSON
a. REPORT	b. ABSTRACT	c. THIS PAGE			19b. TELEPHONE NUMBER *(include area code)*

Standard Form 298 (Rev. 8-98)
Prescribed by ANSI Std. Z39.18

FLOW CONTROL OVER SHARP-EDGED WINGS

Final Report

AFOSR GRANT NUMBER FA9550-04-1-0144

Jose Rullan[1], Pavlos P. Vlachos[2] and Demetri P. Telionis[1]
[1] Engineering Science & Mechanics, [2] Mechanical Engineering
Virginia Polytechnic Institute and State University
Blacksburg, VA 24061

TABLE OF CONTENTS

NOMENCLATURE

α	Angle of attack
C_μ	Momentum Coefficient
U_∞	Freestream velocity
h	Slot width
c	airfoil chord
St	Strouhal number
F^+	Reduced frequency
$f_{shedding}$	Shedding frequency
$f_{actuator}$	Actuator frequency
Re	Reynolds number

1 INTRODUCTION

In recent years there has been an increased interest in flow control, and in particular in aerodynamics, with the purpose of increasing lift and decreasing drag of airfoils and wings. Wings suffer from flow separation at high angles of attack due to viscous effects, which in turn causes a major decrease in lift and increase in drag. This occurs to all types of airfoils, but sharp-edged wings are particularly vulnerable to such detrimental effects. These types of wings are used on supersonic transports as well as in stealth technology due to the fact that flat surfaces and sharp edges help reduce the radar signature of the airplane by reflecting the radar signals away from the radar, while also reducing the wave drag due to the shock wave that otherwise would be detached if round edge airfoils were used. The problems with these types of wing geometries are that they need long runways and require a lot of power for takeoff and landing since at subsonic flight the lift for these airfoils is reduced as well advanced control systems and highly skilled pilots to maintain a safe degree of maneuverability.

Sharp edge airfoils suffer from separation even at low angles of attack such as 8°, because the flow cannot negotiate the sharp turn at the leading edge. As the flow separates, the airfoil behaves as a bluff body. Due to this separation, a reduction in lift will be experienced by the airfoil due to the fact that the airflow on the suction side of the airfoil is separated and vortex shedding starts. The interest in this study is to try to control separated flow, not flow separation. With the implementation of flow control techniques, improvements in the lift coefficient can be obtained in a time-averaged sense. This is achieved by controlling the vortex-shedding phenomenon that in turn will improve a mixing enhancement of high momentum flow from the free stream with low momentum flow in the separated region. This mechanism is known as vortex lift.

1.1 Separated flow

As stated before, the purpose of this research is to control separated flow and not flow separation. It is important to make this distinction, since the former refers to the

effort of working along with a flow field that has already experienced boundary layer separation from a wall while the latter tries to prevent or delay separation, or reattach the flow field. Fiedler et al (1998) classified flow separation and possible techniques to address their situation as shown in Figure 1.

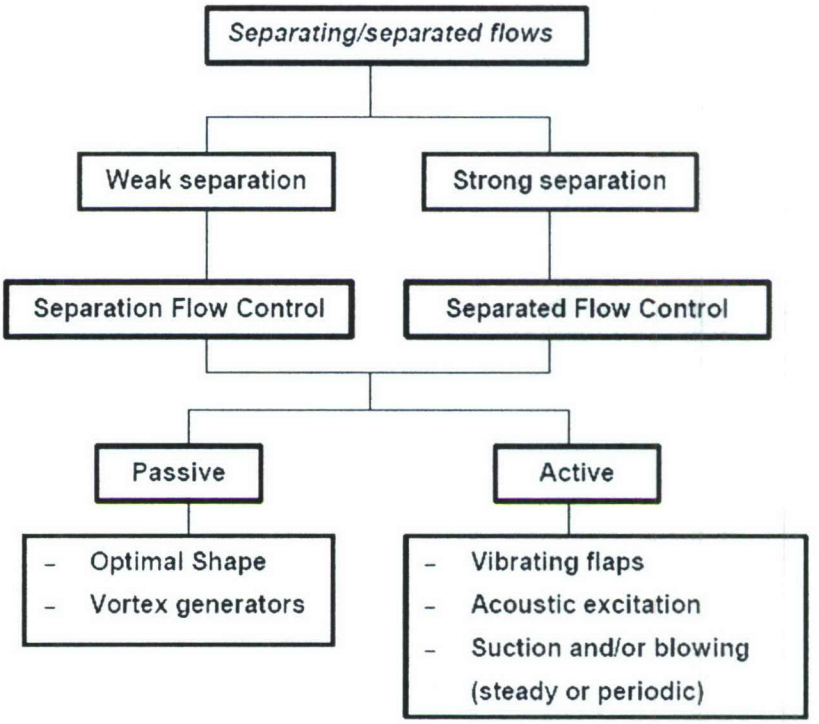

Figure 1: Classification of flow field separation and flow management techniques

Viscous flow theory predicts that a boundary layer forms on a wall due to viscosity forces where there is going to be a substantial variation of the velocity across the streamlines. It also states that a flow will separate in the presence of an adverse pressure gradient. For sharp edge airfoils, separation will always be fixed at the sharp leading edge since separation will occur at sharp corners due to the adverse pressure gradient. Sharp edge airfoils will suffer from massive separation at around eight degrees angle of attack.

When the flow separates from the wall, the boundary layer theory no longer holds since a shear layer will be formed. Vortices will be formed and they will be shed from the separation points located at the leading and trailing edges in an alternate way. These vortices are energized by the interaction of each other so the ones that are shed from the leading edge are in a disadvantage since these leading edge vortices are very weak to

accomplish formation (Roshko 1967) so they may form or not until they reach the wake. This research will try to accomplish the enhancement of the leading edge vortices to see if they roll over the suction side surface thus obtaining a lower pressure and increasing the lift. We need to lay out the physical mechanism of the production, shedding, capture and enhancement of these vortices at post-stall angles of attack. Wu et al (1991) summarizes these four steps of the physics as vortex layer instability-receptivity-resonance.

When flow separates, the result is the continuous shedding of a free shear layer. This shear layer, a vortex layer in itself, is unstable to small perturbations (Kelvin-Helmholtz instabilities) and the instabilities will cause a vortex merging. The upstream layer instability induces stronger and coherent vortex merging downstream (Ho et al 1984) as sketched in Figure 2. This encouragement is repeated thus doubling the size of these global instabilities each time. This interaction of the shear layer with itself is called a feedback mechanism.

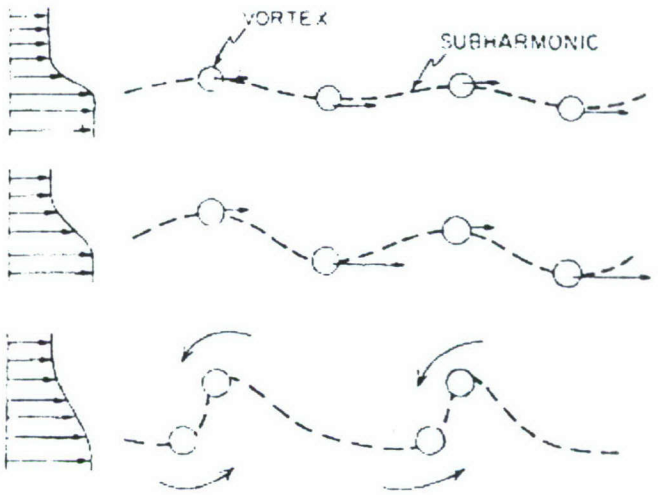

Figure 2: Vortex induction by instabilities in a free shear layer.

It is important not only to understand the vortex layer evolution but its resonance as well. Resonance can best be described from oscillation theory. If a forcing term matches one of the fundamental modes of a linear oscillator then a magnified response will develop and the oscillator's response will be amplified. Even some higher order modes might be amplified and manage somewhat this vortex flow.

Resonance needs the interaction of two periodic events that are in phase with frequencies that are integer multiples of each other. For this to occur a periodic flow feature and a feedback mechanism are needed so the disturbance enables the layer to interact with itself. The purpose is to trigger a self-organizing mechanism of relative small energy input so that the energy is drawn from the random fluctuating motion or vorticity concentration such as the ones produced by mechanical flaps and unsteady jets. Here the vortex shedding frequency is locked and also must of the energy is converted into the vortex itself. The problem vortex-vortex interaction is that the frequency range is usually up to 100 Hz. A good feature is that the forcing frequency does not need to be the optimal resonance frequency to achieve a significant effect.

1.2 Flow control

Flow control is defined by Gad-el-Hak (2001) as the ability to actively or passively manipulate a flow field to effect a desired change. The challenge is to achieve that change with a simple device that is inexpensive to build as well as to operate and has minimum side effects. Control of separated flow is possible by both passive and active means as presented in Figure 3. Passive control refers to the ones that require no auxiliary power and no control loop and sometimes are referred as flow management rather than control. Examples include changing the geometry of the aircraft to increase its aerodynamic properties such as wings equipped with leading edge flaps. These are heavy, require extra hydraulic control and introduce serious problems to sustain the stealth integrity of the aircraft. This type of control is unacceptable in the present case, due to stealth geometry and speed constraints.

On the other hand active flow control refers to the ones where a control loop is used and energy expenditure is required. They are also further divided into predetermined and reactive. Predetermined control loops refer to the application of steady or unsteady energy without regard to the particular state of the flow so no sensors are required. This is the difference with the reactive ones since these employ a sensor to continuously adjust the controller. These reactive ones in turn could be either feedforward or feedback controlled. In the present research, we employ a predetermined loop control.

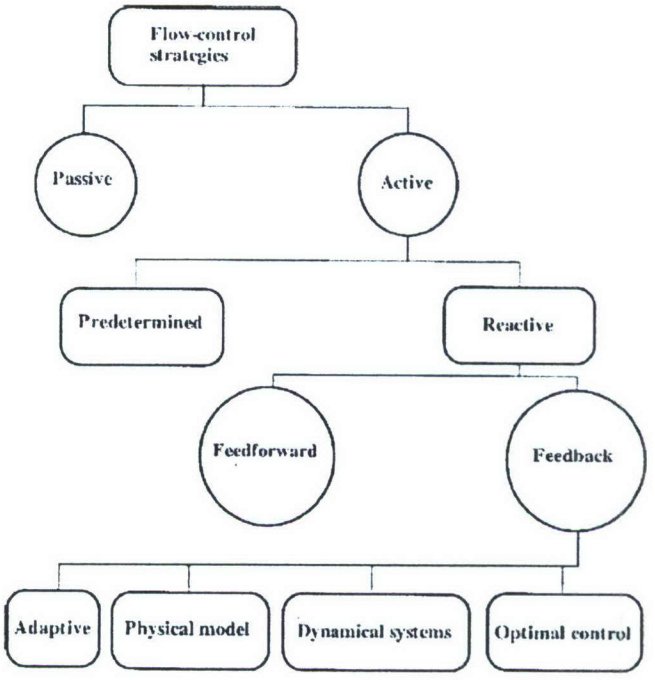

Figure 3: Classification of flow control methods.

1.2.1 Mechanical Flaps

Zhou et al (1993) were the first to try to do control on a sharp edge airfoil. They used a rounded edge airfoil placed backwards in a wind tunnel so the sharp trailing edge faced the oncoming flow. Their test was only at 27° angle of attack but their results indicated that an increase in lift could be achieved.

Hsiao et al (1993) employed a pulsed micro-flap on the leading edge of a wing to control separated flow. They focused on the position, amplitude, and frequency of the flap motion necessary to improve the aerodynamics characteristics of the flow over an airfoil at high angles of attack. Hsiao and Wang found that periodic perturbations can organize and enhance the average strength of the shedding vortices and can increase in a time-average sense the lift by as much as 50%. Hsiao et al (1998) later made modifications to their previous design, finding that the most effective excitation corresponds to a flap motion with the vortex shedding frequency. They also found that larger amplitudes of excitation motion produced a larger lift coefficient.

In order to create the necessary flow disturbance, Miranda (2001) used a small oscillating flap placed on the leading edge of a circular arc sharp-edged airfoil. This pulsing flap creates an unsteady excitation at the leading edge, which is responsible for

affecting the flow in the desired way. They showed an increased in lift of up to 70%. Previous work has demonstrated that the maximum effect on separated flow can be achieved when the actuation frequency is near the vortex shedding frequency. But the flap must penetrate the separated region in order to have any effect on the formation of vortices. That is the reason suggested since the effect was greatly reduced as the angle of attack was increased. They also found that oscillating flaps are not limited in their frequency domain. Indeed, they demonstrated that an oscillating flap could generate a wide range of effective frequencies for the control of separated flow over a sharp-edged airfoil. But such devices may not be attractive to the aircraft designer.

1.2.2 Periodic blowing

A blowing technique has also been tested to control separated flow. Small jets are mounted at the leading edge of airfoils for the purpose of developing periodic perturbations into the boundary layer. The idea is to produce streamwise vortices using transverse steady and oscillating flow jets to increase the cross-stream mixing and lead to stall suppression in adverse pressure gradients. Several studies have been conducted on the use of oscillating blowing. McManus and Magill (1996) studied the separation control in incompressible and compressible flow using pulsed jets. They tested a NACA-4412 airfoil section with a leading-edge flap. The leading-edge flap was fitted with flow control actuators, each actuator consisted of a cross flow jet with pitch and screw angles of 90 and 45 degrees respectively. High-speed flow control valves were used to control the pulsed flow to each jet individually. The leading edge contained three jet nozzles; however only two were used. The valve open-and-close cycle was manipulated using a computer function generator driving a solenoid valve power supply. The valve controller allowed pulse rates up to 500 Hz and volume flow rates in excess of 20 slugs/min for each jet. A constant average mass flow of air was supplied to the jet using a closed-loop servo valve. Their data indicated that maximum lift enhancements occur with a jet pulse Strouhal number of approximately 0.6. However, McManus and Magill found the pulsed jets caused an increase in lift of up to 50 percent over a base line case for $\alpha \leq 10$ degrees. It was found that the effectiveness decreased with the increase in Mach number. The best results were found when the angle of attack was equal to the angle corresponding to C_{lmax}.

Seifert et al (1993) examined oscillatory blowing on the trailing edge flap of a NACA-0015 airfoil. They activated jets mounted in a 2-D slot located on the upper surface above the hinge of the flap. The airfoil was placed at an angle of attack of 20 degrees. Seifert et al. concluded that steady blowing had no effect on lift or drag. However, modulating blowing generated an increase in lift and cut the drag in half.

Synthetic-jet actuators can be used effectively achieve dynamic blowing and suction. Synthetic-jet actuators based on piezoelectric devices are most efficient at the resonance frequency of the device and limited by the natural frequency of the cavity. Such actuators have proven very useful in the laboratory but may not be as effective in practice. Rao et al (2000) designed an actuator, which is essentially a small positive-displacement machine. The same group later designed a similar device and tested a NACA0015 airfoil with rounded leading edges containing six reciprocating compressors, which were driven by two DC motors. These compressors/pistons created a synthetic jet (zero mean flux) at the leading edge of the airfoil. They found that flow separation control was demonstrated at angles of attack and free stream velocities as high as 25° and 45 m/s, respectively. These actuators may have overcome some of the problems faced by other designs but they are complex machines, requiring high-speed linear oscillatory motions and complex mechanical components.

1.2.3 Other actuations

There are other devices tried for active flow control and could be applied to post-stall flow control. Among some recent technology, one of the most talked about in general is piezoresistors. Jacobson et al (1997) designed an actuator that consists of a piezoelectrically-driven cantilever mounted flush with the flow wall and could be used in large arrays for actively controlling transitional and turbulent boundary layers. When driven, the resulting flow disturbance over the actuator is a quasi-steady pair of counter-rotating streamwise vortices with strengths controlled by the amplitude of the actuator drive signal. These vortices decay rapidly downstream of the actuator but they produce a set of high- and low-speed streaks that persist far downstream. Piezoelectric actuators are also mechanical such as the one by Cattafesta et al (2001), where one sheet of piezoceramic was attached to the underside of a shime. Here the actuator works as a flap

and is able to produce significant velocity fluctuations even in relative thick boundary layers.

Another type of actuators considered are called electrohydrodynamic, introduced by Artana et al (2002) where flush mounted electrodes in a flat plate with a DC power supply are used to create a plasma sheet. This plasma sheet seems to induce an acceleration in the flow close to surface thereby increasing its momentum and inducing a faster reattachment as seen in the flow visualization.

1.3 Methodology

So far, efforts have been reported to control the flow separation over airfoils with rounded leading edges, while here we report on the control of separated flow over sharp-edged airfoils. These techniques are equally applicable for the control of separated flows over rounded airfoils. There are two important differences between the actuator requirements for the two cases. First, the location of the actuators for the control of separation over rounded airfoils is not critical since the flow is still receptive to an external disturbance, whereas for the control of separated flow the actuation must interact with the free-shear layer. This fact dictates that the actuator of a sharp-edged wing must be as close as possible to the sharp edge, which leads to the second important difference. The direction of the actuation disturbance must be adjusted to lead the disturbance as much as possible in the direction of the free shear layer. Two additional important parameters are the momentum coefficient C_μ and frequency of the actuation. Different angles of attack and free stream velocities will require a wide variety of possible combinations. Been able to independently control both is a great challenge. These requirements may appear too stringent for the sharp- edged airfoils but on the other hand, they may provide some opportunities for robust control with minimal energy input. It is possible that free shear layers would be more receptive to disturbances right at their initiation that is as close as possible to the sharp leading edge. Another similar situation is the control of asymmetric wakes over pointed bodies of revolution at incidence. In this case, minute disturbances very close to the apex can feed into the global instability of the flow and lead to very large wake asymmetries as shown by Zilliac et al (1990) and Zeiger et al (1997).

It is important to note that periodic blowing is more effective than a steady jet due to resonance. For blowing, the momentum coefficient is define by McCormick (2000) as

$$C_{\mu} = \frac{\left(\rho h u^2\right)_{jet}}{\left(\rho c U^2\right)_{\infty}}$$

where ρ is the density of air and cancels out, h is the slot height, c is the chord of the airfoil and u and U are the respective velocities of the jet and the free stream. This is the relation of the input energy to kinetic energy of the free stream and is suggested in Wu et al (1997) that it should to be at least 1%.

The disturbance frequency likely to be amplify the most is given, using linear stability theory, by the Strouhal number $St = \frac{f_{shedding} \times c \times Sin(\alpha)}{U_{\infty}}$ where $f_{shedding}$ is the shedding frequency, c is the airfoil chord, α is the angle of attack and U_{∞} is the free stream velocity. We are going to assume a value of $St=0.2$ for this research as is thoroughly accepted in literature. Seifert et al (1999) gives the actuation frequency, related to the shedding frequency, the reduced non-dimensional frequency $F^{+} = \frac{f_{actuation}}{f_{shedding}}$. He suggests that this reduced frequency to be $0.4 < F^{+} < 2$ since it seems that harmonics play a role in the dynamic process.

1.4 References

Abiven, C., Vlachos, P. P., (2002). "Super spatio-temporal resolution, digital PIV system for multi-phase flows with phase differentiation and simultaneous shape and size quantification", Int. Mech. Eng. Congress, Nov. 17-22, 2002, New Orleans, LA

Abiven, C., Vlachos P. P., Papadopoulos, G., (2002). "Comparative study of established DPIV algorithms for planar velocity measurements", Int. Mech. Eng. Congress, Nov. 17-22, 2002, New Orleans, LA

Amitay M, Smith B. L. and Glezer, (1998). "Aerodynamic flow control using synthetic jet technology", AIAA Paper 98-0208

Artana, G., D'Adamo, J., Léger, L., Moreau, E., Touchard, G., (2002). "Flow Control with Electrohydrodynamic Actuators" AIAA Journal Vol. 40, pp. 1773-1779

Cahill, J. F., Underwood, W.J., Nuber, R.J., Cheesman, G.A., (1953). "Aerodynamics forces on symmetrical circular-arc airfoils with plain leading-edge and plain trailing-edge flaps" NACA Report 1146

Cattafesta, L.N, Garg, S., Shukla, D., (2001). "Development of Piezoelectric Actuators for Active Flow Control". AIAA Journal Vol. 39, pp. 1562-1568

Didden, N. (1979). "On the Formation of Vortex Rings: Rolling Up and Productions of Circulation." Z. Angew. Math.Phys. Vol 30, pp101-106.

ELD, (1984) 24" Flow Visualization Water Tunnel, Operating and Maintenance Instructions

Fiedler, H. E., (1998). "Control of Free Turbulent Shear Flows". In *Flow Control: Fundamentals and Practices* (ed. Gad-el-Hak, M., Pollard, A., Bonnet, J. P.), pp. 335-429

Gad-el-Hak , M., (2001). "Flow Control: the Future," J. of Aircraft. Vol. 38, No. 3, pp. 402-418

Gilarranz, J. L., Rediniotis, O. K., (2001). "Compact, High-Power Synthetic Jet Actuators For Flow Separation Control," AIAA Paper 2001-0737

Glezer, A. (1998): "The Formation of Vortex Rings". Phys. Fluids, Vol 31, pp. 3532-3542.

Hsiao, F. –B., Wang, T.-Z., Zohar, Y., (1993). "Flow separation Control of a 2-D Airfoil by a Leading-Edge Oscillating Flap," Intl. Conf. Aerospace Sci. Tech., Dec. 6-9, 1993, Tainan, Taiwan.

Hsiao, F. B., Liang, P. F., Huang, C. Y., (1998). "High-Incidence Airfoil Aerodynamics Improvement by Leading-edge Oscillating Flap". J. of Aircraft. Vol. 35, No. 3, pp. 508-510.

Ho, C.-M. and Huerre, P. (1984) "Perturbed free shear layers". Ann. Rev. Fluid Mech. 16, 365

Jacobson, S.A, Reynolds, W.C.,(1998), "Active Control of Streamwise Vortices and Streaks in Boundary Layers", J. of Fluid Mechanics. Vol. 360, pp. 179-211.

McCormick, D. (2000), "Boundary Layer Separation Control with synthetic jets", AIAA Paper 2000-0519

McManus, K., Magill, J., (1996). "Separation Control in Incompressible and Compressible Flows using Pulsed Jets". AIAA Paper 96-1948.

Miranda, S., Telionis, D., Zeiger, M., (2001). "Flow Control of a Sharp-Edged Airfoil", AIAA Paper No. 2001-0119, Jan. 2001

Pope, A., Barlow, J.B., Rae, W.H., *Low speed wind tunnel testing*, 3rd ed. p.353-356.

Prandtl, L. (1904) "Über Flüssigkeitbewegung bei sehr kleiner Reibung", Verhandlugen des III. Internatinalen Mathematiker-Kongres (Heidelberg) pp. 484-491, 1905

Rao, P. Gilarranz, J.L., Ko, J. Strgnac, T. and Rediniotis, O.K., (2000). "Flow Separation Control Via Synthetic Jet Actuation", AIAA Paper 2000-0407

Roshko, A., (1967), "A review of concepts in separated flow", Proceedings of Canadian Congress of Applied Mechanics, Vol. 1, 3-81 to 3-115

Scarano, F. and Rieuthmuller, M. L. (1999). "Iterative multigrid approach in PIV image processing with discrete window offset". Experiments in Fluids, 26, 513-523

Seifert, A., Bachar, T., Koss, D., Shepshelovich, M., Wygnanski, I. (1993). "Oscillatory Blowing: A Tool to Delay Boundary-Layer Separation". AIAA Journal. Vol. 31, No. 11, pp. 2052-2060.

Seifert, A., Pack, L.G., (1999). "Active Control of Separated Flows on Generic Configurations at High Reynolds Numbers". AIAA Paper 1999-3403

Smith B. L. and Glezer A., (1998). "The formation and evolution of synthetic jets". Phys. of Fluids 10, 2281-2297

Wereley S.T., Meinhart C.D. (2001). "Second-order accurate particle image velocimetry". Experiments in Fluids, 31, pp. 258-268.

Wu, J.C., Vakili, A. D., Wu, J.M., (1991). "Review of the Physics of Enhancing Vortex Lift by Unsteady Excitation", Prog. Aerospace Science, Vol. 28, pp. 73-131

Wu, J.M., Lu, X., Denny, A.G.,Fan, M. Wu, J.Z., (1997). "Post Stall Flow Control on an Airfoil by Local Unsteady Forcing". Prog. AIAA Paper No 97-2063

Zeiger, M.D. and Telionis, D.P. (1997). "Effect of Coning Motion and Blowing on the Asymmetric Side Forces on a Slender Forbody". AIAA Paper No 97-0549

Zeiger M. (2003). "The dynamic character of the flow over a 3.5 caliber tangent- ogive cylinder in steady and maneuvering states at high incidence". Dissertation prepared for the Ph.D. Candidacy

Zhou, M. D., Fernholz, H. H., Ma, H. Y., Wu, J. Z., Wu, J. M., (1993). "Vortex Capture by a Two-Dimensional Airfoil with a Small Oscillating Leading-Edge Flap". AIAA Paper 93-3266.

Zilliac, G.G., Degani, D. and Tobak, M. (1990). "Asymmetric Vortices on a Slender Body of Revolution". AIAA Journal, pp 667-675

2 EXPERIMENTAL SETUP AND EQUIPMENT

2.1 Introduction

Measurements were carried out in two wind tunnels and a water tunnel. The water tunnel and the small wind tunnel are located in the ESM fluids laboratory at Norris Hall. The other wind tunnel is the Stability tunnel located in Randolph Hall. Two different models were constructed: one for air pressure measurements in the wind tunnel and another for flow visualization and velocity measurements in the water tunnel. The facilities and the models are here briefly described.

2.2 Wind tunnels

2.2.1 ESM wind tunnel

The ESM wind tunnel is an open-circuit, low-speed tunnel constructed in 1983. To reduce the turbulence level one honeycomb and four nylon-conditioning screens are included in the settling chamber. A five-to-one contraction follows the settling chamber. The test section dimensions are 51 cm x 51 cm x 125 cm (20 in x 20 in x 50 in) and include a removable plexiglass wall for easy access as well as visualization. The tunnel is powered by a 15 hp motor. Adjusting the relative diameters of the drive pulleys sets the tunnel speed. It can achieve free-stream velocities from 4 m/s to 35 m/s. The turbulence level does not exceed 0.51% at a free-stream velocity of 10 m/s, except for regions very near the tunnel walls. The flow across the test section has a velocity variation of less than 2.5%. Figure 1 shows a schematic of the wind tunnel.

The tunnel free stream velocity is obtained by a Pitot tube mounted on one of the side walls, which is connected to the data acquisition system as well as a Edwards-Datametrics Barocel precision transducer model 590D-100T-3Q8-H5X-4D and this in turn was connected to a 1450 Electronic Manometer that would provide a readout of the dynamic pressure. The Barocel has a range of 0-100 Torr with an accuracy of 0.05% of the pressure reading and a full-scale resolution of 0.001% .

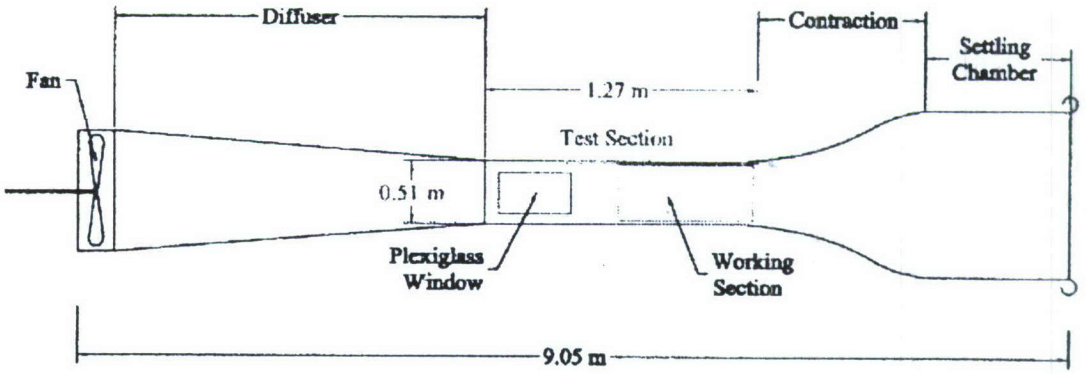

Figure 1: ESM Wind Tunnel Schematic

2.2.2 Virginia Tech Stability wind tunnel

The Virginia Tech Stability wind tunnel is a continuous, closed-loop subsonic wind tunnel. The maximum achievable flow speed is 275 ft/s (83.8 m/s) in a 6-foot by 6-foot by 25-foot (1.83m×1.83m×7.62m) test section. This facility was constructed in 1940 at the present site of NASA Langley Research Center by NASA's forerunner, NACA. Use of the tunnel at Langley in the determination of aerodynamic stability derivatives lead to its current name. In 1959, the tunnel was moved to Virginia Tech where it has been located outside of Randolph Hall.

The settling chamber has a contraction ratio of 9 to 1 and is equipped with anti-turbulence screens. This combination provides an extremely smooth flow in the test section. The turbulence levels vary from 0.018% to 0.5% and flow angularities are limited to 2° maximum. The settling chamber is 3m long and the diffuser has an angle of 3°. The ambient temperature and pressure in the test section is nearly equal to the ambient outdoor conditions due to the presence of a heat exchanger. During testing the control, room is maintained at the same static pressure as the test section. The tunnel fan has a 14-foot (4.27m) diameter and is driven by a 600 hp motor. Shows an schematic of the Stability tunnel.

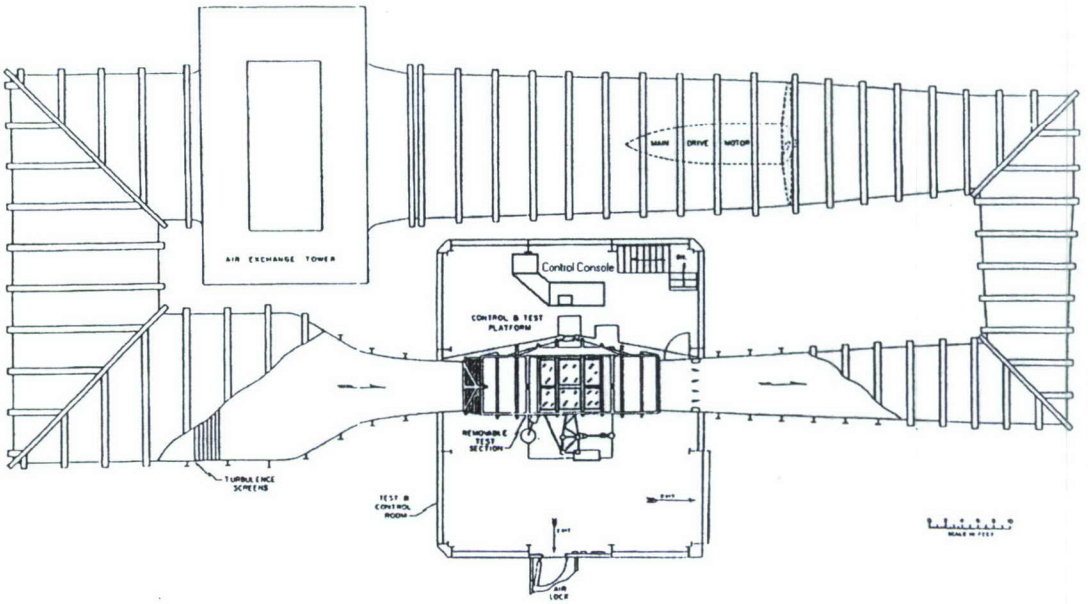

Figure 2: Stability tunnel schematic

2.3 Wind tunnel experimental rig

2.3.1 Model

The model used for this phase is a symmetric circular arc 12 ½ percent chord thickness airfoil. The chord length is 16 in with a resulting maximum thickness of 2 in. Its span is 20 in. It was built in two separate phases: the jet actuator and leading edge and the body of the airfoil.

The design of the jet mechanism took into account the desire of having it as close as possible to the leading edge of the airfoil. The leading edge part of the wing is essentially a wedge prism as shown in

Figure 3. The actuation mechanism consists of two concentric cylindrical surfaces as shown in Figure 4. The inner cylinder is a 7/16"-diameter inner brass tube that contains eight 1/16" wide slots and 1 ½ "long with 1/16 separation between them. The inner cylinder rotates about a fixed axis inside a fixed outer cylindrical surface created by the machined wedge. The inner cylinder is a brass tube, free to rotate on three bushings. One bushing was machined to fit snugly between the brass tubing and the machined leading edge at mid-span. This was done to eliminate possible warping of the tube during rotation.

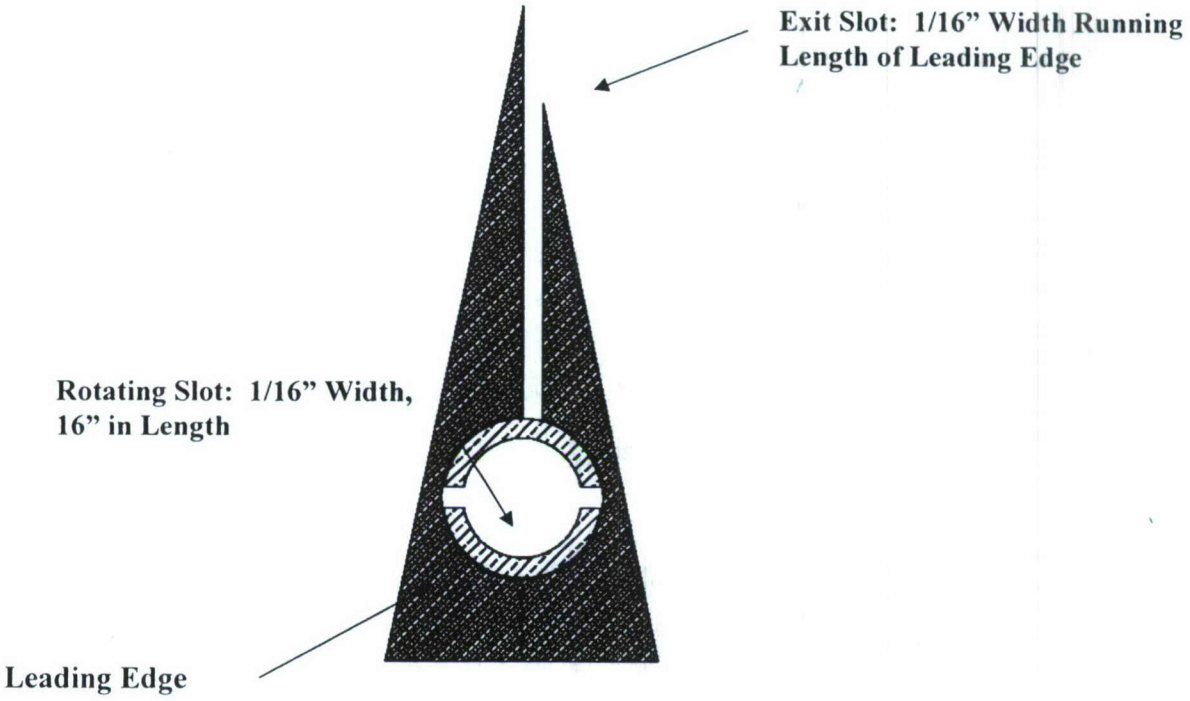

Figure 3: Leading Edge Cross Section

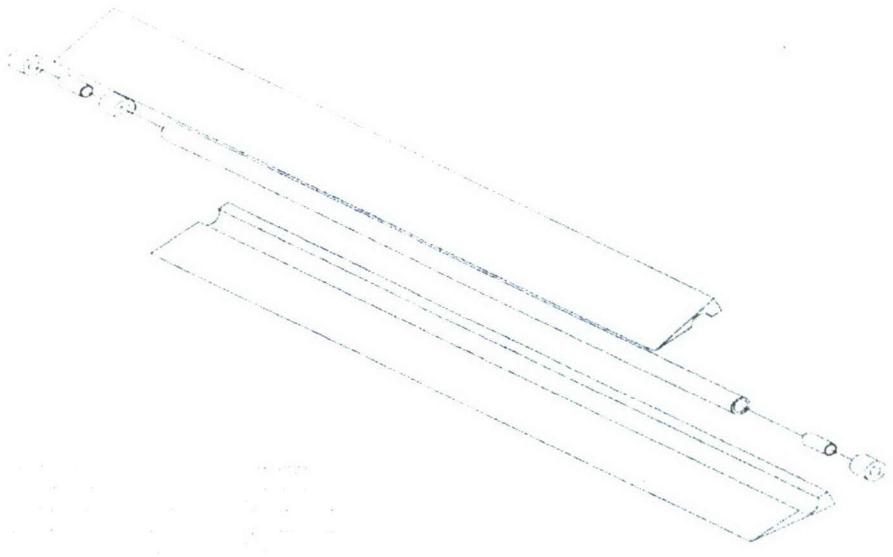

Figure 4: Exploded View of Leading Edge and Flow Control Device

The body was made entirely of aluminum and consists of three holding ribs and two 1/32 sheets that serve as the skin. The ribs have holes through them that provide access to the inside.

Each side has 32 pressure taps aligned and located at 177.8 mm (7 in) from starboard side as can be seen in Figure 5. The taps start at 63.5 mm (2 ½ ") from the leading edge and are spaced at 10.16 mm (0.4 in) along the arc. Stainless steel tubing of 1.27 mm (0.05 in) o.d., 0.8382 mm (0.033 in) i.d. and 6.35 mm (1/4 in) in length was inserted in each tap with tygon tubing R-3603 of 2.38125 mm (3/32 in) o.d. and 0.79375 mm (1/32 in) i.d. connecting them to the pressure transducers.

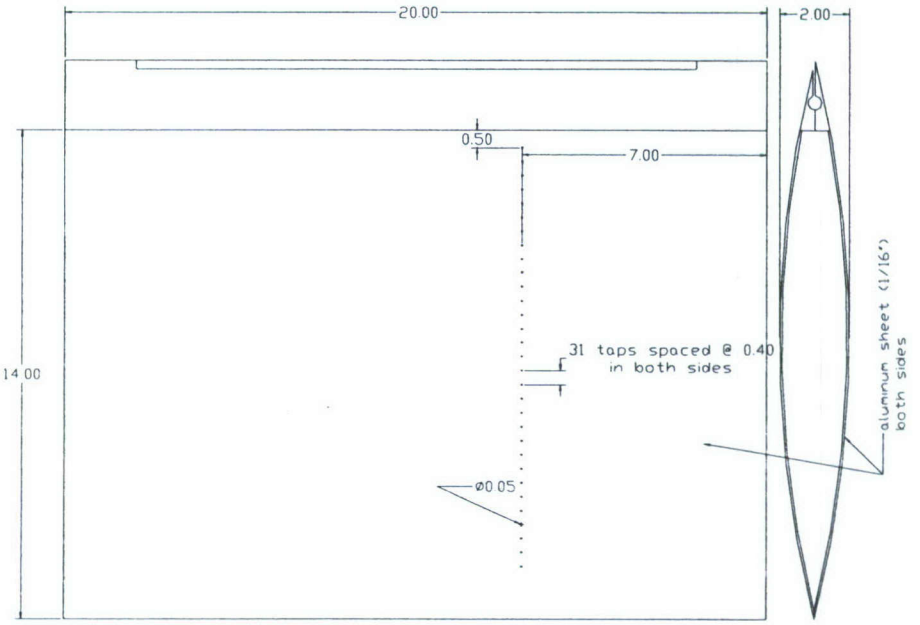

Figure 5: Wind tunnel model

To evaluate the capabilities of the actuator, the assembled leading edge actuator along with a rake of high-frequency-response Pitot tubes were mounted, as shown in Figure 6. Endevco model 8510 pressure transducers were used as sensing elements inside the rake. The output of the pressure transducers was connected to a HP digital signal analyzer, which was used to measure jet frequencies. In addition, these were also connected to a simple PC-driven 12-bit data acquisition system. The rake was mounted on traversing scales so it could easily be displaced to obtain data at different locations relative to the slotted nozzle.

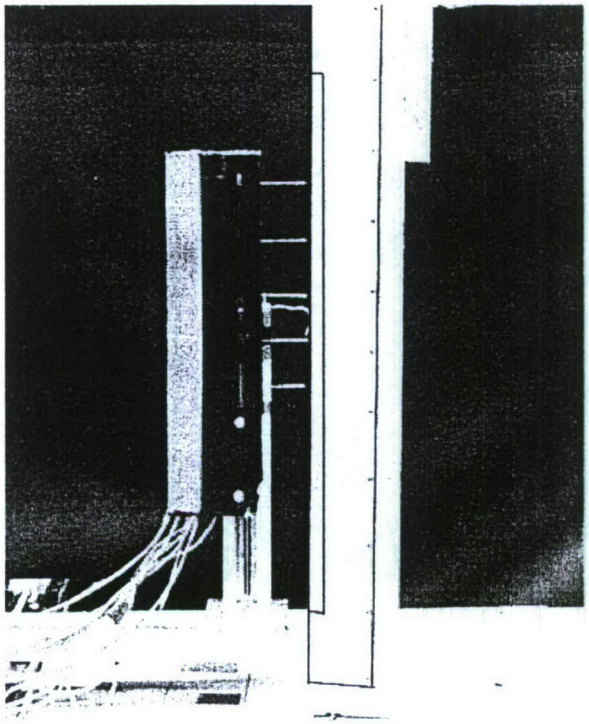

Figure 6: Leading Edge Aligned with Pitot Rake

2.3.2 Data Acquisition system

The pressure transducers used here are Pressure Systems Inc. ESP pressure scanners. These scanners are small, high-density packages containing multiple differential sensors. Two 32 channel scanners were used here, one with 10" of water range and the other with 20" of water range. Each channel is a mini piezoresistive pressure transducer and their output is internally amplified to ±5V full scale. These transducers have an accuracy of 0.10% of full scale after full calibration and a frequency response of 50 Hz. The transducers are differential and the reference pressure taken was the free stream static pressure. The last port in the second ESP was set aside for the tunnel total pressure to obtain the free stream velocity.

Pressure data were acquired using the ESP scanners that were mounted inside the model. The ESP's were connected to dedicated boards for digital addressing as well as voltage regulation. Since the ESP's have a maximum frequency response of 50 Hz they were sampled at 250 Hz and the sampling was done by a data acquisition board from Computer Boards model CIO-DAS08 12-bit A-D converter installed on a 233 MHz Pentium II processor installed computer. The Endevco pressure transducers were

connected to the same setup system although their inputs are acquired as external sources. They were calibrated properly.

This system was developed in house and has proprietary software as well as physical setup. For more detailed information on this data acquisition system the reader is referred to Zeiger (2003).

2.4 Water Tunnel

The ESM Water Tunnel was designed and built by Engineering Laboratory Design (ELD). The system is a closed loop design with the flow arranged in a vertical configuration with an approximate capacity of 9463 liters (2500 gallons) of water. An schematic is provided in figure Among the tunnel components are the flow sections, that includes a return plenum with turning system that divides and directs the flow after the test section, 24 inches return PVC pipe, an inlet plenum, a flow straightener and a three-way contraction convergence. The test section is a 61 cm x 61 cm x 183 cm (24" x 24" x 72") made out of a 1 ¼ inch clear acrylic plexiglass and a removable top that was not used during the present work. The final components of interest are a 17000 liters/min (4500 GPM) single stage pump and a variable speed drive assembly that consist of a 15 kW (20 hp) AC motor and a variable frequency controller that allows for a range of flow velocities in the test section from 3 cm/s (0.1 ft/s) to 50 cm/s (1.5 ft/s).

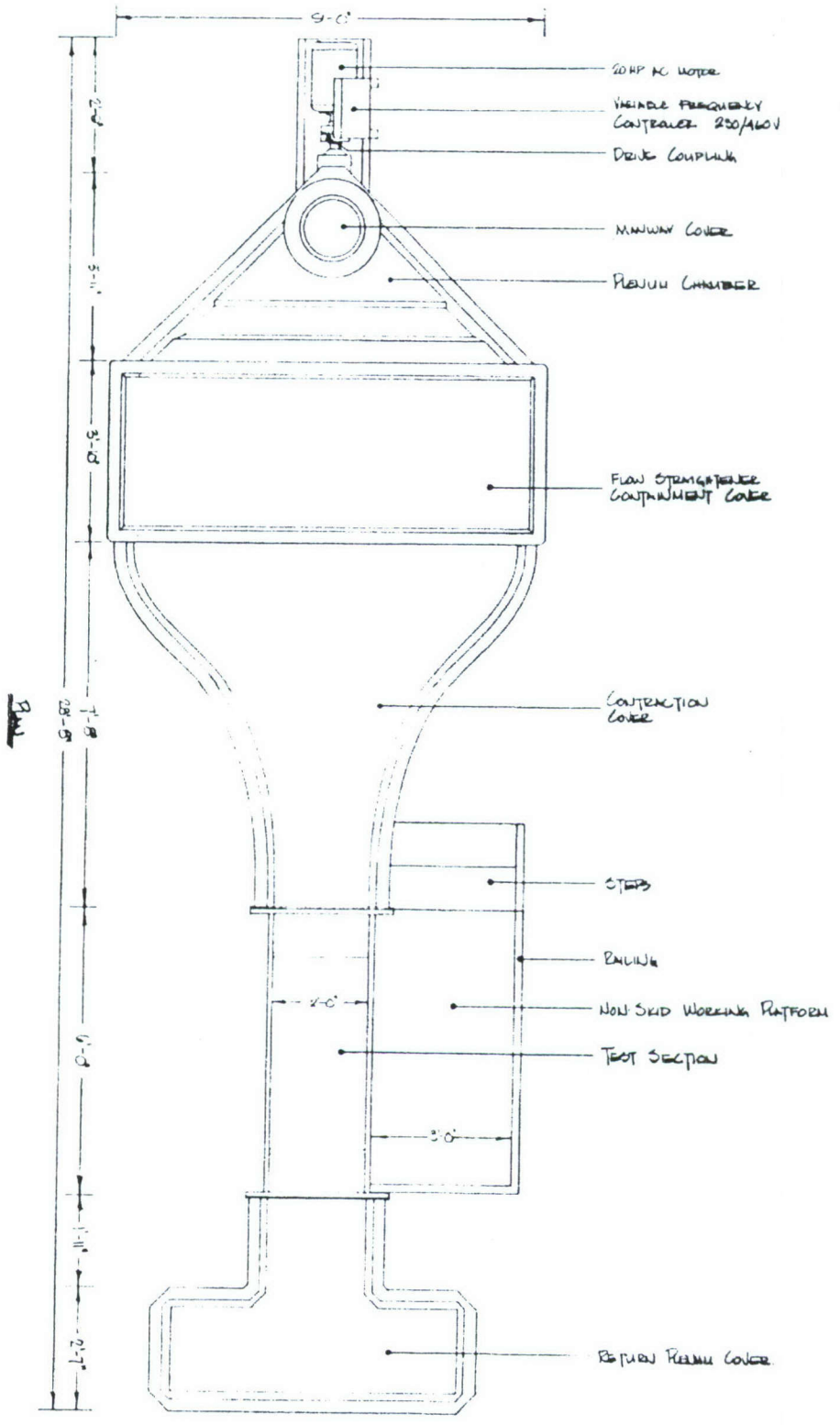

Figure 7: ESM Water tunnel Schematic

2.5 Water Tunnel Model

A first generation water tunnel Sharp Edge Airfoil model has been designed and fabricated out of ABS plastic using a rapid-prototyping facility. This model is shown in Figure 8. Its internal chamber is connected with high precision, computer-controlled gear pumps via the water supply connector shown in the same figure. The pumps allow the generation of pulsing jets with non-zero mean flow, or synthetic jet actuation via blowing and suction action. The airfoil section is geometrically similar to the one fabricated for the wind-tunnel tests. The chord was 100 mm and the maximum thickness was approximately 15% of the chord. The span of the model was 220 mm while a uniform jet-exit slot with 1mm width was placed within 5% from the leading edge. Finally, end plates were installed at the tips of the model in order to assure two-dimensional flow and control of the end effects.

For the experimental results presented here, the Reynolds number based on the chord was Re=25,000. The airfoil was placed at an AOA=25 deg in order to generate a massively separated flow. Based on a Strouhal number of 0.2 the natural shedding frequency was estimated around 1Hz. The latter was chosen as the actuator frequency yielding $F^{+}=1$. The actuator pulsed as a positive net-mass flow actuator with zero offset and an amplitude of $u_{jet}=0.15$m/s with 50% duty cycle. The above numbers result in a $C\mu=0.006$. Three cases will be presented here. First the flow of the pulsing jet alone, second the flow over the airfoil with no control and finally the flow with the control. These cases were investigated using two different magnifications, first with the field of view covering the whole airfoil with 1 mm spatial resolution, and then with fine resolution of 0.5 mm zooming near the actuator jet.

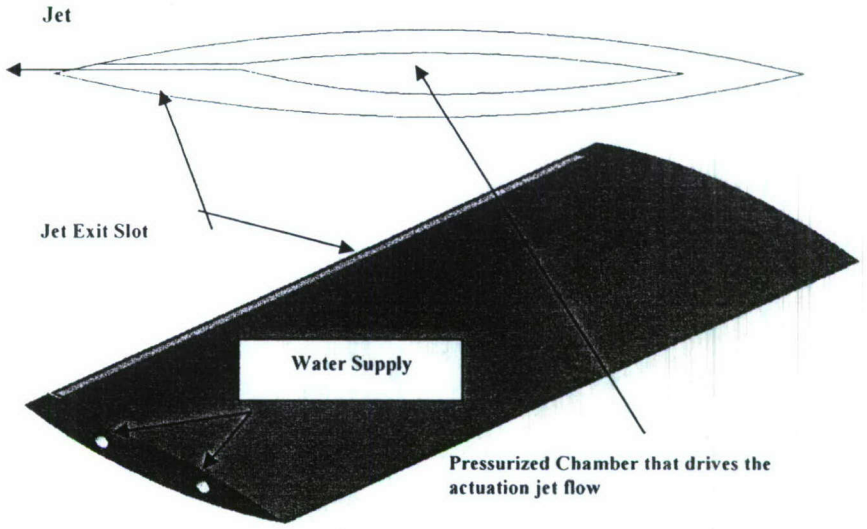

Figure 8: Water tunnel model

2.6 Particle Image Velocimetry System

This is a facility equipped with state of the art, in-house developed Time Resolved Digital Particle Image Velocimetry (TRDPIV). This PIV system is based on an Oxford Systems powerful laser (55 Watts), which is guided through a series of special mirrors and lenses to the area of interest and is opened up to a laser sheet directed across the field as shown in Figure 9. For the research conducted here, the laser sheet was placed in the mid-span of the airfoil aligned parallel to the free-stream. The free stream velocity was 0.25 m/s with corresponding water tunnel free stream turbulence intensity approximately 1%. A traversing system allows adjusting the distance from the models to the laser sheet. The flow is seeded with neutrally buoyant fluorescent particles, which serve as flow tracers. The diameter of the particles is on the order of 100 microns such that the particles accurately follow the flow with no response-lag to any turbulent fluctuations. A CMOS video camera captures the instantaneous positions of the particles. The laser and the camera are synchronized to operate in dual frame single exposure DPIV mode with sampling frequencies of 1000 Hz. This mode of operation allows very detailed temporal resolution, sufficient for resolving the turbulent flow fluctuations present in the wake.

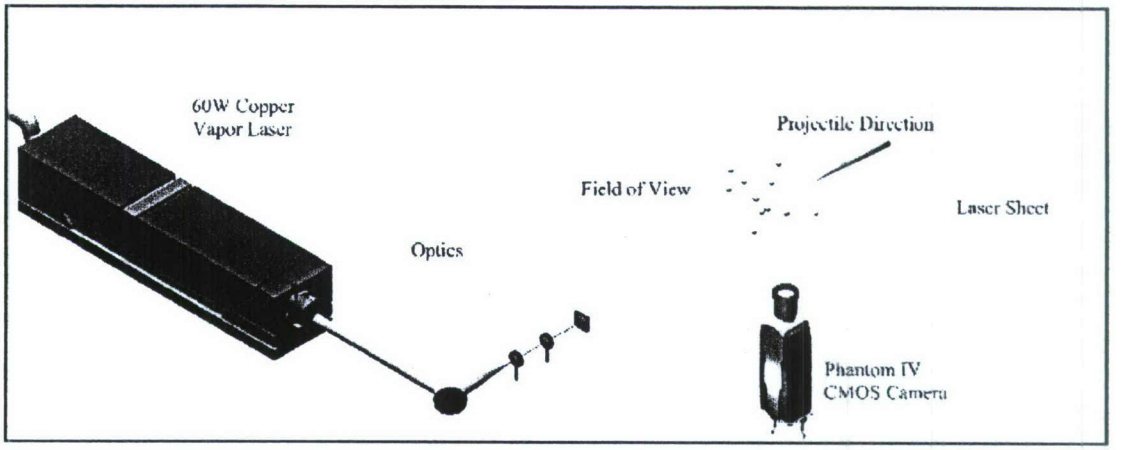

Figure 9: Schematic of experimental setup, which includes a 55-Watt Cu-Vapor pulsing laser, a high speed CMOS camera, optical lenses, and the flow field.

The velocity evaluation is carried out using a multi-grid iterative DPIV analysis. The algorithm is based on the work by Scarano and Rieuthmuller. In addition to their method we incorporated a second-order Discrete Window Offset (DWO) as proposed by Wereley and Meinhart. This is a simple but essential component. Time-resolved DPIV systems are limited by the fact that the time separation between consecutive frames is the reciprocal of the frame rate, thus on the order of milliseconds. This value is relatively large compared with microsecond time-intervals employed by conventional DPIV systems. By employing a second order DWO we provide an improved predictor for the particle pattern matching between the subsequent iterations. Moreover, the algorithm employed performs a localized cross-correlation which, based on our preliminary work, when compared to standard multi-grid schemes for resolving strong vortical flows was proven to be superior. Further details on the system, the algorithm and the associated error analysis can be found in Abiven et al (2002).

For the needs of the present study, the multigrid scheme was employed with a window hierarchy of 32-32-16-16-8 pixel2 and a space resolution of 4 pixel/vector. Two different magnifications were employed resulting in 0.5 mm and 1mm space resolution. The overall performance of the method yield time resolution 1 milliseconds with sampling time up to 2 secs. and average uncertainty of the velocity measurement on the order of 10-3 m/s independently of the velocity magnitude. The vorticity distribution in the wake is calculated from the measured velocities using 4th order, compact, finite-difference schemes 16.

2.7 References

Abiven, C., Vlachos, P. P., (2002). "Super spatio-temporal resolution, digital PIV system for multi-phase flows with phase differentiation and simultaneous shape and size quantification", Int. Mech. Eng. Congress, Nov. 17-22, 2002, New Orleans, LA

Abiven, C., Vlachos P. P., Papadopoulos, G., (2002). "Comparative study of established DPIV algorithms for planar velocity measurements", Int. Mech. Eng. Congress, Nov. 17-22, 2002, New Orleans, LA

Amitay M, Smith B. L. and Glezer, (1998). "Aerodynamic flow control using synthetic jet technology", AIAA Paper 98-0208

Artana, G., D'Adamo, J., Léger, L., Moreau, E., Touchard, G., (2002). "Flow Control with Electrohydrodynamic Actuators" AIAA Journal Vol. 40, pp. 1773-1779

Cahill, J. F., Underwood, W.J., Nuber, R.J., Cheesman, G.A., (1953). "Aerodynamics forces on symmetrical circular-arc airfoils with plain leading-edge and plain trailing-edge flaps" NACA Report 1146

Cattafesta, L.N, Garg, S., Shukla, D., (2001). "Development of Piezoelectric Actuators for Active Flow Control". AIAA Journal Vol. 39, pp. 1562-1568

Didden, N. (1979). "On the Formation of Vortex Rings: Rolling Up and Productions of Circulation." Z. Angew. Math.Phys. Vol 30, pp101-106.

ELD, (1984) 24" Flow Visualization Water Tunnel, Operating and Maintenance Instructions

Fiedler, H. E., (1998). "Control of Free Turbulent Shear Flows". In *Flow Control: Fundamentals and Practices* (ed. Gad-el-Hak, M., Pollard, A., Bonnet, J. P.), pp. 335-429

Gad-el-Hak , M., (2001). "Flow Control: the Future," J. of Aircraft. Vol. 38, No. 3, pp. 402-418

Gilarranz, J. L., Rediniotis, O. K., (2001). "Compact, High-Power Synthetic Jet Actuators For Flow Separation Control," AIAA Paper 2001-0737

Glezer, A. (1998): "The Formation of Vortex Rings". Phys. Fluids, Vol 31, pp. 3532-3542.

Hsiao, F. –B., Wang, T.-Z., Zohar, Y., (1993). "Flow separation Control of a 2-D Airfoil by a Leading-Edge Oscillating Flap," Intl. Conf. Aerospace Sci. Tech., Dec. 6-9, 1993, Tainan, Taiwan.

Hsiao, F. B., Liang, P. F., Huang, C. Y., (1998). "High-Incidence Airfoil Aerodynamics Improvement by Leading-edge Oscillating Flap". J. of Aircraft. Vol. 35, No. 3, pp. 508-510.

Ho, C.-M. and Huerre, P. (1984) "Perturbed free shear layers". Ann. Rev. Fluid Mech. 16, 365

Jacobson, S.A, Reynolds, W.C.,(1998), "Active Control of Streamwise Vortices and Streaks in Boundary Layers", J. of Fluid Mechanics. Vol. 360, pp. 179-211.

McCormick, D. (2000), "Boundary Layer Separation Control with synthetic jets", AIAA Paper 2000-0519

McManus, K., Magill, J., (1996). "Separation Control in Incompressible and Compressible Flows using Pulsed Jets". AIAA Paper 96-1948.

Miranda, S., Telionis, D., Zeiger, M., (2001). "Flow Control of a Sharp-Edged Airfoil", AIAA Paper No. 2001-0119, Jan. 2001

Pope, A., Barlow, J.B., Rae, W.H., *Low speed wind tunnel testing*, 3rd ed. p.353-356.

Prandtl, L. (1904) "Über Flüssigkeitbewegung bei sehr kleiner Reibung", Verhandlugen des III. Internatinalen Mathematiker-Kongres (Heidelberg) pp. 484-491, 1905

Rao, P. Gilarranz, J.L., Ko, J. Strgnac, T. and Rediniotis, O.K., (2000). "Flow Separation Control Via Synthetic Jet Actuation", AIAA Paper 2000-0407

Roshko, A., (1967), "A review of concepts in separated flow", Proceedings of Canadian Congress of Applied Mechanics, Vol. 1, 3-81 to 3-115

Scarano, F. and Rieuthmuller, M. L. (1999). "Iterative multigrid approach in PIV image processing with discrete window offset". Experiments in Fluids, 26, 513-523

Seifert, A., Bachar, T., Koss, D., Shepshelovich, M., Wygnanski, I. (1993). "Oscillatory Blowing: A Tool to Delay Boundary-Layer Separation". AIAA Journal. Vol. 31, No. 11, pp. 2052-2060.

Seifert, A., Pack, L.G., (1999). "Active Control of Separated Flows on Generic Configurations at High Reynolds Numbers". AIAA Paper 1999-3403

Smith B. L. and Glezer A., (1998). "The formation and evolution of synthetic jets". Phys. of Fluids 10, 2281-2297

Wereley S.T., Meinhart C.D. (2001). "Second-order accurate particle image velocimetry". Experiments in Fluids, 31, pp. 258-268.

Wu, J.C., Vakili, A. D., Wu, J.M., (1991). "Review of the Physics of Enhancing Vortex Lift by Unsteady Excitation", Prog. Aerospace Science, Vol. 28, pp. 73-131

Wu, J.M., Lu, X., Denny, A.G.,Fan, M. Wu, J.Z., (1997). "Post Stall Flow Control on an Airfoil by Local Unsteady Forcing". Prog. AIAA Paper No 97-2063

Zeiger, M.D. and Telionis, D.P. (1997). "Effect of Coning Motion and Blowing on the Asymmetric Side Forces on a Slender Forbody". AIAA Paper No 97-0549

Zeiger M. (2003). "The dynamic character of the flow over a 3.5 caliber tangent- ogive cylinder in steady and maneuvering states at high incidence". Dissertation prepared for the Ph.D. Candidacy

Zhou, M. D., Fernholz, H. H., Ma, H. Y., Wu, J. Z., Wu, J. M., (1993). "Vortex Capture by a Two-Dimensional Airfoil with a Small Oscillating Leading-Edge Flap". AIAA Paper 93-3266.

Zilliac, G.G., Degani, D. and Tobak, M. (1990). "Asymmetric Vortices on a Slender Body of Revolution". AIAA Journal, pp 667-675

3 JET CHARACTERIZATION

A thorough understanding of the pulsating jet is needed before any application can be performed. The need for this is to understand how the actuator will behave under different conditions and if there is any coupling between the actuating frequency and the jet velocity as it happens to acoustic actuators and other compact actuators. Moreover, we need to document how the asymmetry of the nozzle affects the profile.

3.1 Pitot-Tube Measurements

The traversing scales, driven by stepper motors and controlled by the data-acquisition system, was used to orient the rake at positions along the leading edge slot, and perpendicular to the slot, seen in Figure 3-4. Velocity profiles were thus generated. We tested the actuator at supply pressures ranging from 40 psi to 100 psi and frequencies between 15 and 60 Hertz. A time record of the waveform for the steady state, as well as for pulsation obtained over the slotted nozzle is shown in Figure 1. For the same applied pressure of 80 psi the time records show that when the jet is pulsated it has a higher velocity than the steady jet. The RMS values of the two signals indicate a difference of almost 23 % increase from steady to a pulsating jet.

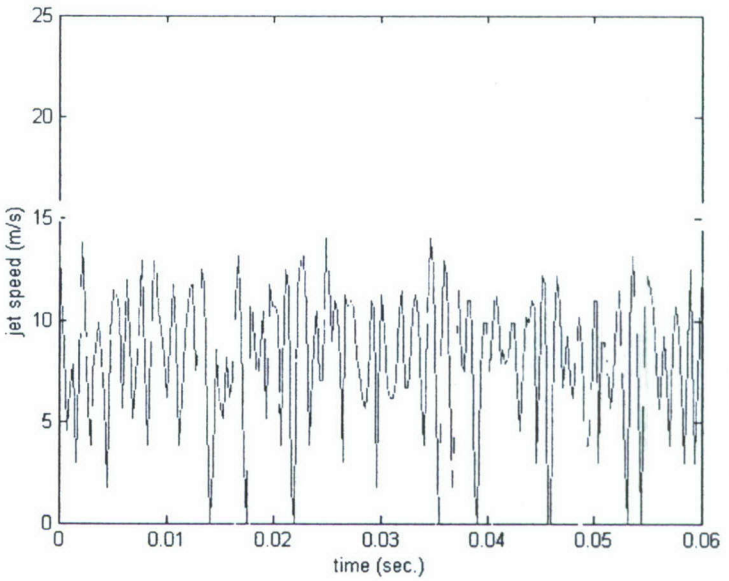

Figure 1: Time records for steady jet and for 63 Hz pulsating jet with the same pressure

Power spectra of such signals (in Figure 2) revealed that the dominant frequency of the jet was twice the driving frequency of the motor. The spectrum confirmed that no motions were generated by nonlinear interactions, since the only other visible frequency was the second mode of the actuation frequency, and therefore this device could generate pulsed jets with any desired frequency within the limitations of the device, without introducing unwanted secondary frequencies. Named frequencies refer to the frequency of the jet, not the rotational frequency of the motor.

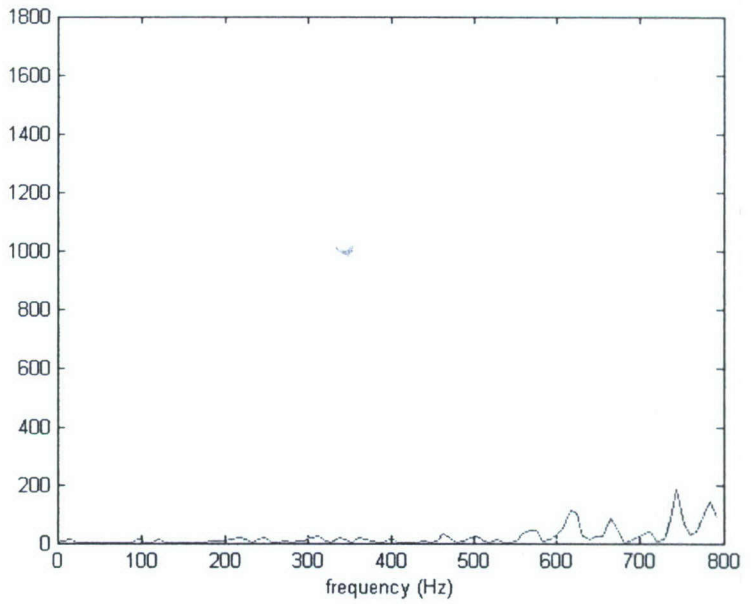

Figure 2: Power spectrum for steady jet and for 63 Hz pulsating jet with the same pressure

Another feature is that this actuator can produce pulsing jets with amplitudes independent of the driving frequency. We measured the velocities across the slot for a range of driving frequencies and for a fixed plenum pressure of 100 psig. The results are presented in Figure 3. These data indicate that the velocities generated by the device are almost completely independent of the driving frequency, and vary by up to 3.1% for data acquired at 100 psig driving pressure and down by 2.2 % for 25 psig and by 7.8% for 80 psig supply pressure. They remain fairly constant with some downward or flat trends as the frequencies are increased.

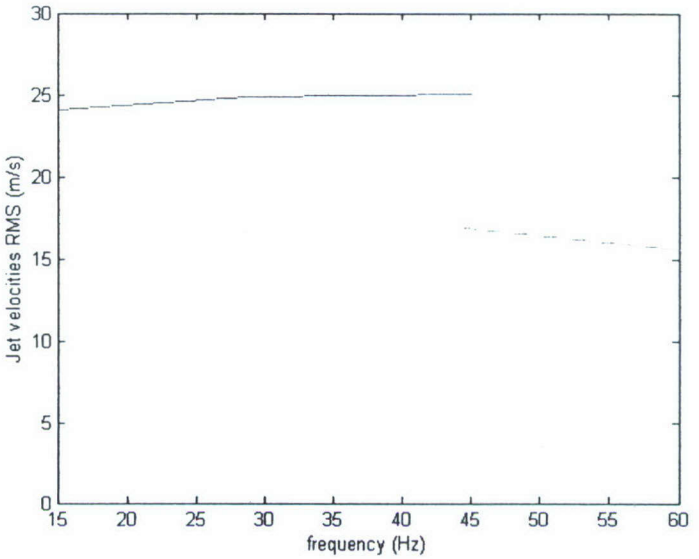

Figure 3: RMS for the jet speed at different pressures. Blue line is for 100 psig, red line is for 80 psig and green line is for 25 psig.

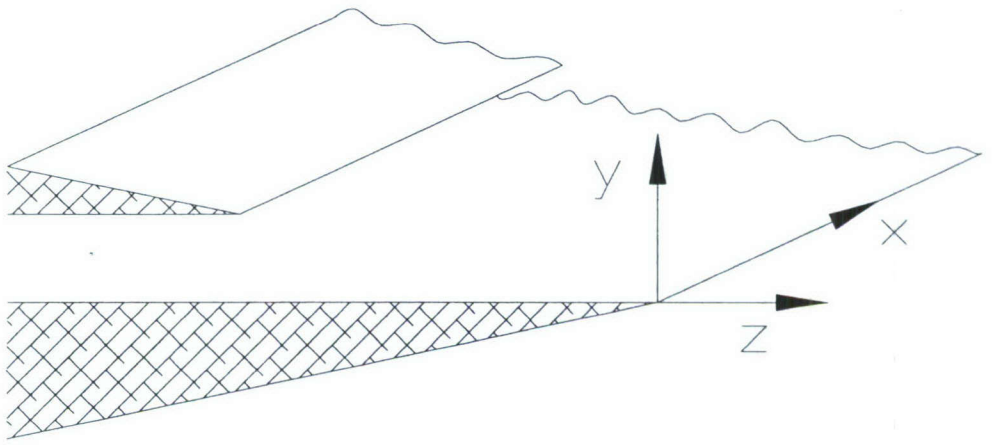

Figure 4: Sketch of coordinate system

Velocity profiles at different distances across the steady jet were also plotted in terms of coordinates laid out in Figure 4. In Figure 5 observed that the location of the maximum velocity is displaced upward, i.e. in the direction of the short side of the nozzle. This implies that there is a deviation of the direction of the jet away from the

direction of the z-axis of the duct as it moves in the outward direction of the edge. Averaged profiles for the pulsed jet are presented in Figure 6, Figure 7 and Figure 8 for three driving frequencies of 15, 29 and 45 Hz. In these three profiles, the vectoring of the jet is more pronounced although not by a high margin. This deviating tendency can be attributed to the asymmetry of the nozzle. As shown in Figure 4, one side of the jet duct is shorter than the other. As a result, the boundary layer on one side becomes a free shear layer before the other. Thus on one side, the free vorticity may start rolling, while the shear layer on the other side is constrained by the flat solid wall and vorticity retains its organization in the form of parallel flat layers. It is essentially a boundary layer. Rolled vortices may now generate regions of low pressure and thus induce changes in the direction of the jet. This is a Coanda effect. Apparently, this effect is mild for steady flow. This is expected, because the distance the free shear layer travels before the other side becomes free is short. For such a distance, no large vortical structures can grow. The situation is different with pulsing jet. An unsteady jet started from rest quickly rolls into two large vortices in two dimensions or a vortex ring in axisymmetric flow as suggested by Didden (1979) and Glezer (1998). In our case, the asymmetry of the two flat sidewalls allows the formation of a vortex on one side but forces vorticity to be confined in an attached boundary layer on the other side. The vortex being formed only on one side induces a low pressure as well as flow away from the long wall. A stronger vectoring away from the axis of symmetry of the wing and therefore a more effective disturbance will probably be introduced in the separated flow. In addition, the increase in frequency does not change further the velocity profiles with respect to the steady blowing case indicating that this further vectoring is a result of the pulsation without regard to magnitude of frequency.

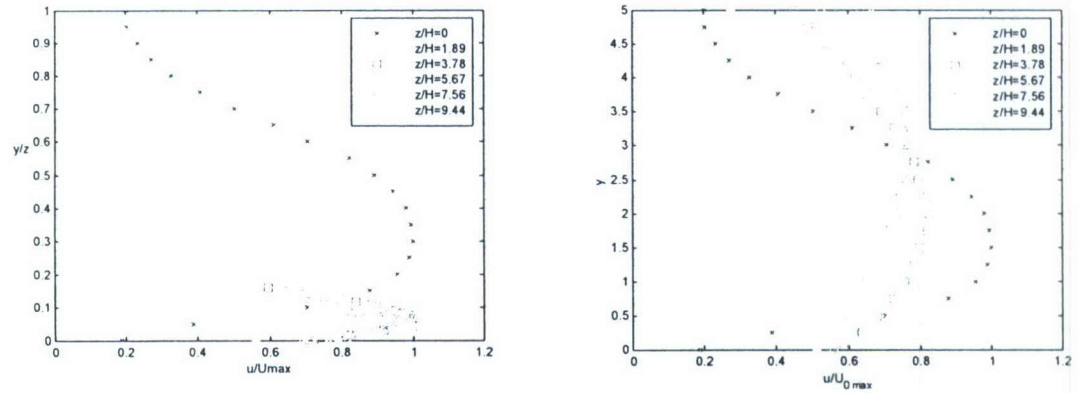

Figure 5: Actuator-jet velocity profiles in self-similar coordinates (left) and actual coordinates (right)

Steady Blowing

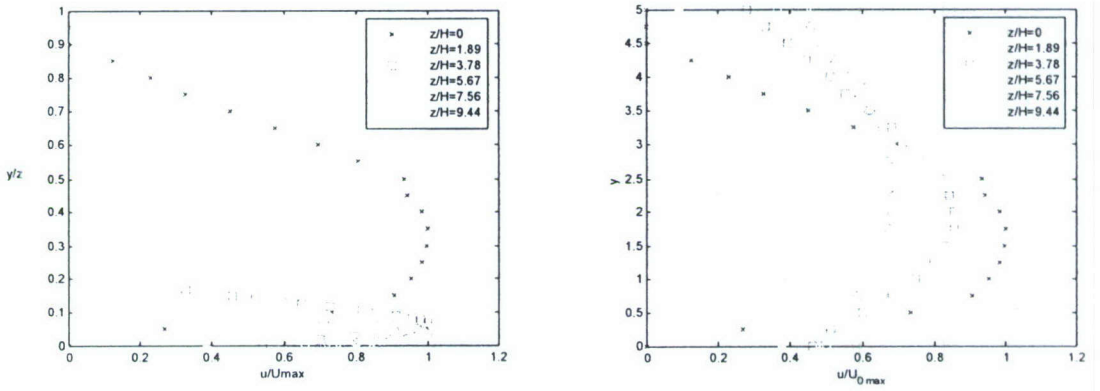

Figure 6: Actuator-jet velocity profiles in self-similar coordinates (left) and actual coordinates (right)

15 Hz

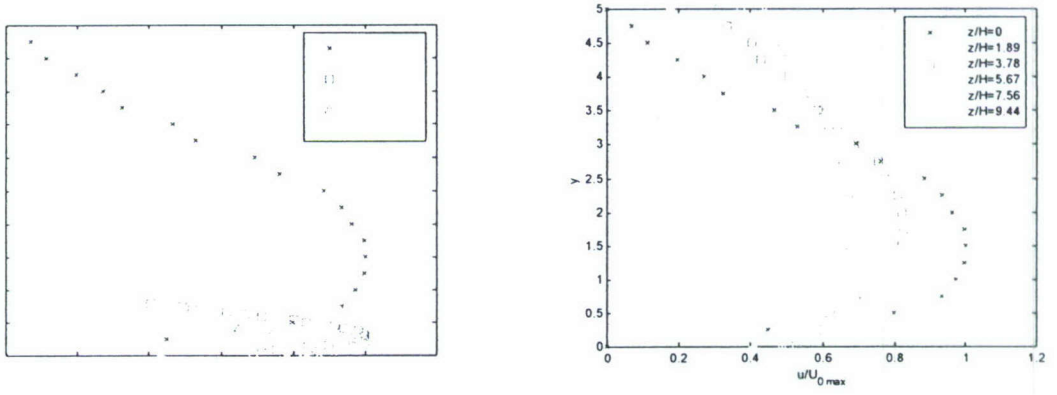

Figure 7 Actuator-jet velocity profiles in self-similar coordinates (left) and actual coordinates (right)

29 Hz

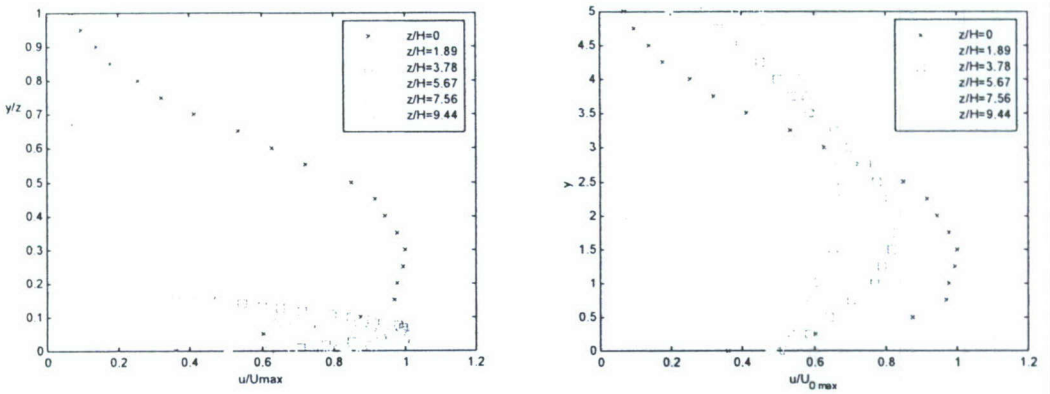

Figure 8: Actuator-jet velocity profiles in self-similar coordinates (left) and actual coordinates (right) 45 Hz

3.2 PIV measurements

Water tunnel tests helped in documenting the development of the actuator jet and shed light on the asymmetry discussed above. A space resolution of 0.5 mm and temporal resolution of 1 millisecond was employed. Figure 9 shows a time sequence of 10 instantaneous velocity fields and vorticity distribution within one cycle of the actuator pulse. The frames are spaced apart by 0.02 secs. The initiation of the jet in the flow is shown in Figure 9-a. The formation of a pair of counter-rotating vortices continues in Figure 9-b. As discussed before, the slot geometry allows the generation of an asymmetric free-shear flow, confined in the lower side of the flow but allowed to accumulate vorticity and roll into a strong vortex in the upper side of the slot. This is better observed in Figures c-e where the clockwise vortex grows in strength as well as in size. As a result, it induces a velocity to the jet that favors the upper-side and effectively vectoring the jet at an angle with respect to the jet exit direction. At this point the dimensionless time is approximately $t^*=15$ which means that the jet reaches a steady state condition. Thus, a jet parallel to the slot forms with the classic shear layer vortices illustrated in Figure 9f-i. The important feature of this sequence is that the impulsive character of the jet favors the formation of a starting vortex on the upper side of the slot. This is equivalent to a passive control mechanism introduced by the slot geometry, inducing the jet to deviate at an angle with respect to the airfoil chord. This is a favorable feature, because when the jet interacts with the incident free stream, it curves and aligns itself better with the leading edge shear layer.

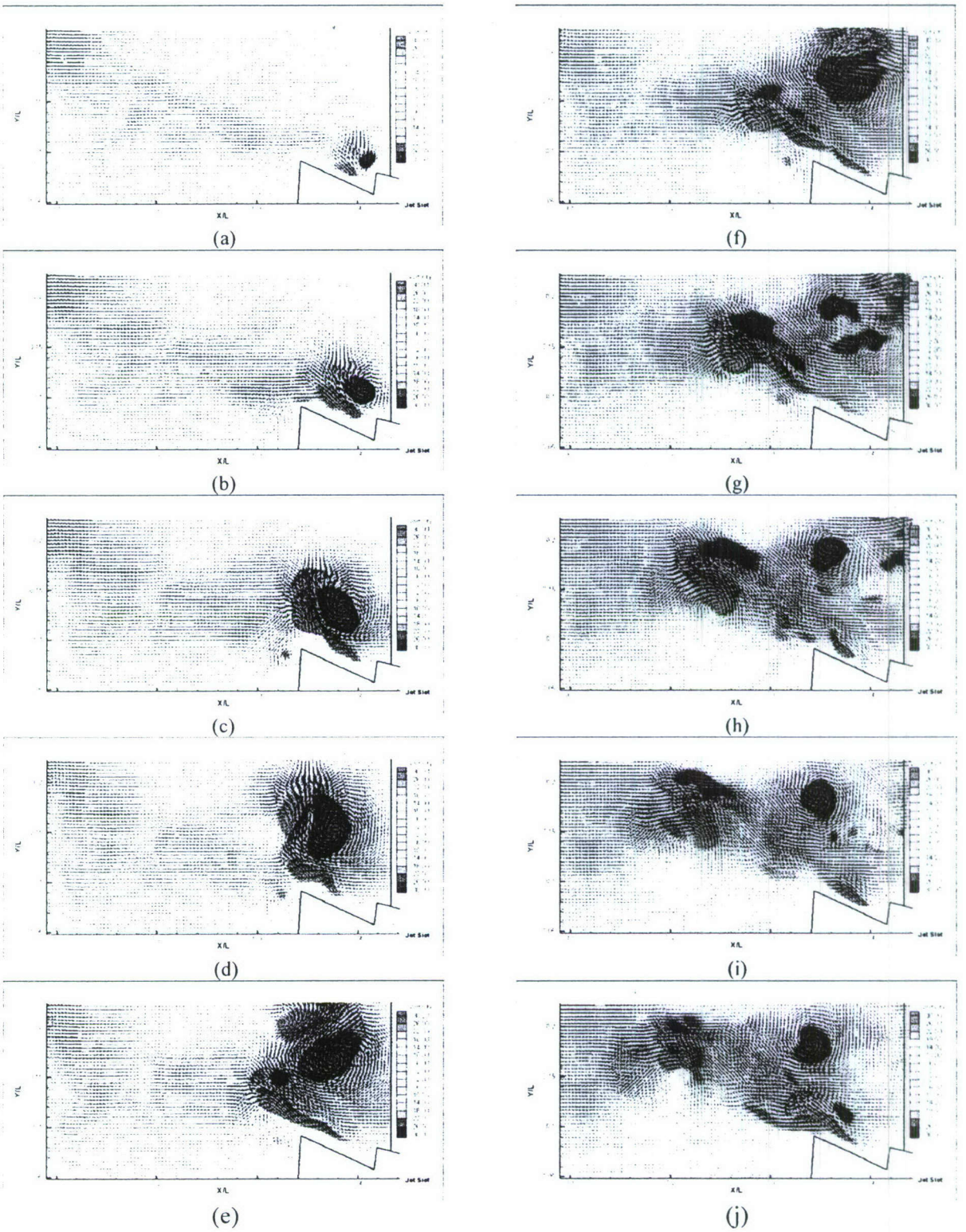

Figure 9: Time sequence of the actuator-jet vorticity contours and velocity distribution flow structure. t_{delay}=0.02 secs

The interaction and alignment with the leading edge shear layer can be observed in the following sequence of instantaneous flow fields. Figure 10-a and b show the separated shear layer before the initiation of the controlling pulsating jet. Clear shear layer instabilities are developing and the flow is highly disorganized. In Figure 10-c the initiation of the jet in the flow generates a clockwise rotating vortex with its locus approximately at x=0.13 y=0.1. This vortex induces a downward velocity to the shear layer vortices thus triggering a vortex pairing and the roll-up of a strong coherent vortex (Figure 10-c-d). In the subsequent figures (e-h), we witness one coherent vortex that interacts strongly with the airfoil increasing the vorticity (positive) levels and potentially inducing a pressure drop that will increase the suction and thus the lift. Remarkably, the dimensionless time required for vortex formation on the suction side is on the order of $t^*=15$ which appears to be the same as the time required for the pulsing jet to reach a steady state. Figure 10-i-j demonstrates that as the strength of the pulsing jet decays, the strength of the suction vortex reduces.

The previous sequence of figures reveals the mechanism for controlling separated flow. The impulsively-started jet vortex interacts with the shear layer and its natural instabilities forcing these instabilities to grow through a vortex pairing process and subsequently forming a strong coherent vortex that increases the vorticity contribution. The continuation of the blowing within the pulsing cycle does not appear to further enhance the process. In contrast, the results indicate that the starting vortex is predominantly affecting the flow. This allows us to speculate that a more efficient way to manage the flow by minimizing the input would be by reducing the duty cycle of the pulsing for the same $C\mu$.

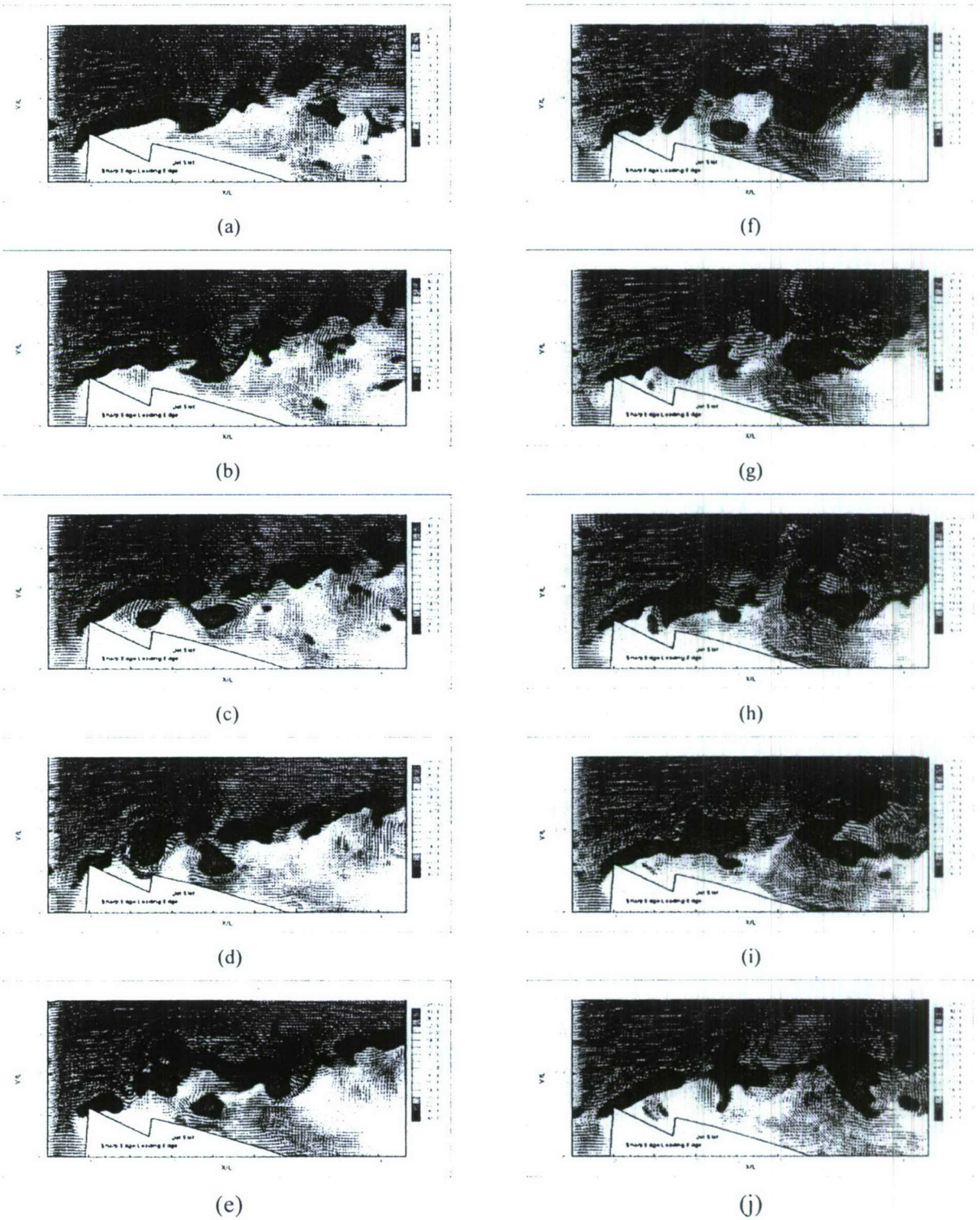

Figure 10: Time sequence of the controlled flow vorticity contours and velocity distribution

3.3 Conclusions

Our experimental data indicate that the velocity profiles generated by this actuator are nearly independent of the frequency. This means that the device is an excellent candidate for a robust flight actuator, where the required frequency and mass flow are changing with aircraft speed and the angle of attack. Another important feature of this device is that it can generate pulsing flow without any linearly oscillating parts, like a pulsating wall or piston. And due to the geometry of the nozzle the jet is going to have a tendency to be more aligned with the shear layer thus possibly reducing the energy need

3.4 References

Didden, N. (1979). "On the Formation of Vortex Rings: Rolling Up and Productions of Circulation." Z. Angew. Math.Phys. Vol 30, pp101-106.

Glezer, A. (1998): "The Formation of Vortex Rings". Phys. Fluids, Vol 31, pp. 3532-3542.

4 FLOW CONTROL OF SHARP-EDGED WINGS WITH PULSED-JET BLOWING

In previous publications the present team reported on how oscillating mini-flaps can control separated flows over sharp edged airfoils. In this report we present results on the control of flows over such airfoils using unsteady mini-jets deployed along the leading edge. We employ the new design of an actuator described in previous sections. This actuator can achieve a wide range of frequencies, and is free of oscillating components. The results indicate that unsteady mini-jet actuation is as effective as leading-edge mini-flaps. Moreover the present data are compared with results obtained with large leading edge flaps.

4.1 Low Reynolds Number Tests

We present the averaged pressure distributions over the suction and the pressure side of the airfoil for two different C_μ values and three angles of attack in the ESM wind tunnel. This setup had the problem that it suffered from solid blockage as defined by Pope et al (1999) since the model reduces the cross-sectional area of the tunnel, and as a result the air velocity around the model is increased. The model created a blockage of almost 21% when it was at 15° angle of attack. The results obtained in the ESM tunnel cannot provide direct information on lift and drag of sharp-edge wings. But our aim here is to explore the effects of flow control by comparing data obtained with and without control. The blowing amplitude was sustained at a constant level and the C_μ was adjusted by changing the free-stream velocity. The reduced frequency F^+ was changed and set at 0, 1, 1.5 and 2.

The pressure distributions do not indicate a clear stall situation for 10° (Figure 1) and even 15° and actually suggests attached flow in the average. For C_μ=0.0285 at a=15° (Figure 3) the control clearly increases the maximum suction. The suction strength is stronger on the leading edge part of the airfoil and it decreases towards the trailing edge. Unlike the other C_μ case that showed almost no improvement, here we observe a 15% drop in suction pressure. This difference suggests that the momentum coefficient C_μ should be at least greater than 1.5%. It also shows a small improvement when the

actuator was operated at larger F^+ than unity. This indicates that the harmonics of the natural frequency get excited and can contribute to the resonance effect. One last observation from the second plot of each figure is that at smaller free stream speed (12 m/s and larger C_μ) the pressure distributions on the suction side for 10° (Figure 1), 15° (Figure 3), 20° (Figure 5) and somewhat for 25° (Figure 6)

Figure 7 seem to be chaotic when there is no control. When control is applied, the chaotic situation is reduced or eliminated. This change in the profiles suggests that the actuation mechanism helps organizing the flow field for this particular situation of blockage.

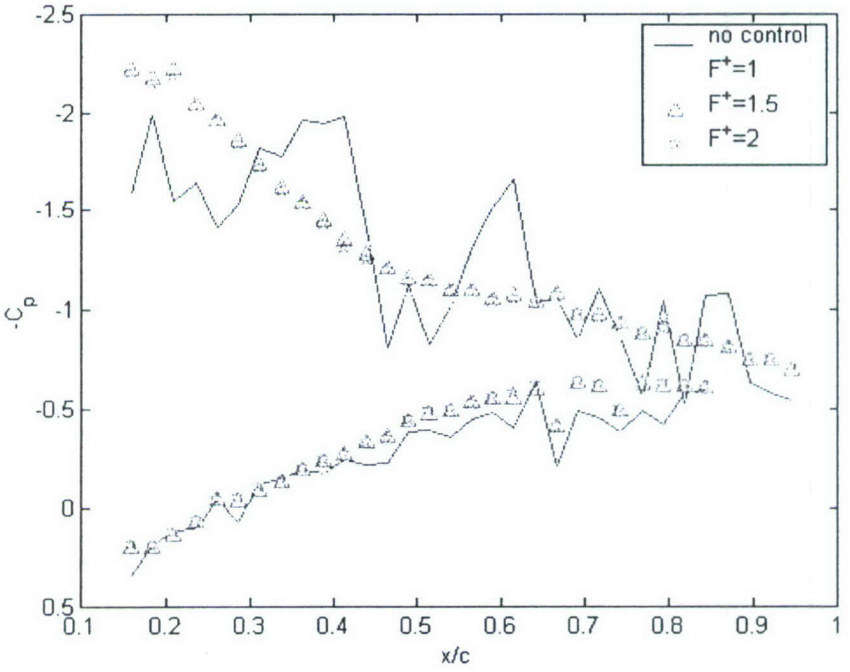

Figure 1: Averaged pressure distributions @ a=10° for Cμ=0.04

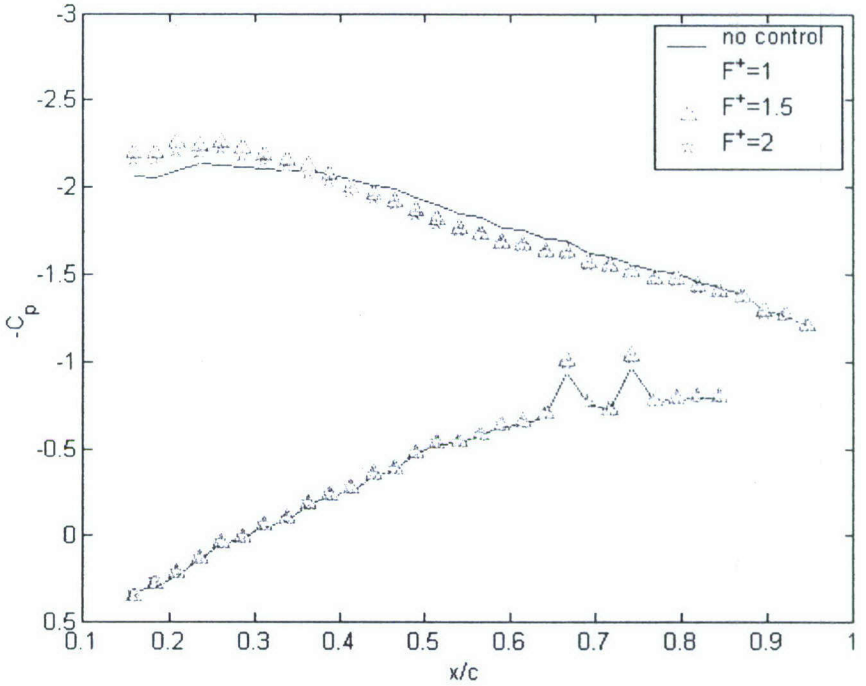

Figure 2: Averaged pressure distributions @ a=15° for Cμ=0.0171 for ESM wind tunnel.

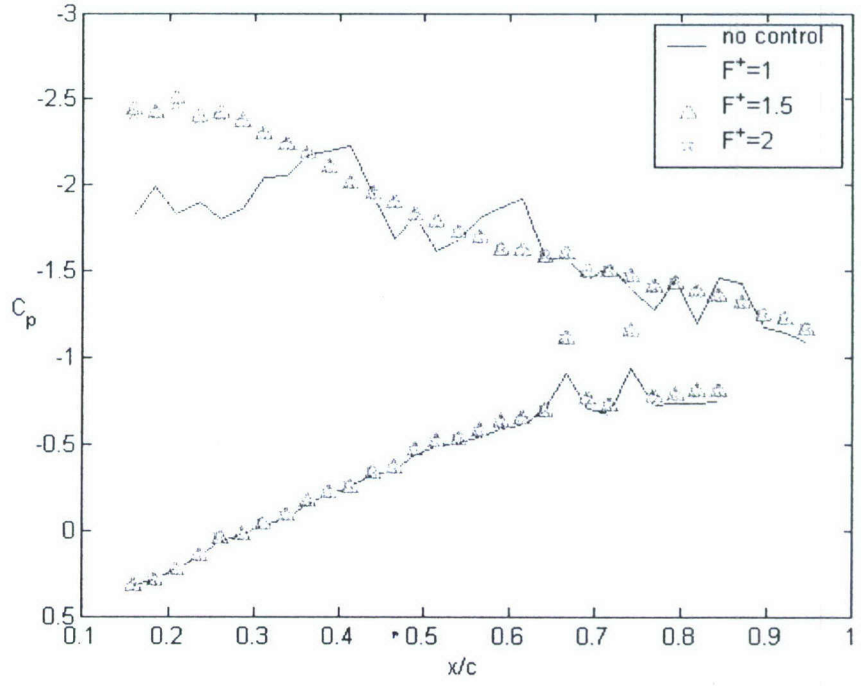

Figure 3: Averaged pressure distributions @ a=15° for Cμ=0.0285 for ESM wind tunnel.

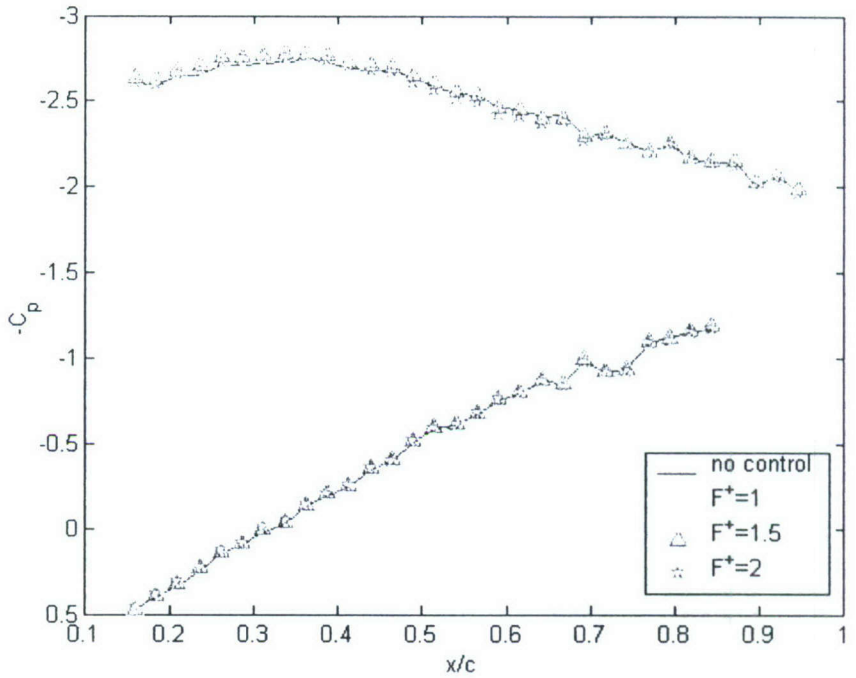

Figure 4: Averaged pressure distributions @ a=20° for Cμ=0.012991 for ESM wind tunnel

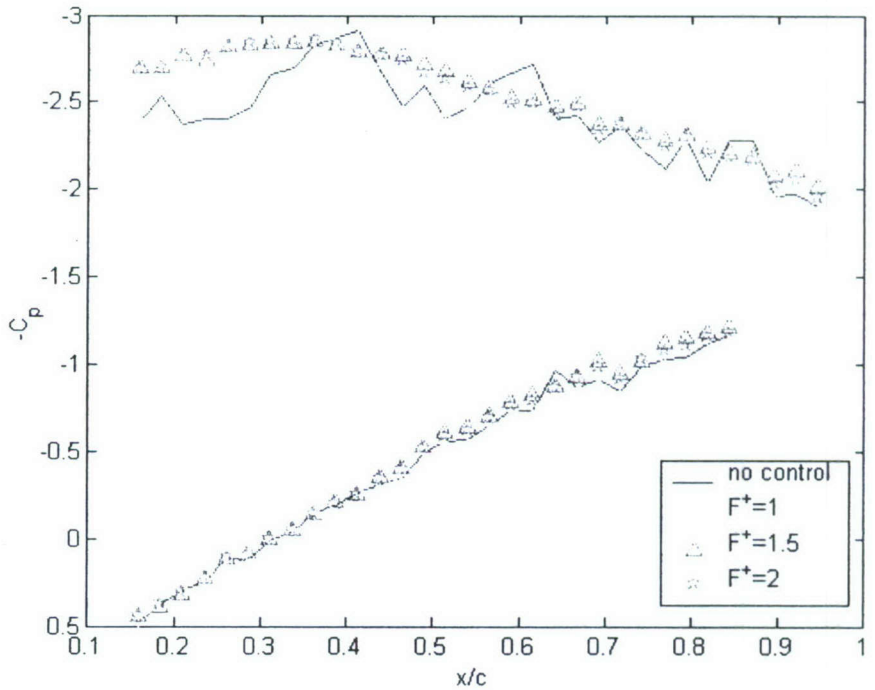

Figure 5: Averaged pressure distributions @ a=20° for Cμ=0.017321 for ESM wind tunnel

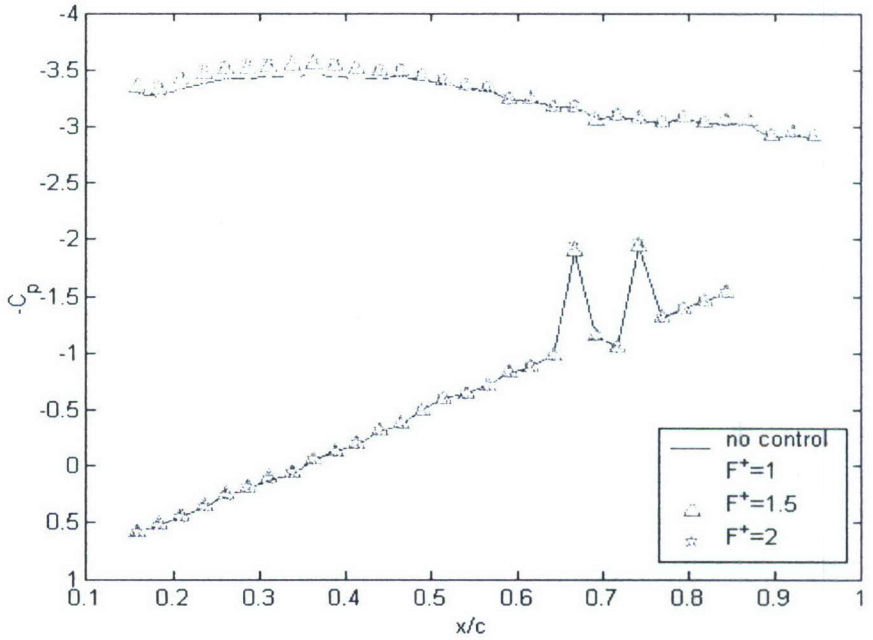

Figure 6: Averaged pressure distributions @ a=25° for Cμ=0.010513 for ESM wind tunnel

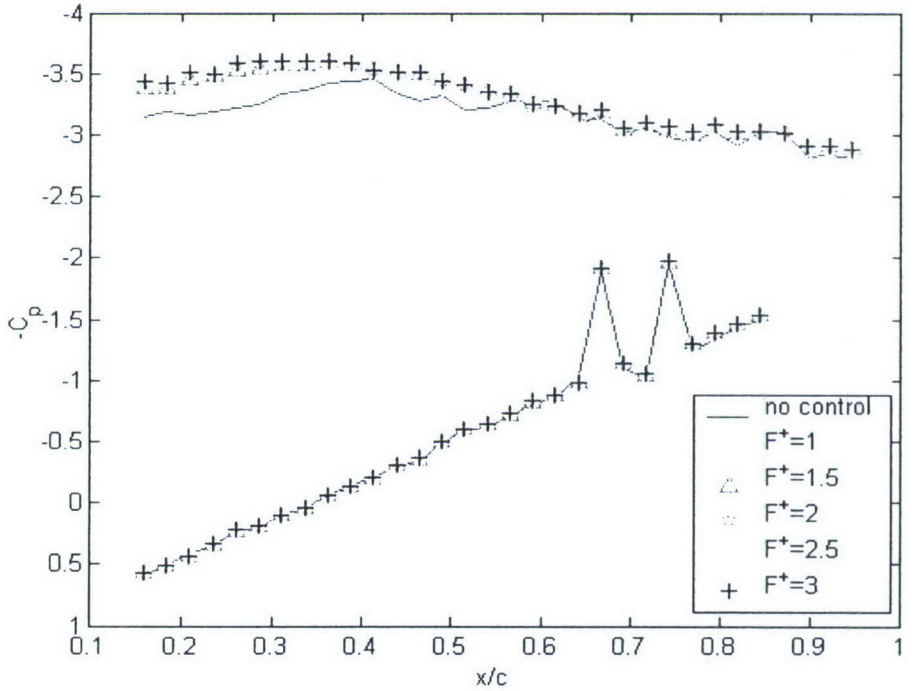

Figure 7: Averaged pressure distributions @ a=25° for Cμ=0.014018 for ESM wind tunnel

4.2 High Reynolds Number Tests

Tests were then carried out in the VA Tech Stability Wind Tunnel. In this tunnel, our model arrangement corresponds to a blockage coefficient 2.2% for an angle of attack of 21°. These tests can therefore simulate well the case of a wing in an infinite domain. The model was equipped with flat end plates to reduce as much as possible the end effects. This technique generates fields that are closer to two-dimensional motions than if the model were to be attached to the tunnel walls. The plates are better because boundary layers growing on the walls are thick and interact with the flow near the roots of the airfoil, giving rise to horseshoe vortices. Tests were carried out at angles of attack of 3° up to 21°, in increments of 3°. Also three different C_μ's were tried: 0.003, 0.01 and 0.03. Due to motor as well as air pressure supply limitations, the runs for the C_μ's were done at different tunnel speeds thus different Reynolds numbers. Figure 8 suggests that there is no Reynolds number dependence.

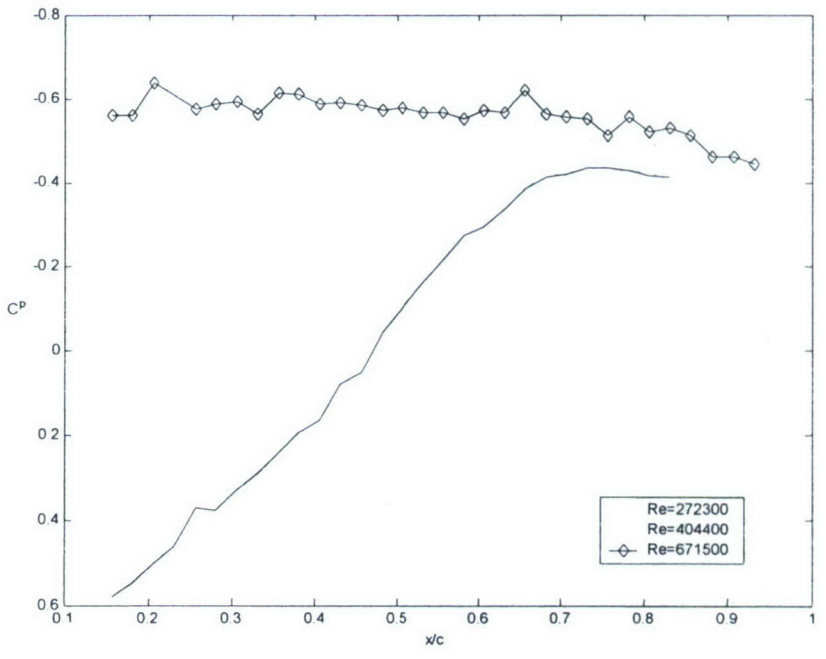

Figure 8: Averaged pressure distributions @ a=12° at different Reynolds number for the no control situation in the Stability wind tunnel.

Average pressure measurements for these angles of attack are shown in Figure 9 through Figure 15. For all these cases, the actuation frequency was set at the estimated

value of the natural shedding frequency. It should be emphasized that because it was very difficult to place pressure taps on the leading edge wedge, we were not able to obtain pressure data very near the leading edge of the wing. For $\alpha=3°$ (Figure 9), there is a peculiar sharp drop near the leading edge on the suction side. We believe that this is due to a separated bubble very near the leading edge. Our control mechanism is not very effective at $\alpha=3°$ and 6°, a behavior we expected, since the flow is attached over most of our relatively thick wing. However, the control actuation lowers the pressure levels in the very front of the airfoil, where the separation bubble resides. The actuation is not effective even at $\alpha=9°$, as shown in Figure 11. But at $\alpha=12°$ (Figure 12), we observe some significant departures from the no-control case. The comparison of the data of these two figures clearly indicates that the flow at $\alpha=9°$ displays the classical behavior of attached flow over airfoils. The suction pressure has its extreme values very near the leading edge. Suction is reduced as we move towards the trailing edge. But for $\alpha=12^0$, the no-control case indicates a flat pressure distribution on the suction side. This is clear indication that the flow is massively separated. And yet, much like the case of oscillating mini-flaps, unsteady blowing at the leading edge brings the pressure distributions closer to those of attached flow, namely, the pressure is lowered near the leading edge and rises near the trailing edge. This is deceiving, because the flow is separated. It is only in the average that the pressure distribution is similar to the distribution of attached flow. The effect is more pronounced with higher levels of C_μ. In Figure 13, Figure 14 and Figure 15 ,$\alpha=15°$, 18° and 21° respectively, the effect of flow control is not as large and in fact, it is progressively reduced as the angle of attack is increasing. It may be possible to achieve greater reductions on the suction pressure with larger values of C_μ, but due to limitations expressed before such tests could not be performed.

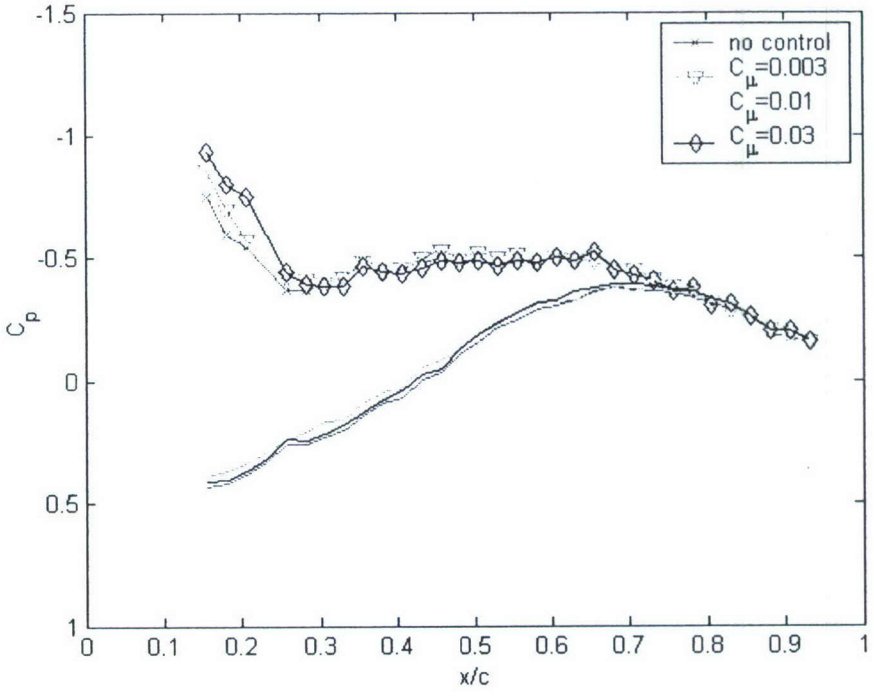

Figure 9: Averaged pressure distributions @ a=3° at Stability wind tunnel

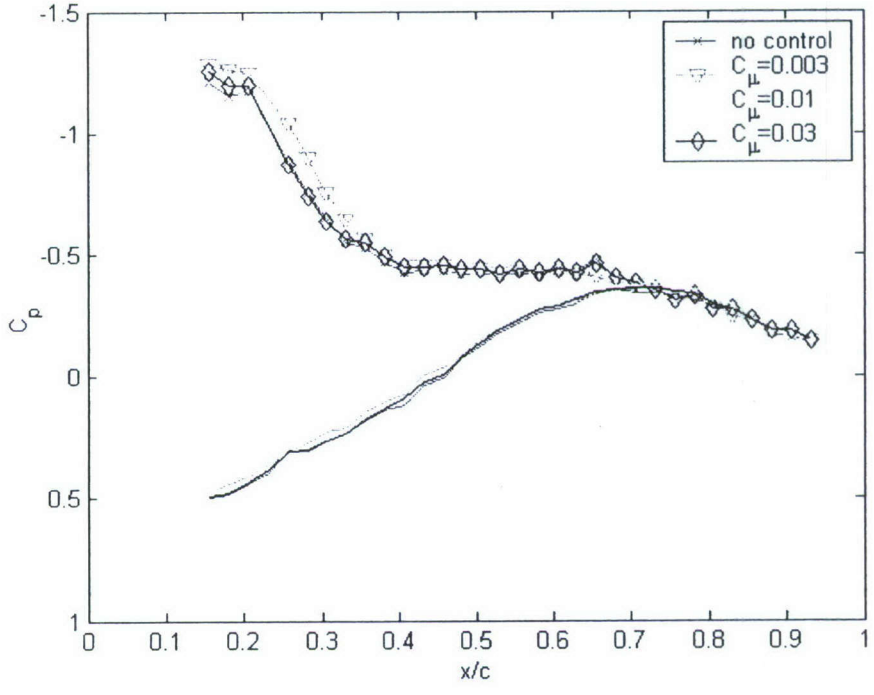

Figure 10: Averaged pressure distributions @ a=6° at Stability wind tunnel

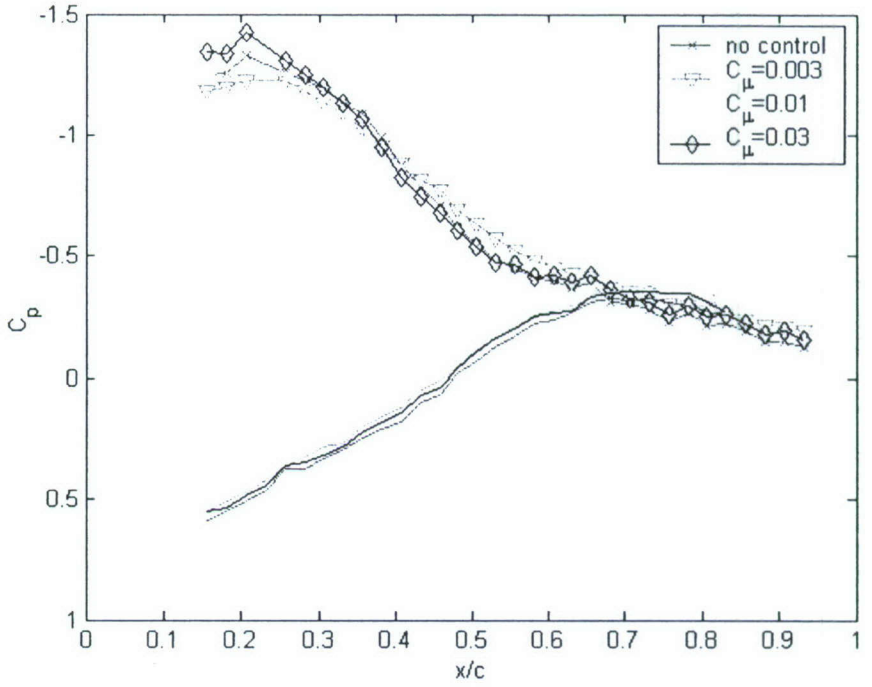

Figure 11: Averaged pressure distributions @ a=9° at Stability wind tunnel

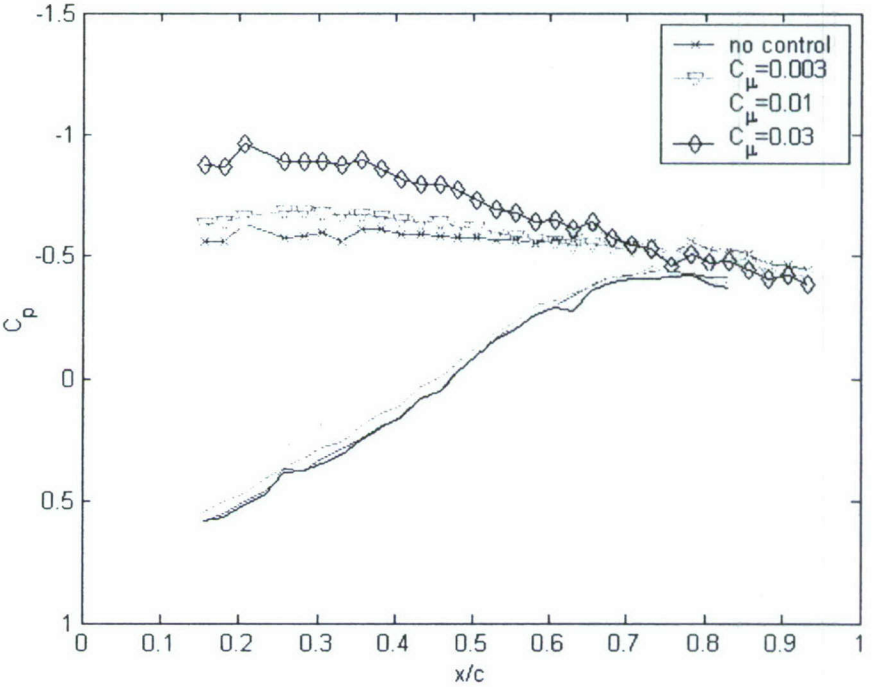

Figure 12: Averaged pressure distributions @ a=12° at Stability wind tunnel

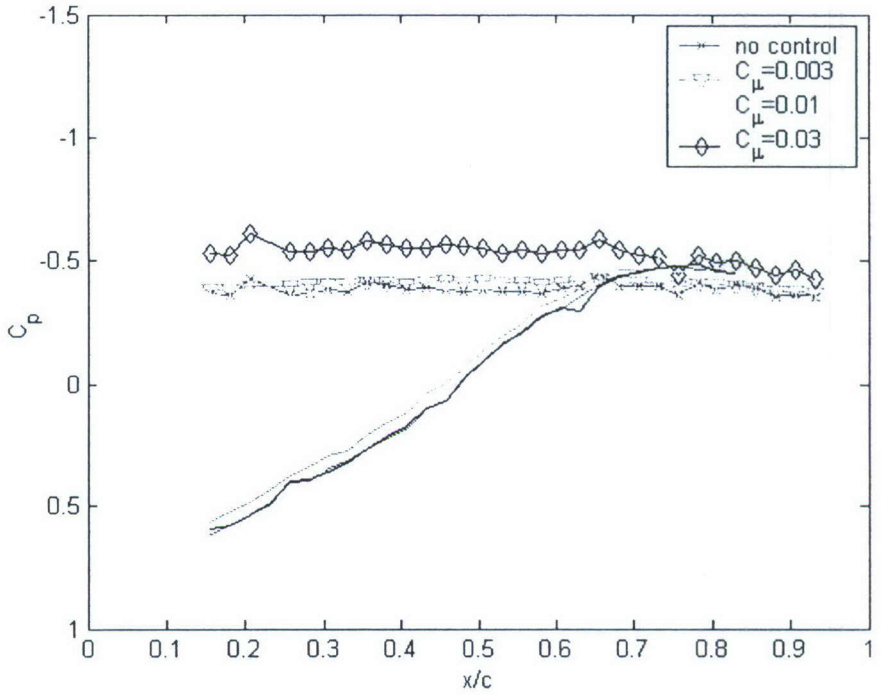

Figure 13: Averaged pressure distributions @ a=15° at Stability wind tunnel

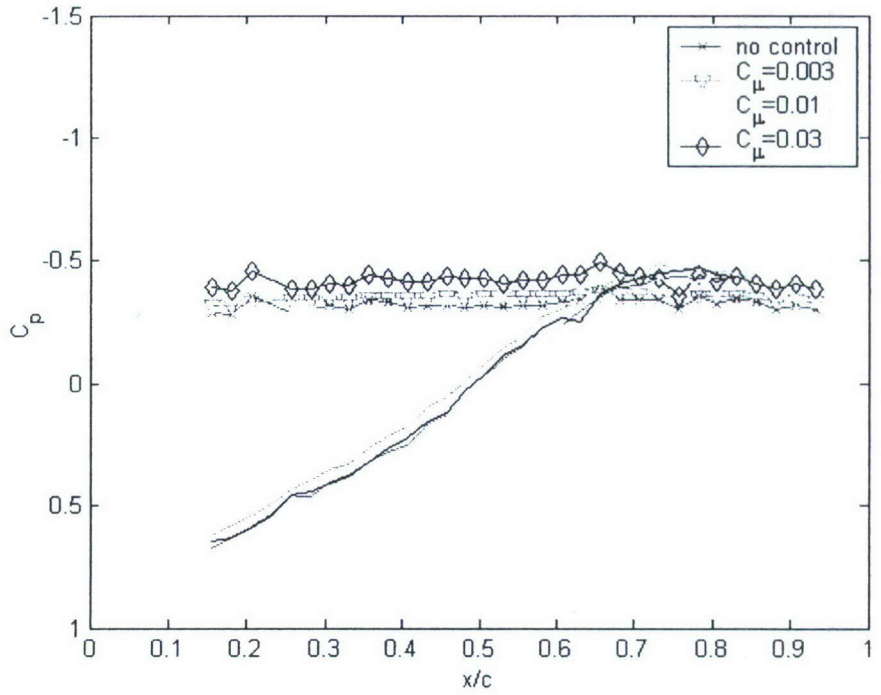

Figure 14: Averaged pressure distributions @ a=18° at Stability wind tunnel.

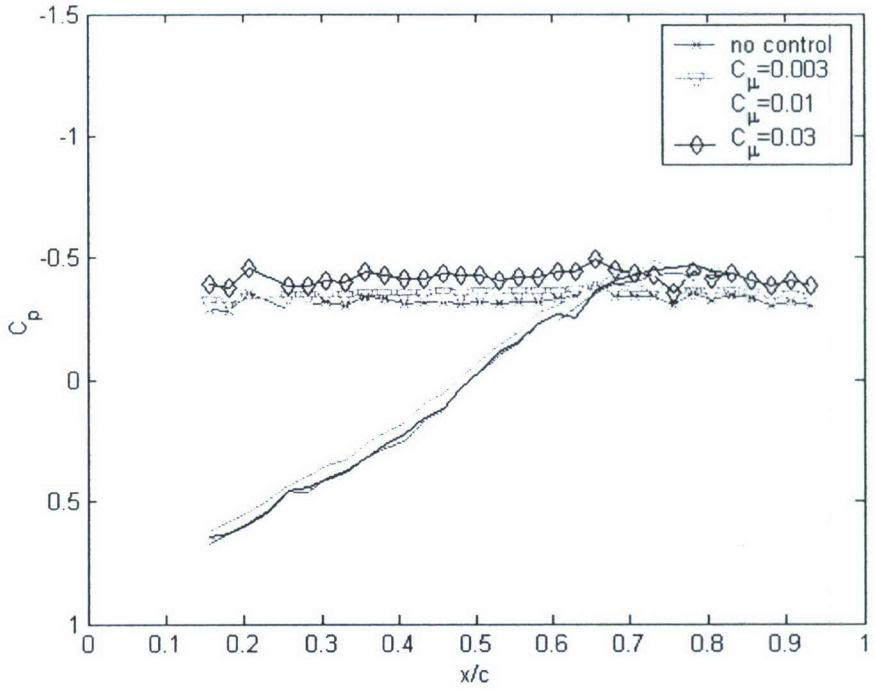

Figure 15: Averaged pressure distributions @ a=21° at Stability wind tunnel.

Lift coefficients were calculated by integrating the pressures over the suction and pressure sides of the wing. The results are presented in Table 1, for the three values of C_μ as well as no control. The benefit on the lift coefficient is large in the post stall area although it is reduced as is increased as seen in the last column, which is a comparison between the no control case and the control case with the highest C_μ. One of the reasons for this is that there were limitations in the actuating frequency. This suggests that even if it is not the natural frequency or one of its harmonics it is still possible to achieve some enhancement and increase the lift.

Table 1: Lift Coefficient C_L for conditions at Stability Tunnel

AOA	No control	C_μ = 0.003	C_μ= 0.01	C_μ= 0.03	Increase in C_L
3	0.4230	0.4150	0.4354	0.4458	5%
6	0.6420	0.6690	0.6277	0.6405	-0.23%
9	0.8410	0.8047	0.8046	0.8571	1.91%
12	0.5719	0.5905	0.6086	0.7344	28.41%
15	0.3881	0.3801	0.4131	0.5117	31.85%
18	0.3538	0.3424	0.3874	0.4395	24.22%
21	0.3618	0.3587	0.3884	0.4116	13.76%

The pattern previously discussed can be seen as well in Table 2, which describes the Lift to Drag ratio for the same conditions. Here the increase is not as pronounced as it is for the Lift coefficient. This indicates that the Drag is increasing as well. The vortex decreases the pressure over the surface but the force obtained is normal to the surface. When the angle of attack is increased the component of the normal force in the direction of the drag is increased as well and the lift component is reduced. This situation could be addressed by keeping the vortex closer to the front of the airfoil and detaching it farther from the trailing edge as the angle of attack is increased.

Table 2 : Lift-to-Drag ratio for conditions at Stability Tunnel

AOA	No control	C_μ = 0.003	C_μ= 0.01	C_μ= 0.03	Increase in C_L
3	7.2248	7.9616	8.0992	8.1356	12.6 %
6	9.3634	10.65213	9.2264	9.3714	2.8 %
9	7.5310	6.9529	7.1952	7.5868	0.74 %
12	3.0834	3.3201	3.1875	3.8473	24.77 %
15	2.1611	2.1575	2.1483	2.4982	15.60 %
18	1.8374	1.8156	1.8567	1.9781	7.65 %
21	1.6635	1.6381	1.6524	1.7168	3.20 %

It is emphasized that the data presented so far are averaged pressure distributions. Instantaneous pressure distributions over the wing at four specific instances are presented in Figure 16. These data provide evidence that large vortices are convected over the airfoil. In fact it is very possible that a dominant single vortex forms and convects, in the process inducing an imprint of a traveling wave of very low pressure. The first frame

shows a dominant peak at about 0.4, while the last shows a new one and the previous one close to the end. This gives an approximate speed of propagation of the wave of 5.6 m/s at a U_∞=10 m/s, since the chord is .4064 m. This speed also shows that the wave frequency is 13.75 Hz while the power spectrum at x/c=0.48 shows two dominant frequencies: 13.4 Hz and 26.8 Hz. This corroborates the earlier estimate of the propagation frequency. It is important to note that power spectrum of signals from other ports showed no dominant frequency on port 28 and above meaning that the vortex probably detached from the surface at x/c=0.85. These spectra also showed that no frequency is defined in the first 2 ports. This suggests that the vortex does not form until x/c=0.2 and that a strong vortex convects over 65% of the suction side.

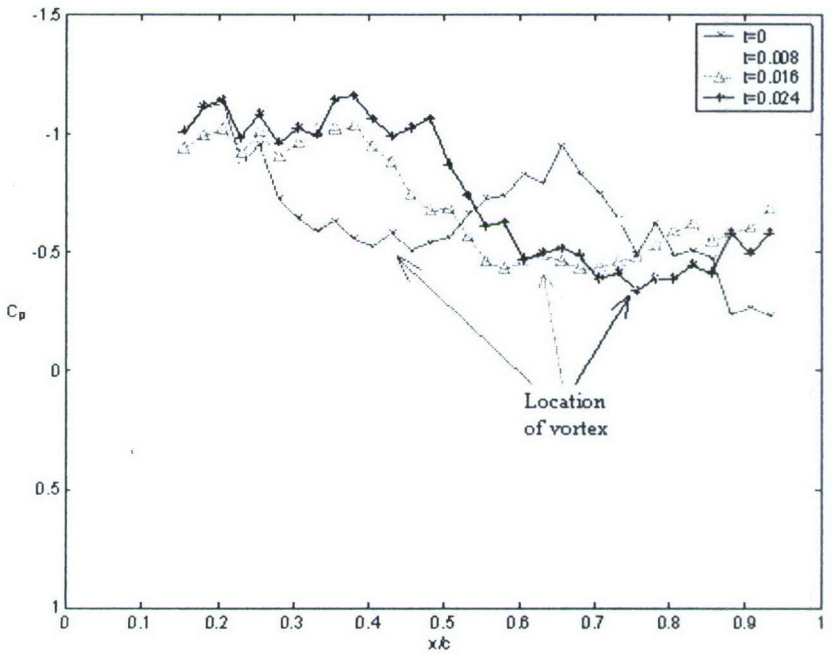

Figure 16: Wave propagation for α=12° with Cm=0.03

It is useful to compare the data of Cahil et al (1953) with the present results although just for reference since their thickness coefficient was 0.06 and the current one is 0.12. Cahil et al. experimented with a circular arc airfoil equipped with leading and trailing edge flaps. Similar flaps are employed by aircrafts like the F-22, in order to increase lift during take off and landing. It is therefore very appropriate to compare the effect of a large leading edge flap, to the effects of flow control. Figure 17 shows that there exist agreement for pressure distributions at $\alpha=6^{\circ}$. In both cases the flow field is nearly attached. Near the leading edge the pressure distribution indicates that a separation

bubble exists, effectively creating a virtual rounding of the leading edge. But at $\alpha=9^0$, the NACA data for no control indicates that the flow is fully separated, whereas the flow over our airfoil with no control appears to be still attached. This can be attributed to the wings' different thickness ratio. With only 6% thickness ratio the NACA airfoil is close to be a flat plate and thus at $\alpha=9^\circ$, the flow over such an airfoil is separated, displaying a nearly flat pressure distribution on the suction side. But with a thickness of 12% the flow over our airfoil stays attached. And for this reason, flow control does not provide any significant improvement. At $\alpha=12^0$ (Figure 19), the flow over the 12% airfoil is separated as well. But now, flow control influences the flow field and thus the pressure distribution. It seems that the actuator can provide the necessary instability for these types of airfoils.

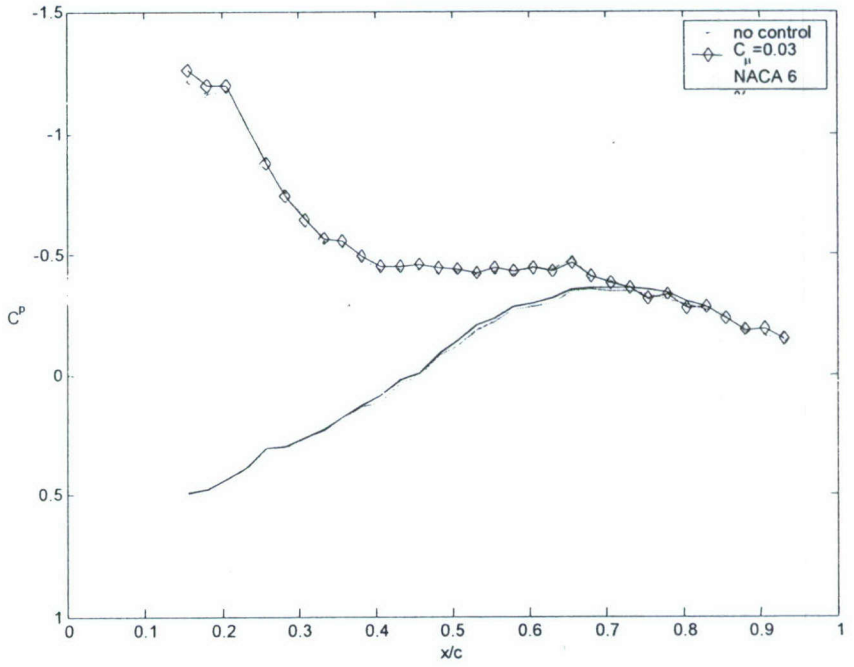

Figure 17: Comparison between NACA airfoil and Stability results @ a=6°

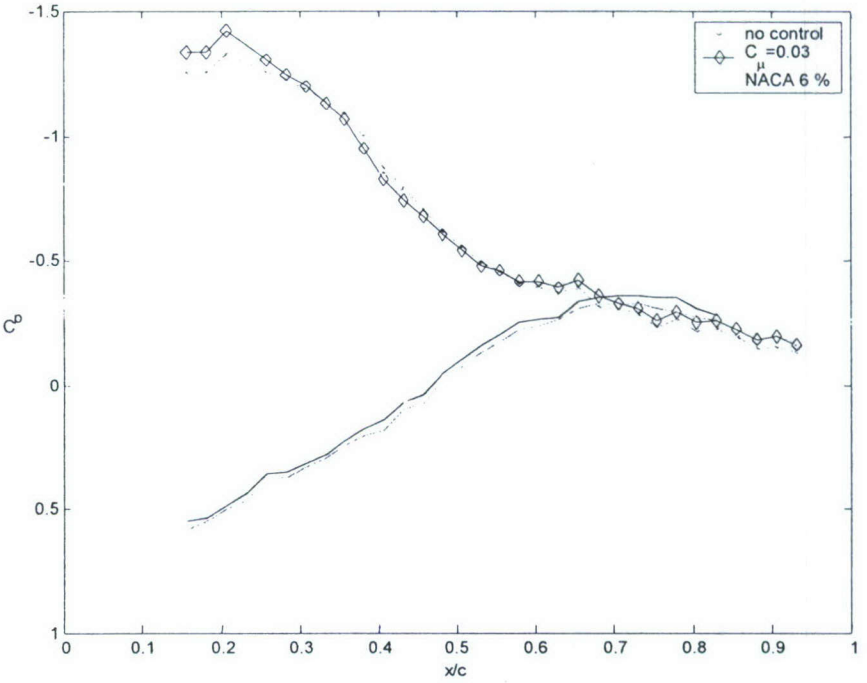

Figure 18: Comparison between NACA airfoil and Stability results @ a=9°

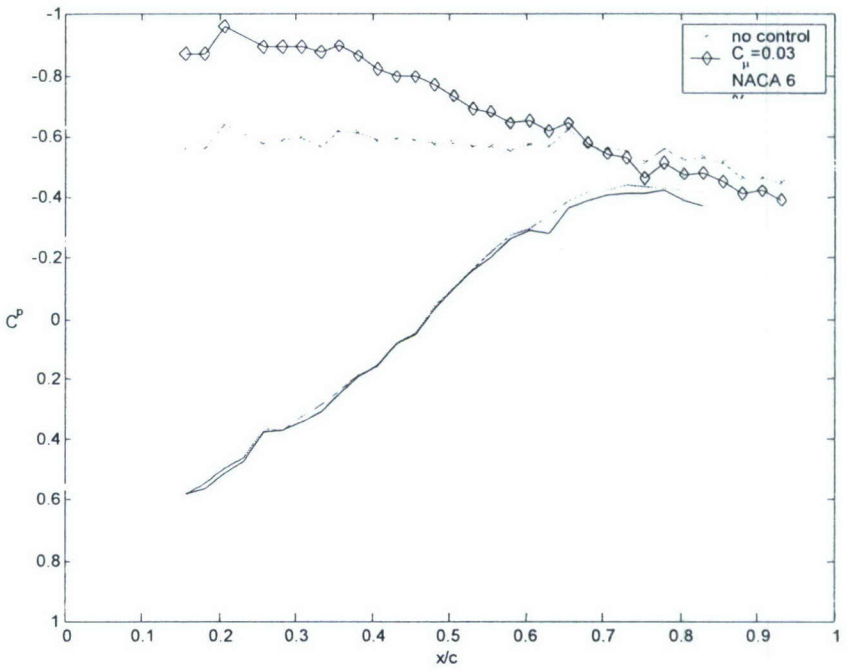

Figure 19: Comparison between NACA airfoil and Stability results @ a=12°

Finally, flow visualization over the entire airfoil was performed to document the global character of the flow. Time average streamlines and vorticity distributions are shown in Figure 20 for an α=15°, F+=1 and C_m=0.02. Observing the two cases, uncontrolled (left) and the controlled (right), there are no radical differences between them. For both cases the flow is attached after the mid-chord. This may be due to the thickness of the airfoil (15%). The suction vortex appears to be more coherent and concentrated in the controlled case. Also, the trailing edge vortex is stronger, more defined and closer to the airfoil for the controlled case. This suggests that the leading edge vortex is stronger and more defined, since the interaction of the two vortices will bring them closer, be energized by the other and initiate the alternate vortex shedding pattern.

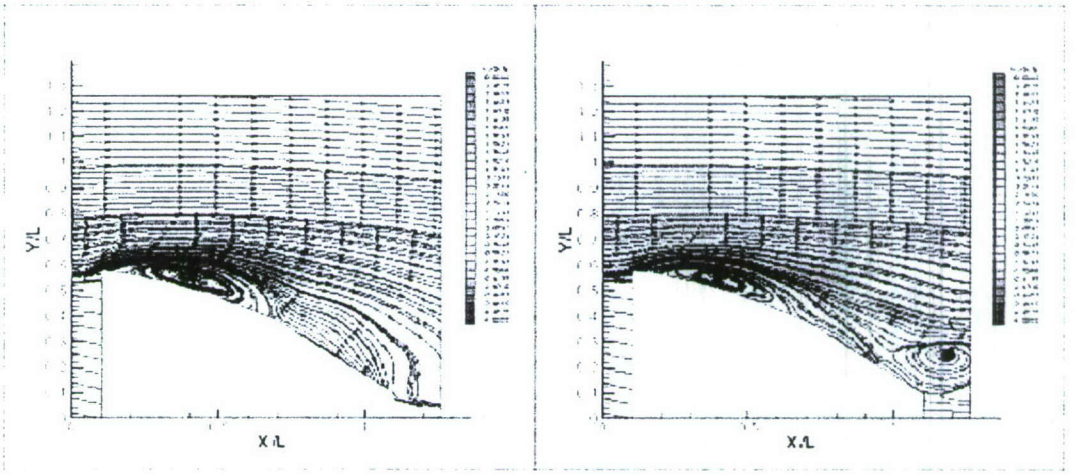

Figure 20: Time averaged streamlines and vorticity contours.
No control (left), control (right).

4.3 Conclusions

The purpose of this research was to develop a flow control mechanism that could generate a pulsing jet along a slotted nozzle to increase the lift of circular-arc airfoils. A novel pulsing jet actuator was designed and constructed. One of the features of this device is that it can generate oscillating disturbances without any mechanical parts like an oscillating flap, which could be detrimental to the radar signature of an airplane. Another feature is that the efficiency of this actuator is practically independent of the frequency. The design proved that uniform and more powerful pulsing jets could be generated along the span of the airfoil. In addition, this actuator did not generate nonlinear interactions

and therefore any secondary frequencies as synthetic jets tend to do. This means that the device is an excellent candidate for a robust flight actuator, where the required frequency is changing with aircraft speed and angle of attack.

The location and geometry of the jet exit revealed that the asymmetry of the walls induces the formation of a starting vortex. This vortex provides a significant vectoring effect that guides the disturbance in the direction of the leading edge free shear layer. Moreover, this vortex interacts with the leading edge shear layer, exciting its natural instabilities and thus forcing the shear layer to roll, forming a strong coherent vortex.

Finally, we demonstrated for the first time, that unsteady blowing right at the leading edge of a sharp-edged circular arc airfoil allows the management of the separated flow, leading to averaged pressure distributions that correspond to higher lift. This was shown to be due to convecting vortices, as detected in the form of a low pressure traveling wave.

4.4 Conclusions

Significant improvement was obtained in the lift coefficient for moderate to high angles of attack. But the effect decreased as the angle of attack was further increased, possibly due to less effective interaction between the disturbance and the shear layer. The data obtained with unsteady blowing indicate that there is a minimum of energy needed in order to exert a proper disturbance to the shear layer. In addition, the research suggests that the harmonics of the natural shedding frequency can have even greater impact than the natural frequency. Finally, the actuating frequency did not have to match the natural frequency since resonance was still achieved when locked to higher actuating frequencies.

4.5 References

Cahill, J. F., Underwood, W.J., Nuber, R.J., Cheesman, G.A., (1953). "Aerodynamics forces on symmetrical circular-arc airfoils with plain leading-edge and plain trailing-edge flaps" NACA Report 1146

Pope, A., Barlow, J.B., Rae, W.H., *Low speed wind tunnel testing*, 3rd ed. p.353-356.

5 THE AERODYNAMICS OF MODERATELY-SWEPT WINGS

Wings swept by 30 to 40 degrees are today very common in fighter aircraft. And yet, there is very little work devoted to the understanding of the aerodynamics of such wings. The problem is that such wings may be able to sustain attached flow behind broken down delta wing vortices, or stall like two-dimensional wings while shedding vortices with generators parallel to their leading edge. In this report, we explore the aerodynamics of swept wings. We present velocity and vorticity distributions along planes normal and parallel to the free stream for a wing with a trapezoidal planform and sharp leading edges. We also present pressure distributions over the suction side of the wing.

5.1 Introduction

At very low sweep angles, namely angles less than 20^0, the flow over sharp-edged wings stalls like the flow over an an unswept wing. Vortices are shed with their axis nearly normal to the free stream. Such vortices are often called "rollers". At high sweep angles, that is larger than 50^0, the flow is similar to delta wing flows that are dominated by leading edge vortices (LEV). We will refer to these vortices here as "streamers". These wings stall due to vortex breakdown.

The effects of sweeping a wing at moderate angles, namely 30^0 to 40^0, and moderate to high angles of attack are very little understood. And yet, such wings are today the norm for most fighter aircraft. The problem is that in this range of parameters, the flow may stall like the flow over an unswept wing, shedding large vortices in an unsteady fashion, or it could stall like a delta wing, sustaining a leading-edge vortex (LEV) that breaks down. The significant difference between the two modes is that delta wing vortices, or streamers, are attached to the leading edge of the wing and shed vorticity by directing it in the core of the vortex and then telescoping it downstream, whereas rollers, grow and

then shed by rolling over the wing and detaching from its surface. This is essentially the phenomenon of unsteady stall.

It is imperative that we understand the basic aerodynamics of these phenomena, before we attempt to control them at high Reynolds numbers. To this end, we have been conducting flow visualizations and PIV measurements at both low and high Reynolds numbers. We found that both stalling modes are possible on a planform with a sweep angle of 40^0. But even with what appears like two-dimensional stall, there is some recirculation in planes normal to the free stream that appears like LEV. We therefore conclude that there is indeed a hybrid mode of stalling. The exciting implication is that with flow control, we should be able to dictate the mode of stalling and therefore the effectiveness of flow control.

Research on delta wing flows for sweep angles as low as 50^0 indicate that delta wing vortices are present but break down very close to the leading edge[1-5]. In fact even before break down, these vortices display wake-like flow where the velocity is very low in the core of the vortex. In some cases[2] it was found that the low aspect ratio wing at medium angles of attack does not behave like a delta wing but rather like an unswept wing. A sweep angle of 50^0 is not low enough to demonstrate the transition from the vortex breakdown stall to the two-dimensional unsteady stall. More recently, Yaniktepe and Rockwell[6] studied the flow over a wing with a sweep angle of 38.7^0. They provided evidence that up to an angle of attack, α of 25^0, the flow appears to be dominated by delta wing tip vortices. At the highest angle of attack, the vortices seem to be displaced inboard.

In both the studies of Ol and Gharib[2] and Yaniktepe and Rockwell[6], the flow field was interrogated along planes normal to the free steam. In our studies we cut the fields with planes that are both normal and parallel to the free stream. We are interested in the possibility that the control mechanisms could actually dictate the desired stall mechanism. We provide evidence that our wing stalls by shedding rollers.

Impressive advancements have been made in controlling the flow over wings with rounded leading edges, but very little work has been devoted to the control of the flow over sharp-edged wings. The present authors[7,8] have demonstrated that flows over sharp edges can be effectively controlled with lift increases as high as 70%. Control of delta

wing flows has been successful but the efforts were focused so far for relatively high sweep angles[9-11]. The objective of this project is to capitalize on our experience and extend the work to moderately swept wings and wings with practical planforms.

The majority of contributions on airfoil flow control are based on separation control. Their aim is to delay separation and stall altogether. There is another area of airfoil and wing flow control, which so far has received little attention but which has greater potential in defense applications. This is the management and control of separated flow. Such flows are encountered over sharp-edged wings at low to moderate angles of attack or over wings in deep stall. The idea is to accept the fact that in some situations, the flow is fully separated, and periodic shedding of vortices is established. The aim then becomes to control the dynamic development of vortical structures in order to improve the performance of the lifting surface. These are the type of flows that develop over wings moderately swept and the focus of the present research.

We discuss in this paper the results of experiments conducted in a water tunnel and a wind tunnel with a trapezoidal planform wing model typical of wings used in industry. These models were tested at low and moderate Reynolds numbers, namely Re=42,000 and 1,200,000. In the water tunnel we employ Digital Particle Image Velocimetry (DPIV). For wind tunnel testing, we assembled the hardware that allows us to test large stainless steel models. We have also developed seven-hole probe measurement techniques that return sectional circulation values and vorticity distributions that will allow us to confirm the effectiveness of flow control.

5.2 Facilities, Models and Equipment

Facilities and Models

Experiments were carried out in the Engineering Science and Mechanics (ESM) water tunnel and in the VA Tech Stability Wind Tunnel. The ESM Water Tunnel was built by Engineering Laboratory Design (ELD) and operates in a closed loop in a vertical plane with up to 2,500 gallons of water. The settling chamber leads to the 24" x 24" x 72" Plexiglas test section via a three-way convergence. A 4500-gpm pump driven by a 20-hp motor provides flow which can attain a maximum speed of 1 m/s, corresponding to a maximum Reynolds number per unit length of 9900/cm. The free stream turbulence level

in the test section is less than 2%. The Virginia Tech Stability wind tunnel is a continuous, closed-loop subsonic wind tunnel. The tunnel fan is 14-foot (4.27m) in diameter and is driven by a 600 hp motor. The maximum achievable flow speed is 275 ft/s (83.8 m/s) in a 6'X6'X25' (1.83m×1.83m×7.62m) test section. The settling chamber has a contraction ratio of 9 to 1 and is equipped with anti-turbulence screens. This combination provides an extremely smooth flow in the test section. The turbulence level varies from 0.018% to 0.5% and flow angularities are limited to 2° maximum.

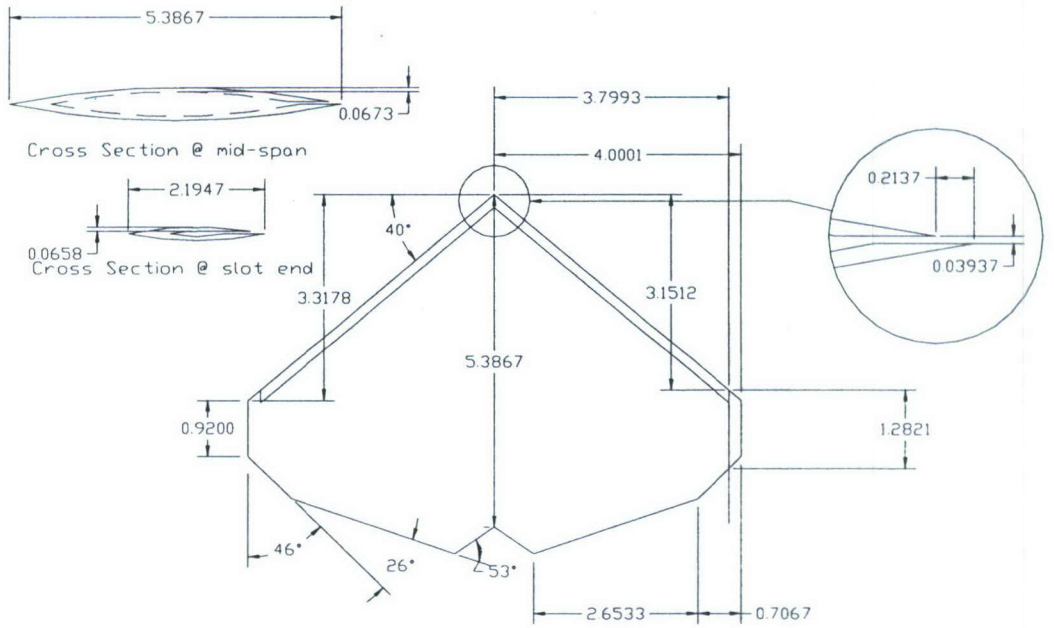

Figure 1. Engineering drawing of the trapezoidal planform model for water tunnel testing.

The model for this experimental investigation has a trapezoidal planform shown in Fig. 1. In this Figure the dimensions, in inches, correspond to a small model designed for testing in the water tunnel. This model is equipped with an internal compartment that can generate a pulsing jet in the leading edge for flow control. Lockheed Martin, a co-sponsor of this effort has availed to us a large, 2.5-feet-span, stainless steel model, equipped with pressure taps. This model is geometrically similar to the model shown in Fig. 1. Pressure taps are distributed along lines parallel to the root of the wing at distances z/c= 0.063, 0.1508, 0.2424, 0.3339, 0.4061, 0.4588, 0.5115, 0.5641, 0.6238, and 0.6904. Along the axial direction the distribution of pressure ports varies with the span. There are 17 next to the root and nine near the tip. The model is mounted on a sting that permits changes of

the angle of attack while keeping the aerodynamic center of the wing at the same elevation in the test section. The wing mounted on the sting is shown in Fig. 2. Short splitter plates were mounted along the root of its wing, to simulate the fuselage, or a plane of symmetry. This aerodynamic conditions are not the same with those imposed along the plane z=0 of the wing model shown in Fig. 1, nor are they equivalent to the conditions imposed by a fuselage model. We will estimate these effects by comparing with data obtained earlier with a full model that includes the fuselage.

Particle Image Velocimetry

Particle-Image Velocimetry (PIV) is a powerful tool that we employ. The most common implementation of the method, (currently commercially available) focuses on a single-exposure double-frame digital cross correlation approach. A high-resolution (1Kx1K pixels) CDD camera that can sample up to 30 fps, results in a sampling frequency of the flow field of only 15Hz, is usually synchronized with a Nd:YAG pulsing laser that illuminates the interrogation area. The velocity field is traditionally treated as a linear transfer function that corresponds to a flow pattern displacement between two consecutive images. This transfer function is revealed in a statistical manner incorporating second order statistical moments of the image patterns (Westerweel[13,14]).

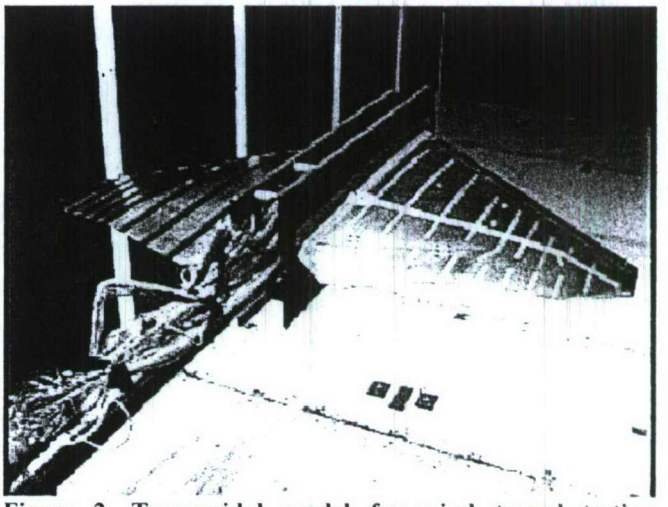

Figure 2. Trapezoidal model for wind tunnel testing mounted on sting

A major disadvantage of this approach is the inability to provide sufficient frequency resolution, which is necessary, in order to investigate any high-frequency phenomena that occur in turbulent, separated flows. A system developed by the authors at VA Tech has overcome the difficulty of low sampling frequency. This was accomplished with the integration of a high-power (50 W) pulsing laser with special type of optics and a unique CMOS, capable of acquiring up to 1000 frames per sec (fps) resulting to a DPIV system with 1 KHz maximum sampling frequency[15]. To our knowledge, there are no results

published in the open literature that employ high-speed CMOS technology cameras to perform DPIV measurements. Our ongoing research to integrate this technology with our existing PIV system demonstrated very high sensitivity, equivalent to 1000 ASA, and signal-to-noise ratio in the order to 100,000:1. The great advantage of this new technology is that each pixel is treated as an individual sensor and any cross-coupled interaction between neighborhood pixels is eliminated. The conditioning of the signal is performed on the sensor. Thus, the spatial and temporal resolution of our PIV system is increased by almost an order of magnitude in comparison with our previous configuration, and two orders of magnitude compared with systems that are commercially available.

Members of our group were able to perform dual-frame cross-correlation time-resolved DPIV by employing single and multiple exposures. The first example of single-exposure double frame cross-correlation time resolved DPIV was presented by Vlachos et al.[15]. However this implementation was limited to very low-speed liquid flows (U~10 cm/s). In a different approach, we performed multiple exposures per frame and we evaluated the vectors using standard cross-correlation. This approach was employed in the analysis of the characteristics of turbulent shear layers by Vlachos et al.[16] and in the investigation of the post-vortex-breakdown region characteristics of delta wings by Klute et al.[17].

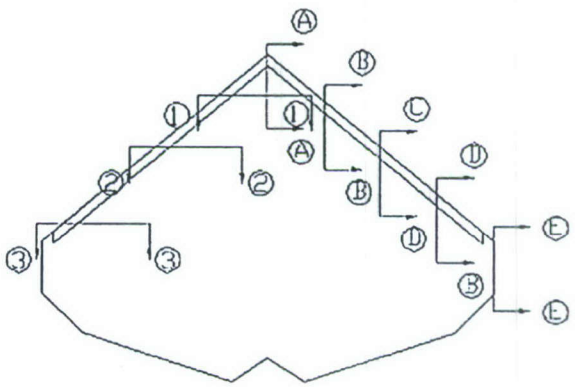

Figure 3. Laser cuts for the water tunnel flow visualization and PIV.

One major drawback of conventional DPIV systems results from limitations inherited from the velocity evaluation methods. Our group recently launched an effort to integrate and combine some of the most effective and well established of these proposed methods[18]. The outcome is a dynamically adaptive hybrid algorithm for the evaluation of the velocity vectors that overcomes these limitations to a great extent, thus increasing accuracy and space resolution. The overall performance of the method, if quantified,

yields space resolution in the order of 0.5 mm average, time resolution in the order 1milisec with sampling time up to 4secs and uncertainty of the velocity measurement in the order of 0.1% of the reference velocity.

The advancements in this effort are employed in the global characterization of the separated flow over the sharp airfoil, providing insight on the interaction of the shear layers with the incident free stream and their roll-up to coherent vortices. These data will be used to analyze the flow control mechanism, providing spatio-temporal correlations, information about the interaction of the various frequency modes in the flow field and the route to the formation of coherent structures in the separated flow region. Data were obtained along laser cuts as shown in Fig. 3. Cuts A, B, C, D and E are parallel to the free stream, while cuts 1,2 and 3 are normal to the free stream. These cuts are located along z/c= 0,01,038,057 and 077 and x/c=0.1856, 0.3712 and 0.5568, respectively.

5.3 Sensors and Actuators

Pressure scanners are employed to monitor the pressure distribution over the wing. ESP scanners by Pressure Systems Inc. are used. Two 32-channel ESPs are employed to monitor the pressure distribution along ten spanwise stations of the wing over the suction side and seven stations over the pressure side. A calibrated 5-hole embedded sensor probe, produced by the Aeroprobe Corporation was used to take velocity measurements in the wake of the wings. The probe can measure the three components of the velocity as well as static and dynamic pressure with a frequency response of well over 1000 Hz. The probe was mounted to a two-axis motorized traversing system and placed at the model's trailing edge.

The ability to demonstrate vortex shedding lock-on control for a closed-loop, adaptive wing configuration will rely on robust sensing and actuation schemes which are realizable for a full-scale aircraft. An equally important consideration is the design and demonstration of feasible closed-loop control algorithms that can affix the shear layer excitation at the sensed vortex shedding frequency for constant and changing airspeeds.

5.4 Results and Discussion

A. Flow Visualization and PIV Results

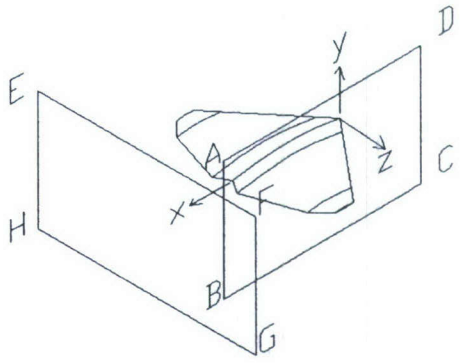

Figure 4. Schematic of planes of data

The velocity field over the airfoil was explored in water tunnel tests using flow visualization and Time-Resolved DPIV. These data were processed using an in-house developed multi-grid iterative DPIV, with second-order, Discrete Window Offset (DWO). Time-resolved DPIV systems are limited by the fact that the time separation between consecutive frames is the reciprocal of the frame rate, thus on the order of milliseconds. This value is relatively large compared with microsecond time-intervals employed by conventional DPIV systems. By employing a second-order DWO we provide an improved predictor for the particle pattern matching between subsequent iterations. Moreover, the algorithm employed performs a localized cross-correlation, which, when compared to standard multi-grid schemes for resolving strong vortical flows was proven to be superior.

For both flow visualizations and PIV measurements, we cut the field by laser sheets parallel and perpendicular to the free stream as shown schematically in Fig. 4. We have data for four angles of attack along the eight planes marked in Fig. 3. Our flow visualization on a Trefftz plane, namely plane EFGH shown in Fig. 5 indicates results very similar to those of Yaniktepe and Rockwell[6], which imply that the flow develops leading edge vortices. We found that such visualizations could be deceiving. For the same configuration, cutting the flow by a plane parallel to the free stream essentially passes a section through a LEV. Leading edge vortices have a nearly circular cross-section if they are cut normal to their axis. But if cut by a plane inclined with respect to their axis, they should show vorticity of the same sign along a closed and nearly elliptical contour. Moreover, the velocity component along the axis of a LEV should be jet-like. The PIV data along a plane parallel to the flow shown in Fig. 6 are void of such characteristics. Instead they indicate vorticity only on the upper side, which is compatible

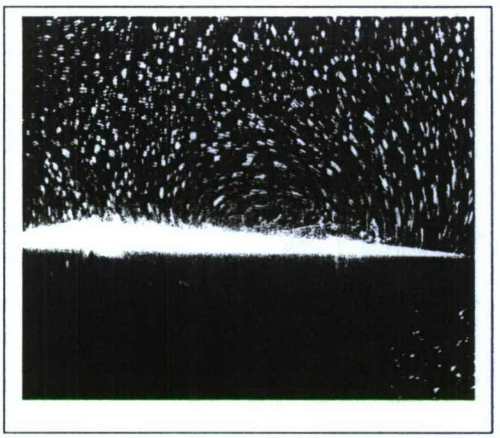

Figure 5. Flow visualization along a Trefftz plane.

with two-D stall. The axial velocity distribution indicates wake-like behavior, which confirms the fact that we have two-D stall. A detail of this flow is shown in Fig. 7.

In Figs. 8 through 10 we present data along planes parallel to the free stream along different spanwise directions, as shown in Fig.3 and indicated in the caption of the frames. The planform of the wing was added in a perspective way to help visualizing the location of the planes of data. In this and the following figures we present a very small portion of the actual number of data, to avoid cluttering the images. But quantities like vorticity have been calculated using all data along the full grid. If a delta wing vortex were present at these locations, then our planes would have cut across them and would have indicated a closed loop of vorticity. These data therefore indicate that the flow separates in the form of rollers. Note that near the root of the wing, the separated region tends to close near the trailing edge, whereas further outboard, the wakes are open. It should be emphasized that these are averaged fields. Our instantaneous frames indicate that the flow field involves the rolling and shedding of rollers.

In Figs. 11 through 14 we present data obtained along planes normal to the oncoming stream, namely planes 1,2 and 3 which are positioned at x/c=0.1856, x/c=0.3712 and x/c=0.5568, respectively. These correspond to the flow visualization of Fig. 4. The data indicate some recirculation that is reminiscent of delta wing vortices. However, vorticity distributions point to the opposite direction. The fact again that vorticity is present only on the top of the domain of recirculation, implies that these planes only cut free shear layers that delineate a separated region.

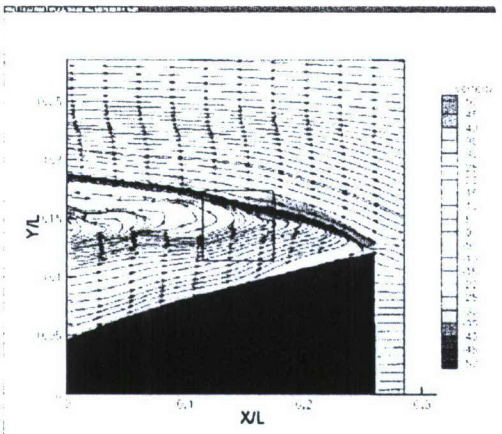

Figure 6. Streamlines and vorticity contours over the wing obtained along a plane parallel to the stream halfway outboard.

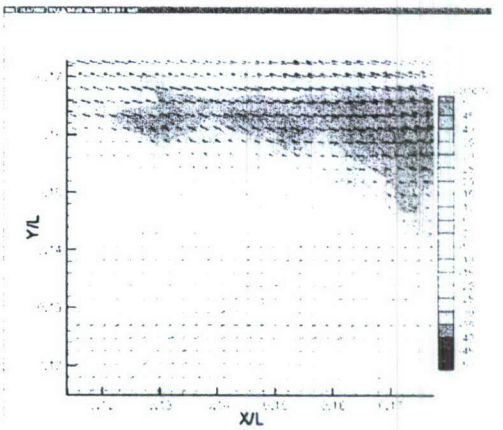

Figure 7. Detail of field of Fig. 6 contained in the rectangular frame shown there.

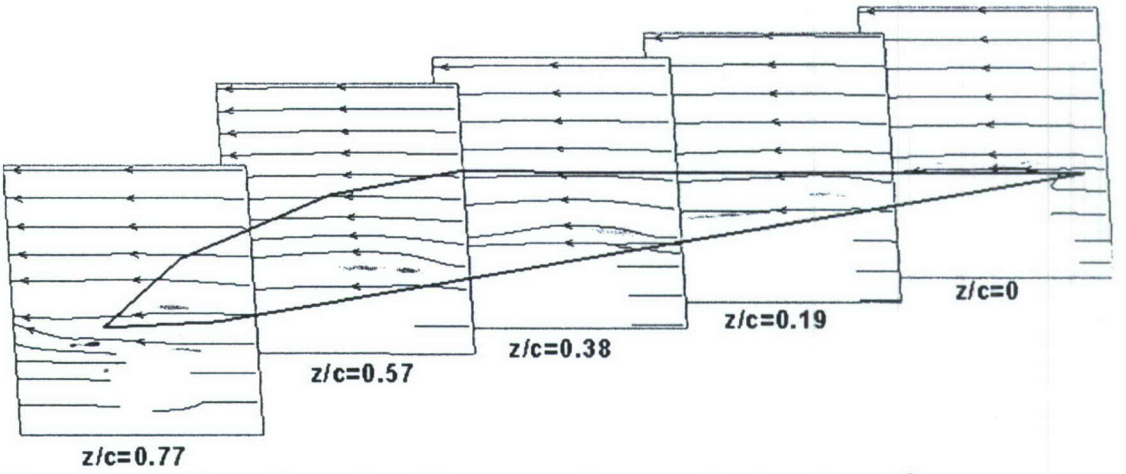

Figure 8. Streamlines and vorticity contours along spanwise planes for $\alpha = 7^0$.

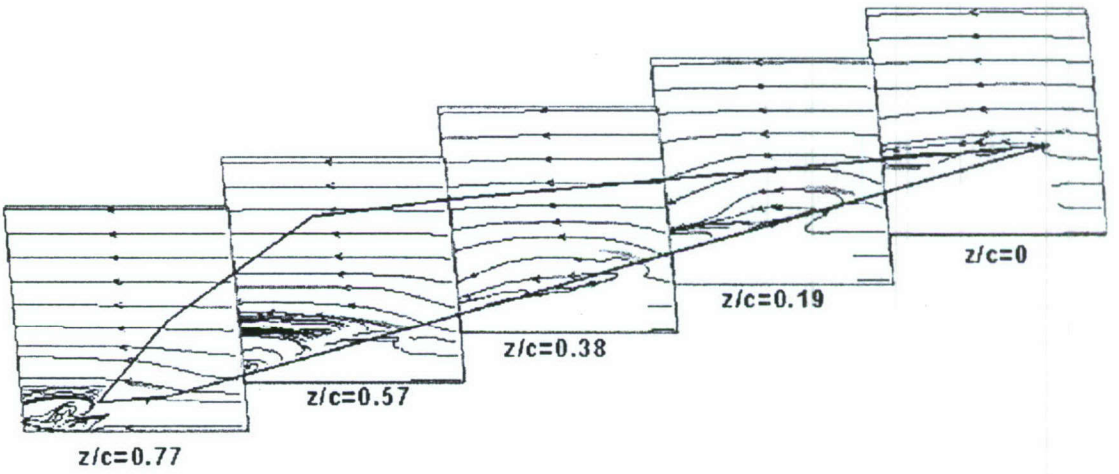

Figure 9. Streamlines and vorticity contours along spanwise planes for $\alpha = 13^0$.

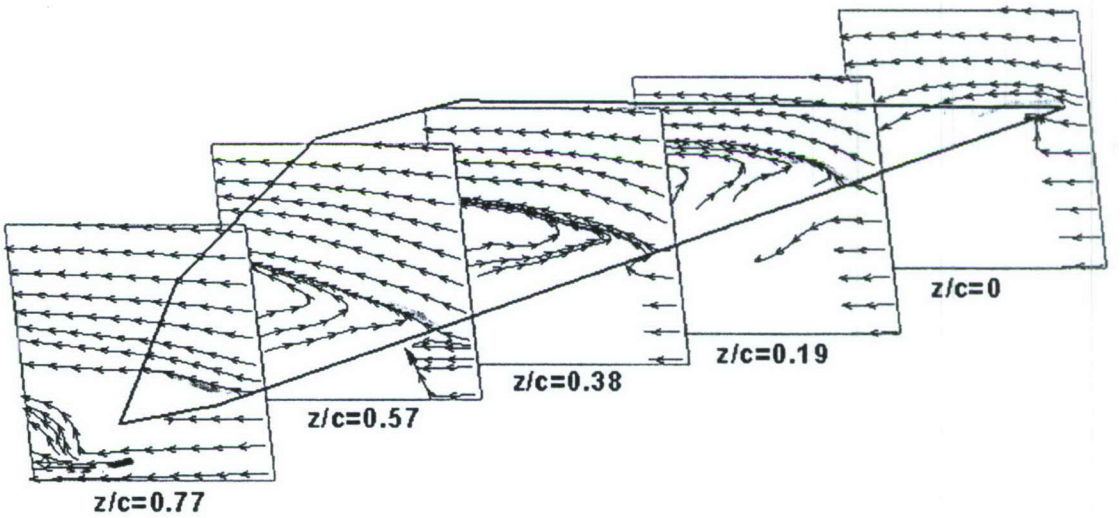

Fig. 10 Streamlines and vorticity contours along spanwise planes for $\alpha = 25^0$.

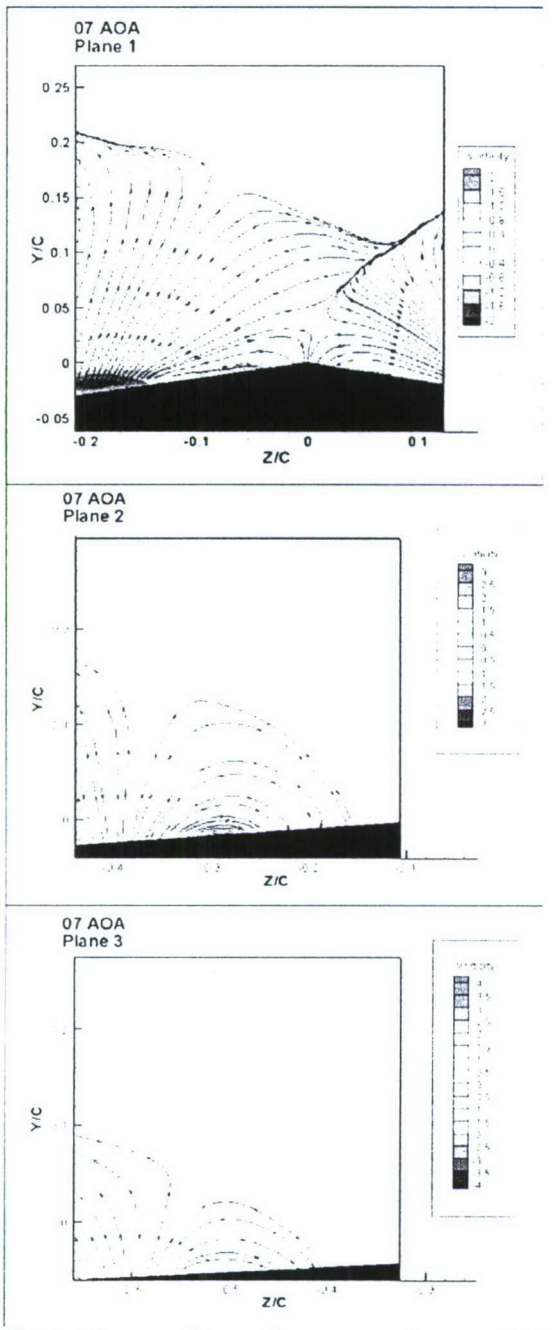

Figure 11. Streamlines and vorticity contours along Trefftz planes for $\alpha=7^0$.

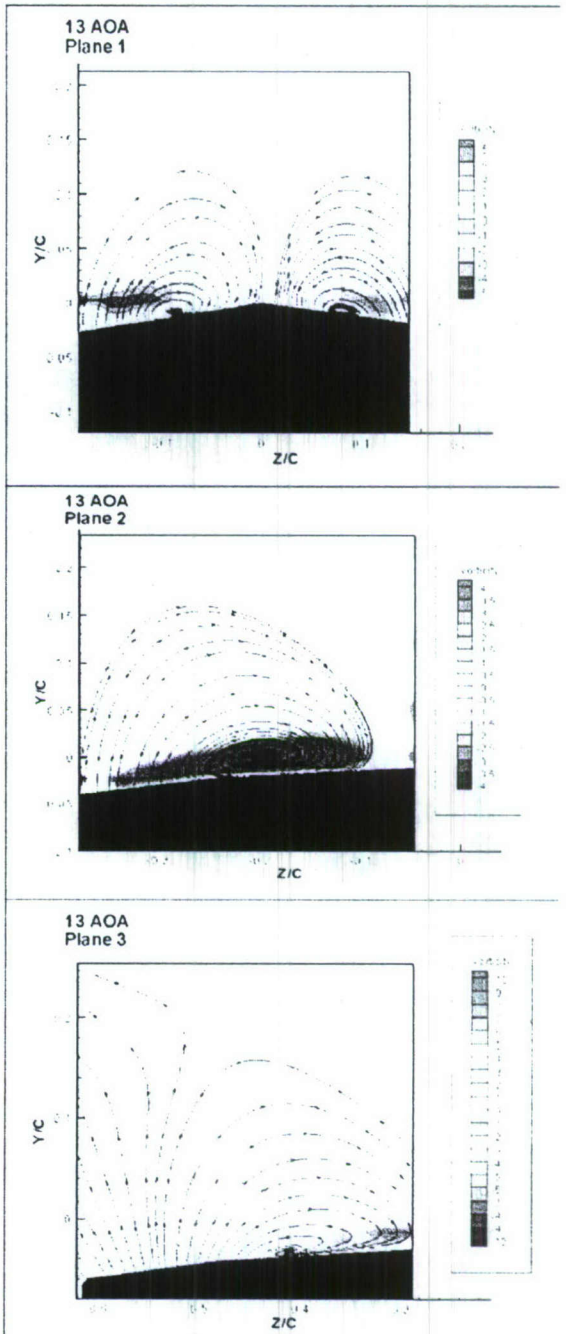

Figure 12 Streamlines and vorticity contours along Trefftz planes for $\alpha=13^0$.

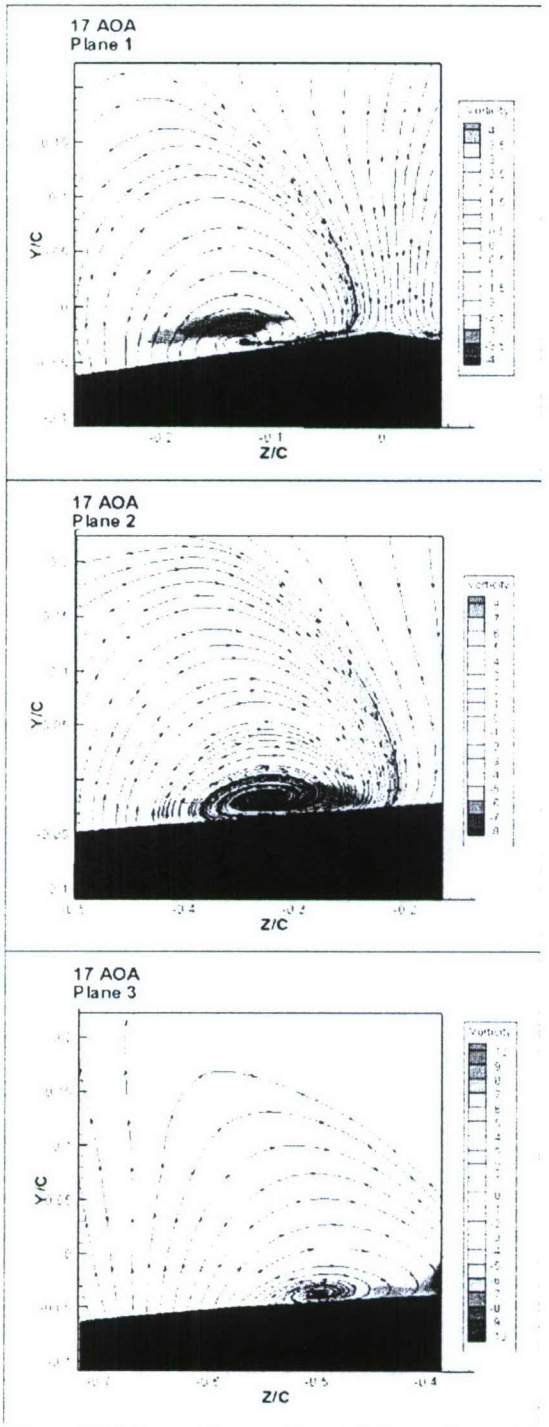

Figure 13 Streamlines and vorticity contours along Trefftz planes for $\alpha=17^0$.

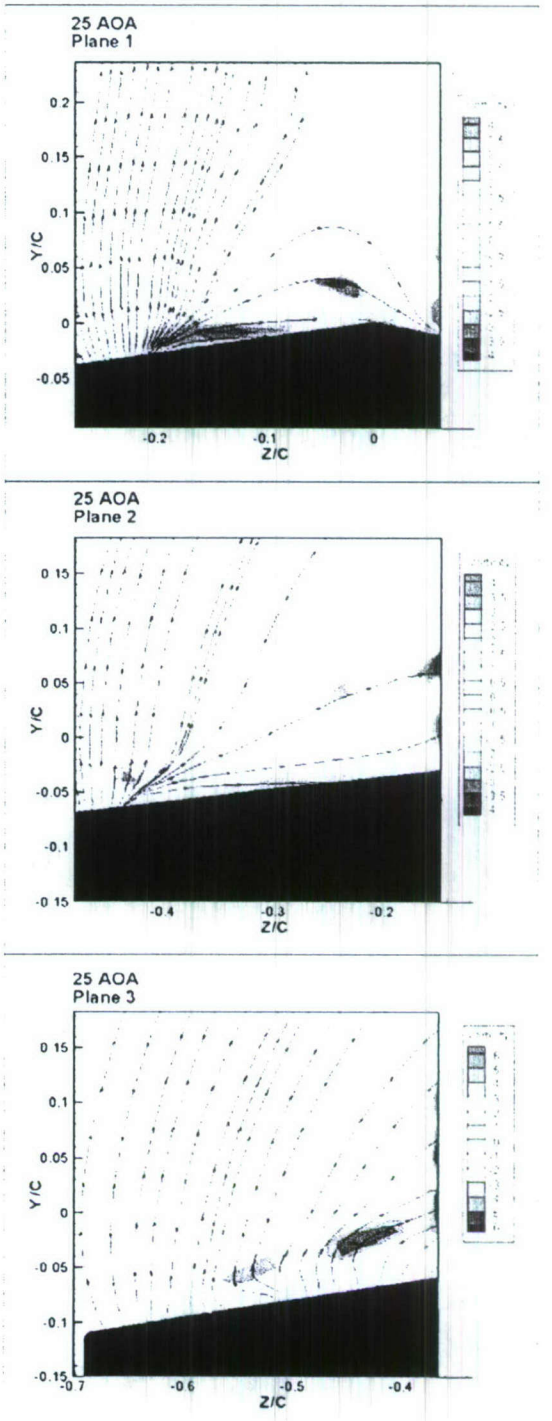

Figure 14 Streamlines and vorticity contours along Trefftz planes for $\alpha=25^0$.

B. Pressure Distributions and Trefftz Plane Results

Pressure distributions were obtained over the large model for a Reynolds number of 1,200,000, at angles of attack of 7°, 13°, 17° and 21°. In Figs. 15 through 18 we present data for four angles of attack, as indicated in the figure captions. In these figures the horizontal axis represents the distance along the chord. But the data are projected as if the wing is viewed from its tip in a direction normal to the root axis, or say the fuselage of the aircraft. Since the leading edge is swept, the pressure curves begin at higher values of the x coordinate as we move from the root to the tip.

All these pressure distributions may appear unfamiliar to researchers who study flows over wings with rounded edges. At high angles of attack, the flow is fully separated and thus, the suction side sustains a uniform pressure distribution. But at low angles of attack, there is a distinct region of very low pressure near the leading edge. This may be interpreted as a leading edge vortex, common on delta wings. This may well be the case, since the low pressure is fixed on the wing. But earlier experiments[7] indicate exactly this type of pressure variation over sharp-edged wings with no sweep. This vortex could therefore be captured on the wing regardless of the sweep angle. Our data indicate that the imprint of this vortex, is confined to the root area of the wing and it retreats closer to the wing as the angle of attack increases. The flow over the wing must be fully separated for $\alpha > 12^0$, in agreement with the data obtained at lower Reynolds numbers.

Areas of recirculation near the leading edge of a wing could also be due to a separated bubble. Such a phenomenon is common at Reynolds numbers below 100,000, and involves a free shear layer that transitions to turbulence, and them reattaches. But these bubbles cannot sustain very low pressures or considerable lengths, as indicated in Figs. 15 and 16.

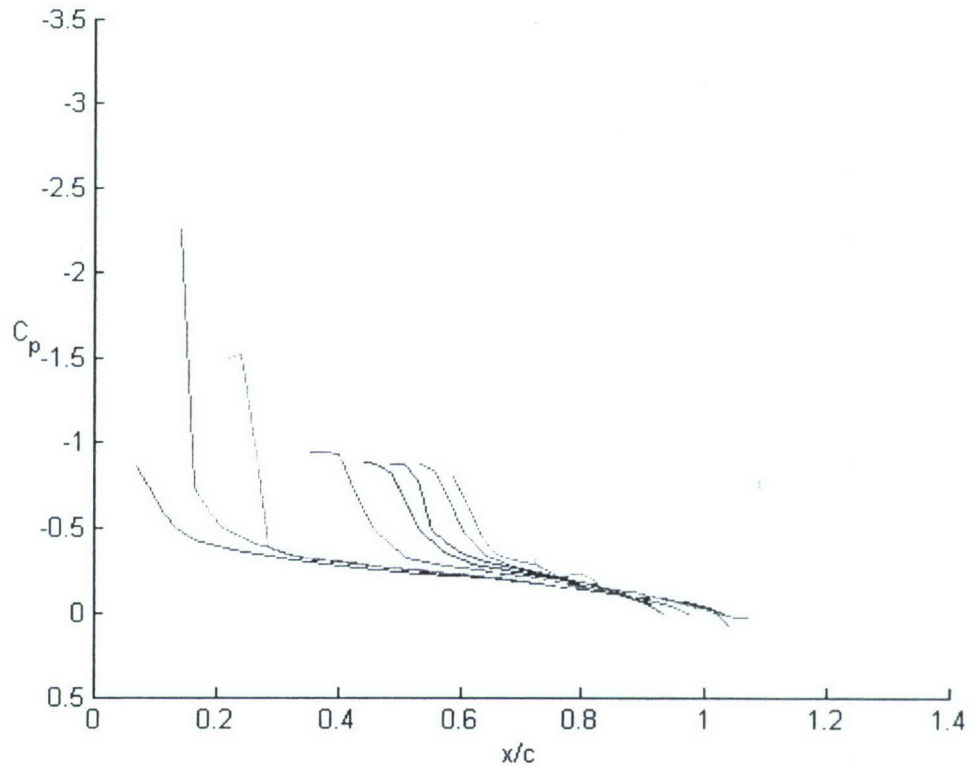

Figure 15. Pressure distribution for $\alpha=7^0$, at spanwise stations of z/c= 0.063, 0.1508, 0.2424, 0.3339, 0.4061, 0.4588, 0.5115, 0.5641, 0.6238, and 0.6904.

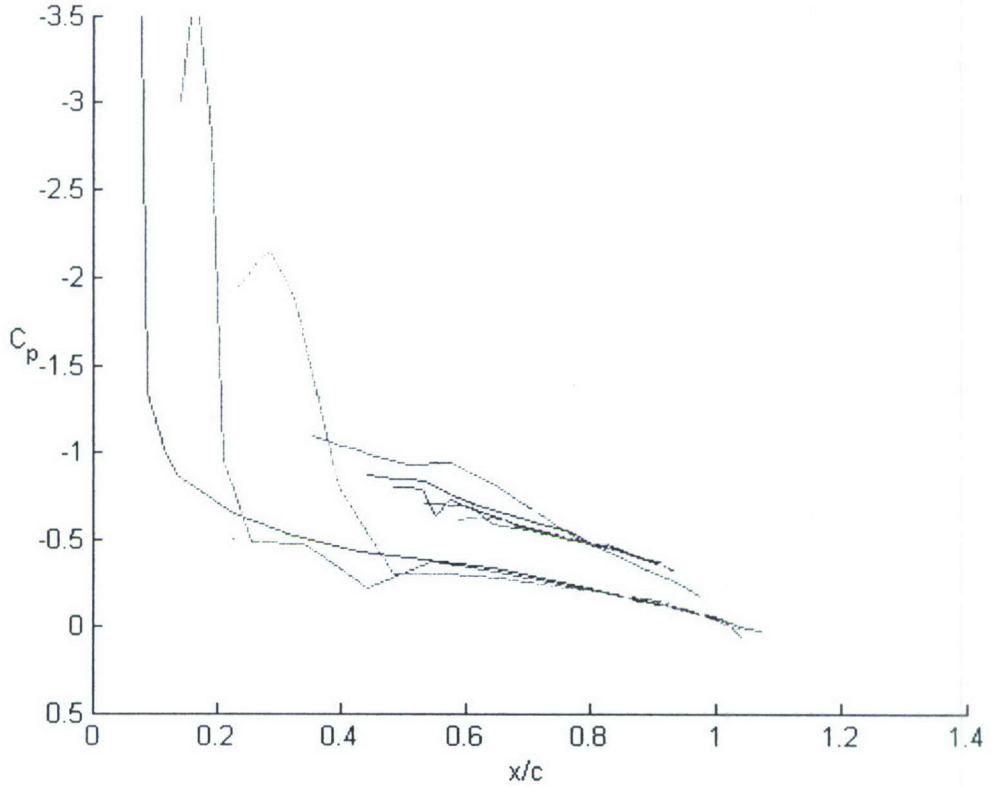

Figure 16. Pressure distribution for $\alpha=13^0$, at spanwise stations of z/c= 0.063, 0.1508, 0.2424, 0.3339, 0.4061, 0.4588, 0.5115, 0.5641, 0.6238, and 0.6904.

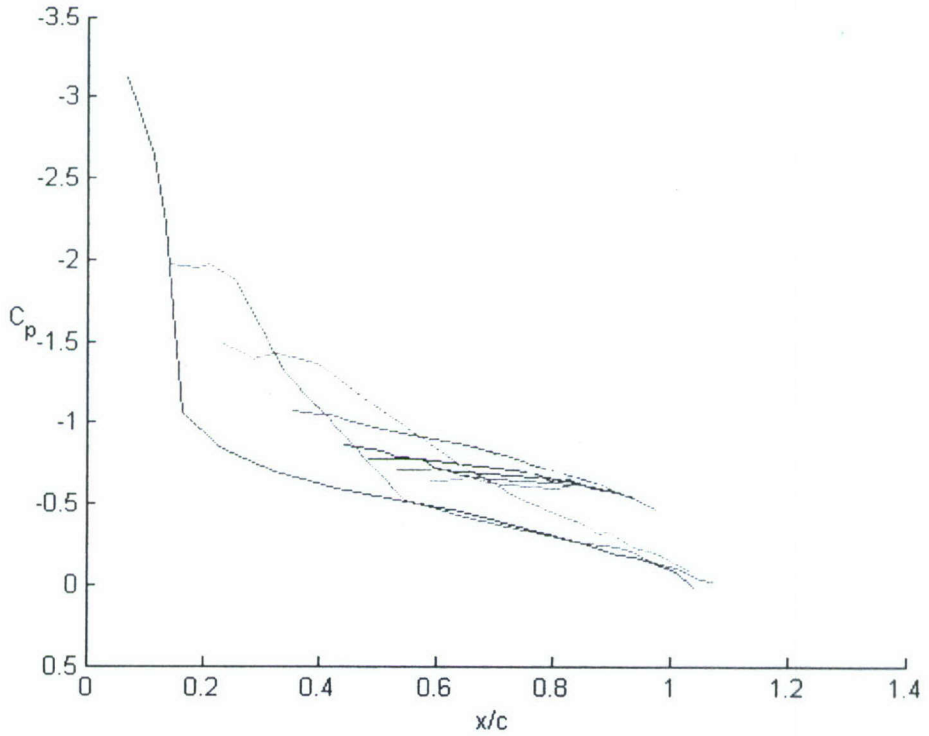

Figure 17. Pressure distribution for $\alpha=17^0$, at spanwise stations of z/c= 0.063, 0.1508, 0.2424, 0.3339, 0.4061, 0.4588, 0.5115, 0.5641, 0.6238, and 0.6904.

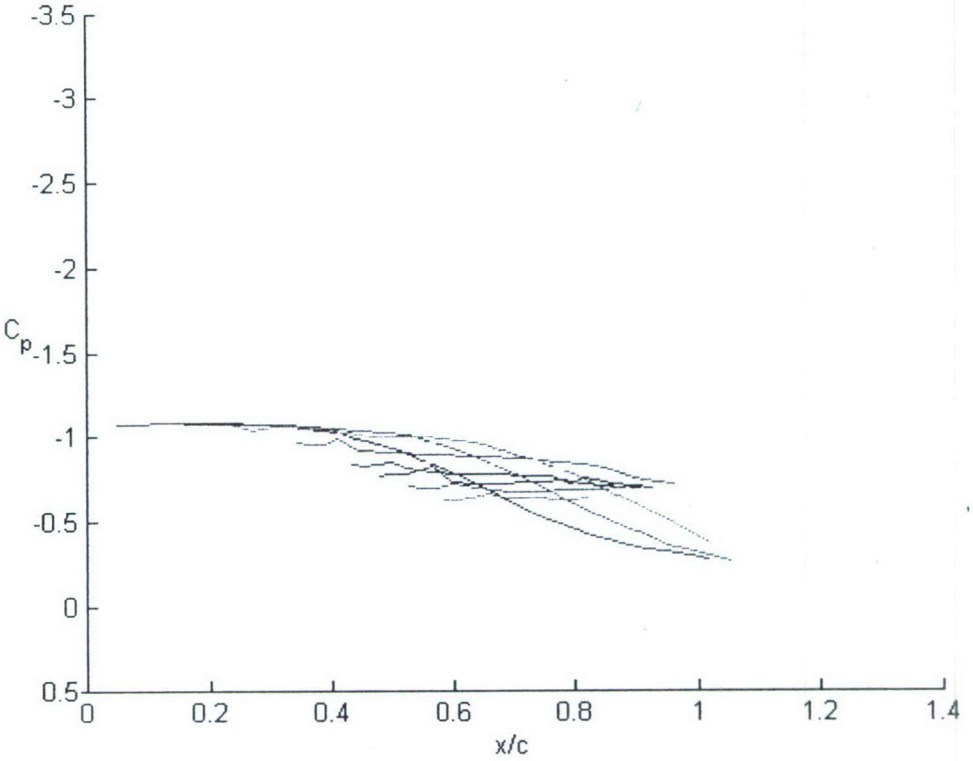

Figure 18. Pressure distribution for $\alpha=21^0$, at spanwise stations of z/c= 0.063, 0.1508, 0.2424, 0.3339, 0.4061, 0.4588, 0.5115, 0.5641, 0.6238, and 0.6904.

We turn now to data obtained on a Trefftz plane normal to the free stream and placed at x/C=1 (just behind the trailing edge), as indicated in Fig. 3. The five-hole probe was traversed on a rectangular grid covering the domain -0.5<y/c<.1 and 0<z/c<1.0 domain. In Figs. 19 through 22 we present results for angles of attack of 13^0 and 21^0. In these figures we display the in-plane velocity component in terms of arrows. In Figs. 19 and 21, the streamwise velocity component is displayed in terms of color/shade contours and in Figs 20 and 22 the in-plane vorticity component is presented in the same way. The velocity vectors in Figs. 19 and 20 indicate the presence of a tip vortex. We note that this vortex is broken down, as is clearly indicated by the wake-like character of the streamwise velocity component. Figure 19 indicates a much more dominant wake-like effect and very slow velocity downstream of the major portion of the wing. It should be noted here that the broken-down delta wing vortices retain their character and display a wake-like profile, which however is confined to the core of the vortex. This is not the

case for the flow field of Fig. 20. For $\alpha=21^0$, the situation is clearer. Now we observe evidence of a massive separated region, with streamwise velocity magnitudes approaching zero and a few pockets of reversed flow. In the vorticity contours of Fig. 22, there seems to be no vorticity present, except a weak amount very near the tip. Apparently the tip vortex will sustain its presence even at higher angles of attack.

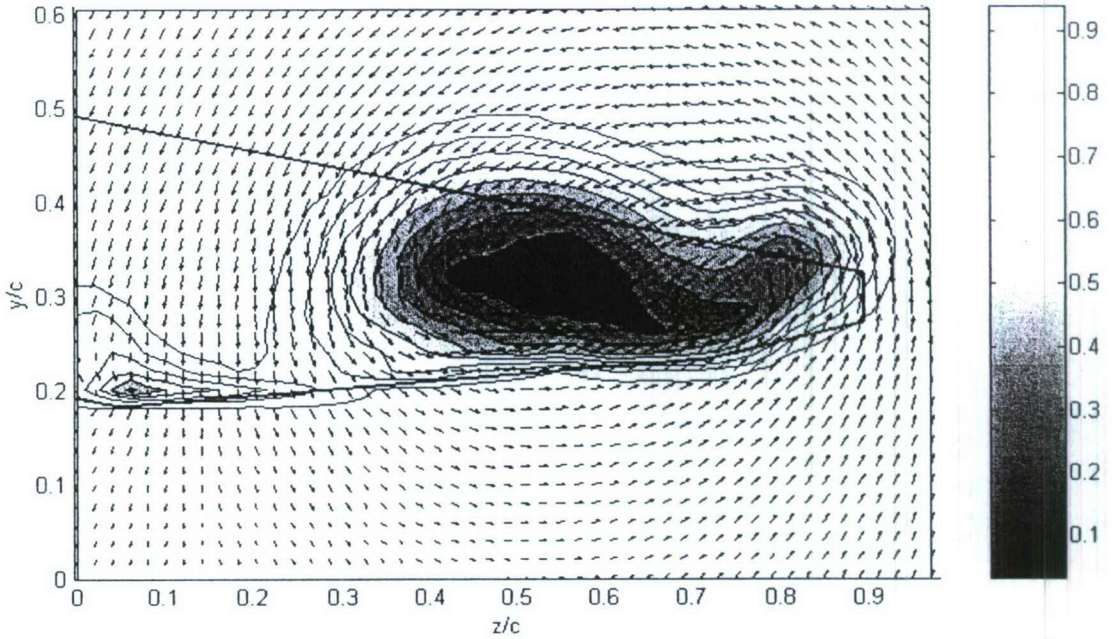

Figure 19. Axial velocity contours for $\alpha=13^0$

Even though there is no evidence of delta wing vortices in planes normal to the free stream, it appears

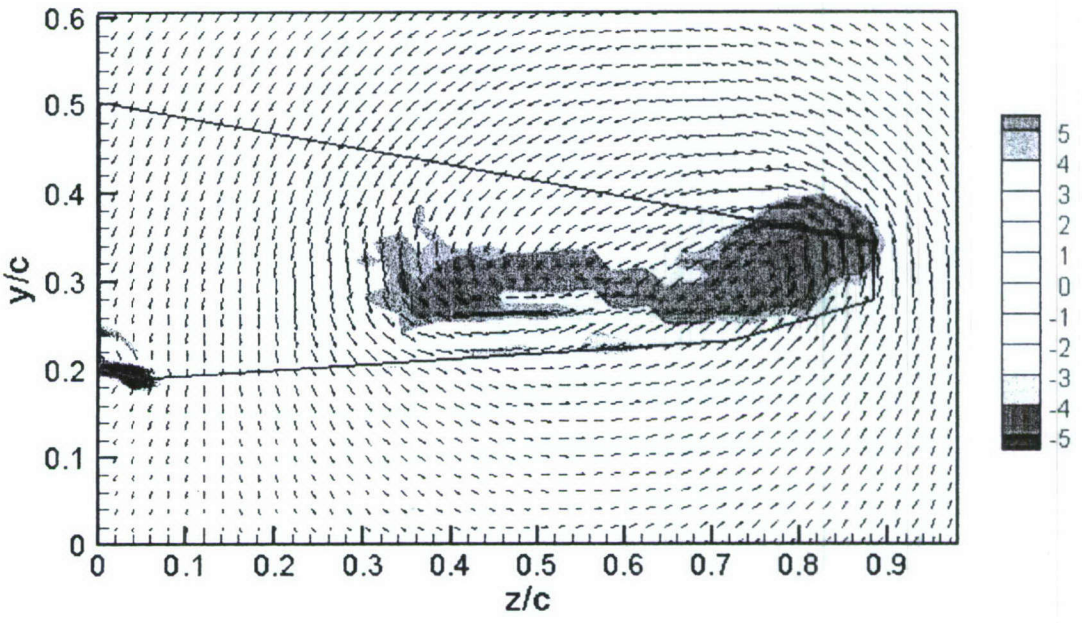

Figure 20. Vorticity contours for $\alpha=13^0$.

that there is a tendency for the velocity vectors in these planes to follow some pattern of recirculation, consistent with the direction induced on all finite wings. This is evident in Figs 19 to 22 but also in Figs. 11 to 15. This is true even though the flow is fully separated.

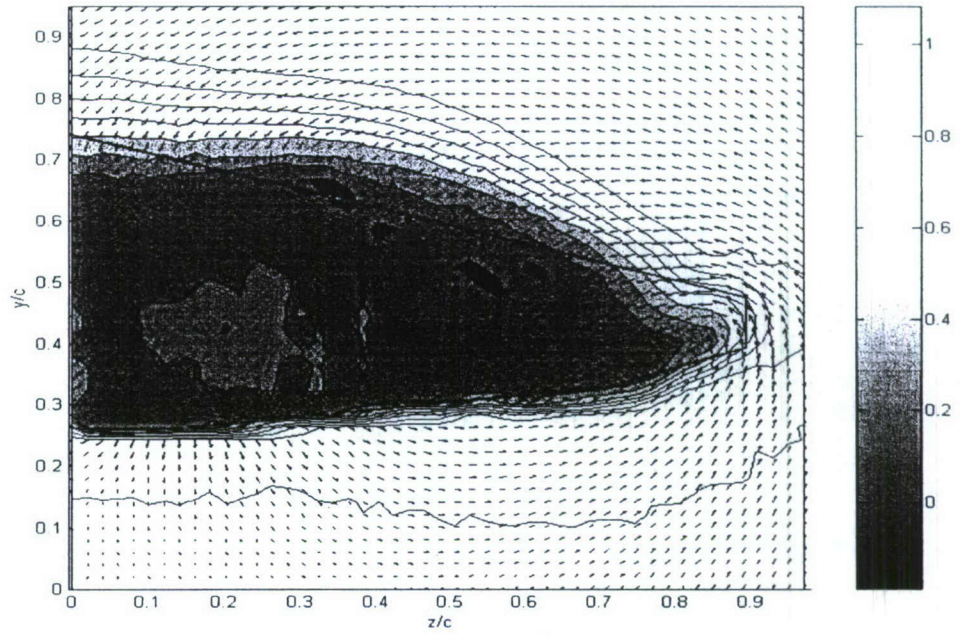

Figure 21. Axial velocity contours for $\alpha=21^0$.

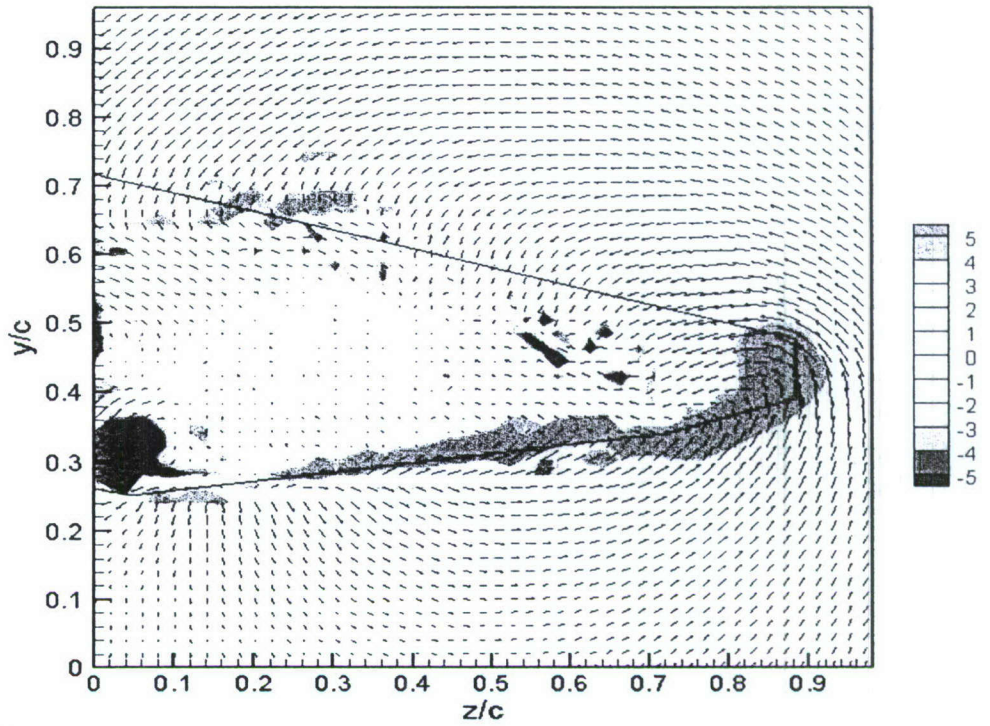

Figure 22. Vorticity contours for $\alpha=21^0$.

5.5 Conclusions

There are two distinct modes of stall for wings with low sweep. The delta wing mode, whereby leading edge vortices break down but remain more or less in the same position over the wing and 2-D stall whereby vortices form, grow and then detach and shed in the wake. Both modes are possible over a planform with a 40^0 sweep, but our research indicates that the flow develops in the form of 2-D stall. We presented evidence that in the inboard part of the wing, an attached vortex can be sustained, reminiscent of delta-wing type of a tip vortex, but further in the outboard region 2-D stall dominates. The flow is unsteady and vortices are shed periodically. We anticipate and already generated preliminary evidence (not shown here) that unsteady blowing right at the leading edge of a sharp wing can reduce the size of the separated flow over the pressure side of a wing in 2-D mode of stall. This is the most effective means of increasing lift in the average, even if the flow remains fully separated. We also have evidence that our control method can actually dictate the character of the flow, and force wing section that sustains a delta wing vortex to stall in the 2-D mode.

5.6 References

[1]Miau, J. J., Kuo, K. T., Liu, W. H., Hsieh, S. J., Chou, J. H., and Lin, C. K., "Flow Developments Above 50-Deg Sweep Delta Wings with Different Leading-Edge Profiles," *Journal of Aircraft*, Vol. 32, No. 4, July-August 1995, pp. 787-794.

[2]Ol, M. V. and Gharib, M., "Leading-Edge Vortex Structure of Nonslender Delta Wings at Low Reynolds Number," *AIAA Journal*, Vol. 41, No. 1, January 2003, pp. 16-26.

[3]Gursul, I., Taylor, G., and Wooding, C., "Vortex Flows over Fixed-Wing Micro Air Vehicles," *40th AIAA Aerospace Sciences Meeting & Exhibit*, Paper No. 2002-0698, AIAA, January 2003.

[4]Taylor, G. S., Schnorbus, T., and Gursul, I., "An Investigation of Vortex Flows over Low Sweep Delta Wings," *AIAA Fluid Dynamics Conference*, Paper No. AIAA-2003-4021, Orlando, FL, June 23-26, 2003.

[5]Gordnier, R. E. and Visbal, M. R., "Higher-Order Compact Difference Scheme Applied to the Simulation of a Low Sweep Delta Wing Flow," *41st AIAA Aerospace Sciences Meeting and Exhibit*, Paper No. AIAA-2003-0620, AIAA, Reno, NV, January 6-9, 2003.

[6]Yaniktepe, B. and Rockwell, D., "Flow Structure on a Delta Wing of Low Sweep Angle," *AIAA Journal*, Vol. 42, pp. 513-523.

[7]Rullan, J., Vlachos, P. P., Telionis, D. P. and Zeiger, M. D., "Flow Control of Unswept and Swept, Sharp-Edged Wings via Unsteady Blowing," *42nd Aerospace Sciences Meeting*, Paper No. AIAA-2004-0226, January 2004.

[8]Miranda, S., Vlachos, P. P., Telionis, D. P. and Zeiger, M. P., "Flow Control of a Sharp-Edged Airfoil," Paper No. AIAA-2001-0119, 2001, also *AIAA Journal*, 2005 (in press).

[9]Guy, Yair, Morrow, Julie, A., McLaughlin, Thomas, E., "Velocity Measurements on a Delta Wing with Periodic Blowing and Suction," *38th Aerospace Sciences Meeting and Exhibit*, Paper No. AIAA-2000-0550, Reno, NV, January 10-13, 2000.

[10]Guy, Y., Morton, S. A. and Morrow, J. A., "Numerical Investigation of the Flow Field on a Delta Wing with Periodic Blowing and Suction," *AIAA Fluids 2000*, Paper No. AIAA-2000-2321, Denver, CO, June 19-22, 2000.

[11]Folk, C., and Ho, C.-M., "Micro-Actuators for Control of Delta Wing with Sharp Leading Edge," Paper No. AIAA-2001-0121.

[12]Washburn, A. E., and Amitay, M., "Active Flow Control on the Stingray UAV: Physical Mechanisms," *42nd Aerospace Sciences Meeting & Exhibit*," Paper No. AIAA-2004-0745, Reno, NV, January 5-8 2004.

[13]Westerweel, J., *Digital Particle Image Velocimetry, Theory and Application*, Delft University Press, 1993.

[14]Westerweel, J., *Optical Diagnostics in Fluid and Thermal Flow*, SPIE 2005, pp. 624-635.

[15]Vlachos, P. P., Donnelly, M. J. and Telionis, D. P., "On the Wake of a Circular Cylinder Piercing a Water Free Surface," *Proceedings of FEDS'98*, FEDS98-5177, 1998 ASME Fluids Engineering Division Summer Meeting.

[16]Vlachos, P. P. and Telionis, D. P., "Turbulence Characteristics in the Wake of a Circular Cylinder Near the Free Surface," FEDSM2000-11320, Boston, MA, 2000.

[17]Klute, S. M., Vlachos, P. P. and Telionis, D. P., "High-Speed DPIV Study of Vortex Breakdown," *Fluid Dynamics Symposium, Fluids 2000 Conference*, also *AIAA Journal* (in press).

[18]Asimopoulos, N., Vlachos, P. P., Telionis, D. P., "A High Speed, High Particle Density Particle Tracking Method for Turbulent Flows," ASME FEDSM'99-7139.

6 FLOW CONTROL OF DIAMOND PLANFORM WINGS – VELOCITY FIELDS

Wings swept by 30 to 40 degrees are today very common in fighter aircraft. And yet, there is very little work devoted to the understanding of the aerodynamics of such wings. The problem is that such wings may be able to sustain attached flow behind broken down delta wing vortices, or stall like two-dimensional wings while shedding vortices with generators parallel to their leading edge. In this paper, we explore the effectiveness of leading-edge control of the flow over such wings. Our results indicate that two-D-like vortices are periodically generated and shed. At the same time, an underline feature of the flow, a leading edge vortex is periodically activated, penetrating the separated flow, eventually emerging downstream of the trailing edge of the wing.

Nomenclature

U_∞ = Characteristic velocity (free stream)
b=semis-span
c = root chord
C_μ = momentum coefficient
T= period of pulsing jet
x,y,z = coordinate system (see Fig. 3)
α= Angle of attack

6.1 Introduction

In this paper we report on the continuation of the work we presented at the 43rd Aerospace Sciences Meeting[1]. In Ref. 1 we discussed the flow over a trapezoidal wing planform at low and moderate angles of attack. We presented velocity fields and pressure distributions for steady flows at different Reynolds numbers. In the present paper we explore the effect of flow control over the same wing planform. Some of the introductory comments included in Ref. 1 are applicable here as well, and are repeated with some minor modifications.

The work described in this sequence of AIAA papers is focused on wings with moderate sweep angles. At very low sweep angles, namely angles less than 20^0, the flow over sharp-edged wings stalls like the flow over an unswept wing. Vortices are shed with their axis nearly normal to the free stream. Such vortices are often called "rollers". At high sweep angles, that is larger than 50^0, the flow is similar to delta wing flows that are

dominated by leading edge vortices (LEV). We will refer to these vortices here as "streamers". These wings stall due to vortex breakdown.

The effects of sweeping a wing at moderate angles, namely 30^0 to 40^0, and moderate to high angles of attack are very little understood. And yet, such wings are today the norm for most fighter aircraft. The problem is that in this range of parameters, the flow may stall like the flow over an unswept wing, shedding large vortices in an unsteady fashion, or it could stall like a delta wing, sustaining a leading-edge vortex (LEV) that breaks down. The significant difference between the two modes is that delta wing vortices, or streamers, are attached to the leading edge of the wing and shed vorticity by directing it in the core of the vortex and then telescoping it downstream, whereas rollers, grow and then shed by rolling over the wing and detaching from its surface. This is essentially the phenomenon of unsteady stall.

Research on delta wing flows for sweep angles as low as 50^0 indicate that delta wing vortices are present, but break down very close to the leading edge[1-5]. In fact even before break down, these vortices display wake-like flow where the velocity is very low in the core of the vortex. In some cases[2] it was found that the low aspect ratio wing at medium angles of attack does not behave like a delta wing but rather like an unswept wing. A sweep angle of 50^0 is not low enough to demonstrate the transition from the vortex breakdown stall to the two-dimensional unsteady stall. More recently, Yaniktepe and Rockwell[6] studied the flow over a wing with a sweep angle of 38.7^0. They provided evidence that up to an angle of attack, α of 25^0, the flow appears to be dominated by delta wing tip vortices. At the highest angle of attack, the vortices seem to be displaced inboard.

In both the studies of Ol and Gharib[2] and Yaniktepe and Rockwell[6], the flow field was interrogated along planes normal to the free steam. In our studies we cut the fields with planes that are both normal and parallel to the free stream. We are interested in the possibility that the control mechanisms could actually dictate the desired stall mechanism.

Impressive advancements have been made in controlling the flow over wings with rounded leading edges, but very little work has been devoted to the control of the flow over sharp-edged wings. The present authors[7,8] have demonstrated that flows over sharp

edges can be effectively controlled with lift increases as high as 70%. Control of delta wing flows has been successful but the efforts were focused so far for relatively high sweep angles[9-11]. The objective of this project is to capitalize on our experience and extend the work to moderately swept wings and wings with practical planforms.

The majority of contributions on airfoil flow control are based on separation control. Their aim is to delay separation and stall altogether. There is another area of airfoil and wing flow control, which so far has received little attention but which has greater potential in defense applications. This is the management and control of separated flow. Such flows are encountered over sharp-edged wings at low to moderate angles of attack or over wings in deep stall. The idea is to accept the fact that in some situations, the flow is fully separated, and periodic shedding of vortices is established. The aim then becomes to control the dynamic development of vortical structures in order to improve the performance of the lifting surface. These are the type of flows that develop over wings moderately swept and the focus of the present research.

We discuss in this paper the results of experiments conducted in a water tunnel with a trapezoidal planform wing model typical of wings used in aeronautical industry. The model was tested[1] at a Reynolds numbers of Re=30,000. We employ Digital Particle Image Velocimetry (DPIV) along planes parallel to the stream and perpendicular to the stream. We report results obtained with a high- speed digital camera that provides instantaneous data.

6.2 Facilities, Models and Equipment

Experiments were carried out in the Engineering Science and Mechanics (ESM) water tunnel. This tunnel was built by Engineering Laboratory Design (ELD) and operates in a closed loop in a vertical plane with up to 2,500 gallons of water. The settling chamber leads to the 24" x 24" x 72" Plexiglas test section via a three-way convergence. A 4500-gpm pump driven by a 20-hp motor provides flow which can attain a maximum speed of 1 m/s, corresponding to a maximum Reynolds number per unit length of 9900/cm. The free stream turbulence level in the test section is less than 2%.

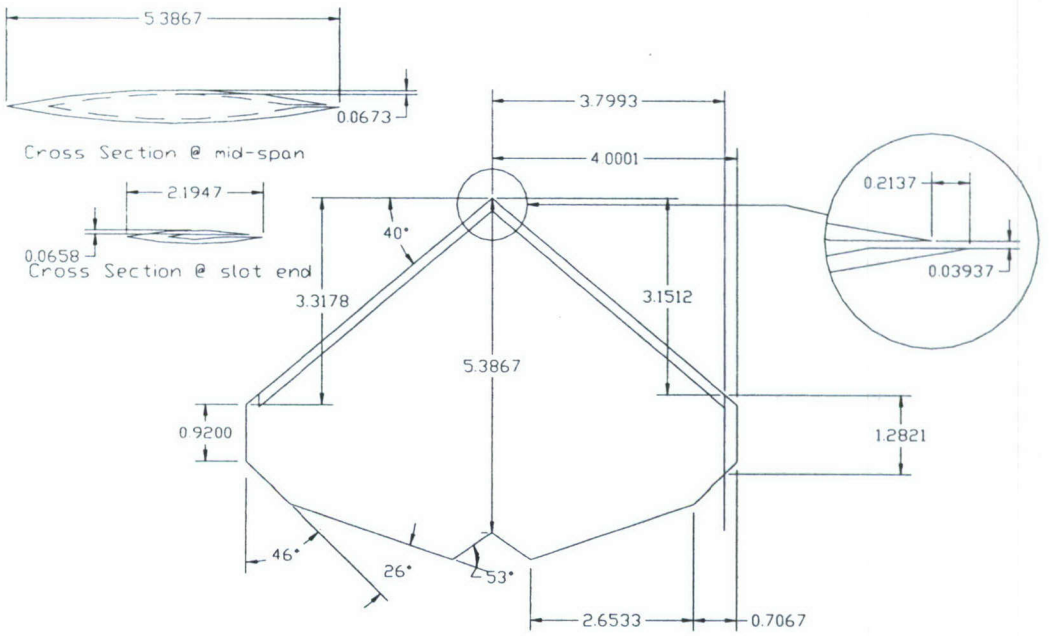

Figure 1. Engineering drawing of the trapezoidal planform model for water tunnel testing.

The model for this experimental investigation has a trapezoidal planform shown in Fig. 1. In this Figure the dimensions, in inches, correspond to a small model designed for testing in the water tunnel. This model is equipped with an internal compartment that can generate a pulsing jet in the leading edge for flow control. It is geometrically similar to a stainless-steel model provided by Lockheed Martin, a co-sponsor of this effort which we have tested earlier[1].

6.3 Particle Image Velocimetry

Particle-Image Velocimetry (PIV) is a powerful tool that we employ. The most common implementation of the method, (currently commercially available) focuses on a single-exposure double-frame digital cross correlation approach. A high-resolution (1Kx1K pixels) CDD camera that can sample up to 30 fps, results in a sampling frequency of the flow field of only 15Hz, is usually synchronized with a Nd:YAG pulsing laser that illuminates the interrogation area. The velocity field is traditionally treated as a linear transfer function that corresponds to a flow pattern displacement between two consecutive images. This transfer function is revealed in a statistical manner incorporating second order statistical moments of the image patterns (Westerweel[13, 14]).

A major disadvantage of this approach is the inability to provide sufficient frequency resolution, which is necessary, in order to investigate any high-frequency phenomena that occur in turbulent, separated flows. A system developed by the authors at VA Tech has overcome the difficulty of low sampling frequency. This was accomplished with the integration of a high-power (50 W) pulsing laser with special type of optics and a unique CMOS, capable of acquiring up to 2000 frames per sec (fps) resulting to a DPIV system with 1 KHz maximum sampling frequency[15]. To our knowledge, there are no results published in the open literature that employ high-speed CMOS technology cameras to perform DPIV measurements. Our ongoing research to integrate this technology with our existing PIV system demonstrated very high sensitivity, equivalent to 1000 ASA, and signal-to-noise ratio in the order to 100,000:1. The great advantage of this new technology is that each pixel is treated as an individual sensor and any cross-coupled interaction between neighborhood pixels is eliminated. The conditioning of the signal is performed on the sensor. Thus, the spatial and temporal resolution of our PIV system is increased by almost an order of magnitude in comparison with our previous configuration, and two orders of magnitude compared with systems that are commercially available.

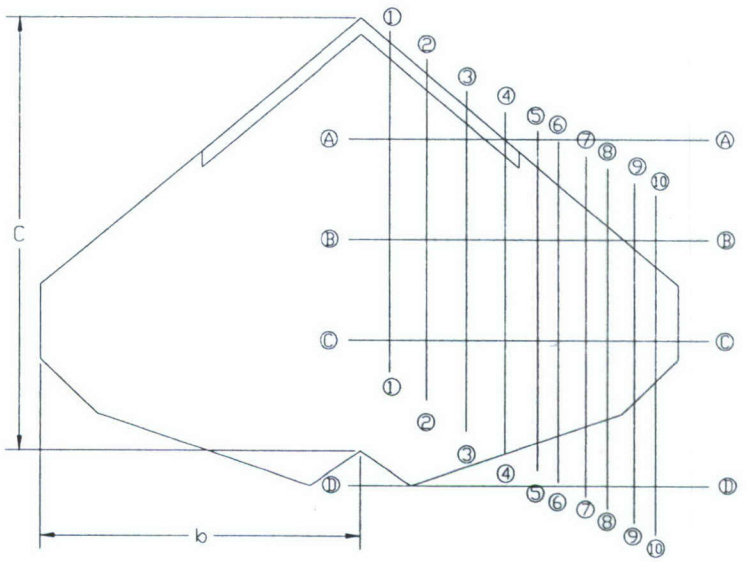

Figure 2. Laser cuts for the water tunnel flow visualization and PIV.

Members of our group were able to perform dual-frame cross-correlation time-resolved DPIV by employing single and multiple exposures. The first example of single-exposure double frame cross-correlation time resolved DPIV was presented by Vlachos et al.[15]. However this implementation was limited to very low-speed liquid flows (U~10 cm/s). In a different approach, we performed multiple exposures per frame and we evaluated the vectors using standard cross-correlation. This approach was employed in the analysis of the characteristics of turbulent shear layers by Vlachos et al.[16] and in the investigation of the post-vortex-breakdown region characteristics of delta wings by Klute et al.[17].

Table 1:Laser Cut Locations

planes	Z/C	Z/b
1	0.068	0.092
2	0.156	0.209
3	0.249	0.334
4	0.340	0.456
5	0.417	0.559
6	0.467	0.626
7	0.531	0.711
8	0.581	0.778
9	0.644	0.863
10	0.694	0.930

planes	X/C
A	0.28
B	0.513
C	0.746
D	1.086

One major drawback of conventional DPIV systems results from limitations inherited from the velocity evaluation methods. Our group recently launched an effort to integrate and combine some of the most effective and well established of these proposed methods[18]. The outcome is a dynamically adaptive hybrid algorithm for the evaluation of the velocity vectors that overcomes these limitations to a great extent, thus increasing accuracy and space resolution. The overall performance of the method, if quantified, yields space resolution in the order of 0.5 mm average, time resolution in the order 1milisec with sampling time up to 4secs and uncertainty of the velocity measurement in the order of 0.1% of the reference velocity.

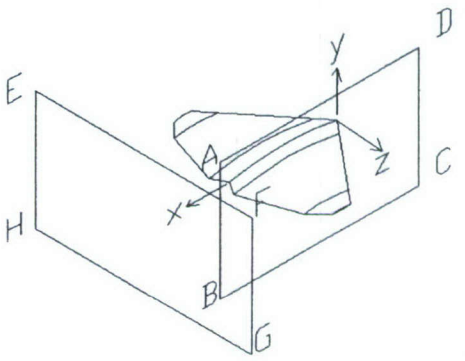

Figure 3. Schematic of planes of data acquisition.

The advancements in this effort are employed in the global characterization of the separated flow over the sharp airfoil, providing insight on the interaction of the shear layers with the incident free stream and their roll-up to coherent vortices. These data are used to analyze the flow control mechanism, providing spatio-temporal correlations, information about the interaction of the various frequency modes in the flow field and the route to the formation of coherent structures in the separated flow region. Data were obtained along laser cuts as shown in Fig. 2. The coordinate system is shown in Fig. 3. The laser cuts were along planes parallel the yz plane, like plane EFGH in Fig. 3 and parallel to the xy plane, like plane ABCD. Cuts 1 through 10 are parallel to the free stream, while cuts A, B, C and D are normal to the free stream. The locations of these planes are shown in Table 1.

6.4 Flow Control Mechanism

Pulsing jets were activated using a pump connected to the wing cavity. The data described in this paper were obtained with a slot spanning only 50% of the leading edge slot starting at the root of the wing. This control mechanism therefore activates only the inboard potion of the wing. The jet was activated at the natural shedding frequency that corresponds to the angle of attack of 13^0, namely 1.71 Hz. This was calculated in terms of a Strouhal number which was measured earlier for this configuration. The corresponding period was therefore T=0.585 sec. The pump operation was monitored with a flow meter. A specific point on the periodic signal of the flow meter was arbitrarily chosen as the origin of time. All instantaneous frames are presented with time measured from the common origin. We obtained data at a rate of 1,000 frames per second and recorded 1700 frames for each plane. In this way, each sequence of instantaneous frames includes more than one period of the actuation disturbance. With interrogation windows of 32X32 pixels, we obtained vectors along grids with sizes of 97X61 to 97X77. Each instantaneous frame therefore contains over 5900 velocity vectors.

1.1 Results and Discussion

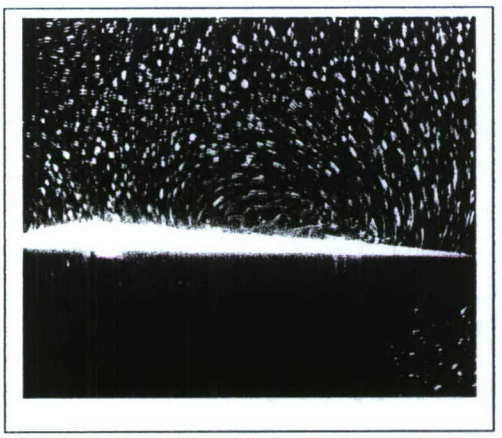

Figure 4. Flow visualization along a Trefftz plane.

Time-Resolved DPIV data were processed using an in-house developed multi-grid iterative DPIV, with second-order, Discrete Window Offset (DWO). Time-resolved DPIV systems are limited by the fact that the time separation between consecutive frames is the reciprocal of the frame rate, thus on the order of milliseconds. This value is relatively large compared with microsecond time-intervals employed by conventional DPIV systems. By employing a second-order DWO we provide an improved predictor for the particle pattern matching between subsequent iterations. Moreover, the algorithm employed

performs a localized cross-correlation, which, when compared to standard multi-grid schemes for resolving strong vortical flows was proven to be superior.

For both flow visualizations and PIV measurements, we cut the field by laser sheets parallel and perpendicular to the free stream as shown schematically in Fig. 2 and 3. All the data presented here were obtained with the wing at an angle of attack of 13^0. Flow visualization on a Trefftz plane, namely plane EFGH shown in Fig. 4 indicates results very similar to those of Yaniktepe and Rockwell[6], which imply that the flow develops leading edge vortices. We found that such visualizations could be deceiving. For the same configuration, cutting the flow by a plane parallel to the free stream essentially passes a section through a LEV. Leading edge vortices have a nearly circular cross-section if they are cut normal to their axis. But if cut by a plane inclined with respect to their axis, they should show vorticity of the same sign along a closed and nearly elliptical contour. Moreover, the velocity component along the axis of a LEV should be jet-like. The PIV data along planes parallel to the flow are void of such characteristics. Instead they indicate vorticity only on the upper side, which is compatible with two-D stall. The axial velocity distribution indicates wake-like behavior, which confirms the fact that we have two-D stall.

In Fig. 5, we present a preview of the phenomena we will discuss in this paper. The three frames in this Fig. 6re instantaneous data along Plane D-no-control, Plane D-with-control and Plane 5-with-control. In this figure we display all the velocity vectors available in each frame. But in the following figures we display only a very small portion of the actual number of data, to avoid cluttering the images. Quantities like vorticity have been calculated using all data along the full grid. In this and all the following figures vorticity is displayed in the form of contours. The top frame in this Fig. 5 indicates the presence of a typical wing-tip vortex. Since there is very little vorticity near the center of the vortex, the core of the vortex must be broken down. This should be expected for a wing with low sweep angle and a moderate angle of attack, and has been reported earlier by Yaniktepe and Rockwell[6]. These authors experimented with a delta wing swept with almost the same angle as ours. The basic difference between the two models is that ours is cropped. In the second frame of Fig. 5 we present one of the instantaneous frames for flow control. As we will discuss later, a second axial vortex, a streamer, develops

upstream and penetrates all the way to Plane D. We chose one of the instantaneous frames that most clearly indicate the presence of this vortex. Finally, in the last frame of this Figure we present instantaneous data along Plane 5 when control is activated.

Fig. 6 presents instantaneous data along xy planes. The three columns in this figure correspond to Planes 2, 3 and 4, and each row corresponds to eight equally spaced instances within one period although we present the first five instances. With the activation of the leading edge, a recirculation region is initiated at T=3T/8 almost simultaneously in Plane 2 and 3. And in subsequent times the disturbance grows and displaces downstream. The vorticity associated with this vortex-like structure is mostly present along its periphery, the area where one would expect to find shear layers. This phenomenon therefore could be classified as a two-D stall vortex. But as we will see later, the other vorticity component normal to Planes 2, 3 and 4 is actually larger. So this is a truly three-dimensional phenomenon.

In Fig. 7a and 7b we now present instantaneous data on Planes A and 3. We now see that the disturbance that so far appeared as a roller resembling two-dimensional stall is actually the generation of an axial vortex. At first the vortex appears as a tip vortex, or a delta wing vortex. But as it evolves, it moves in the inboard direction. We will later find that it moves a little further towards the wingtip direction from the current location of $Z/C \cong 0.25$ though not getting close to it..

Fig. 8a and 8b presents data very similar to those of Fig. 7a and 7b, which is instantaneous data along two mutually perpendicular planes, here Planes C and 8, but this pair was chosen further outboard. We observe a sequence of very similar events. Yet it should be recalled that only the first half of the wing is activated. And yet the actuation is enough to trigger a roll up of vorticity that has move to $Z/C \cong 0.5$. This time the vortex will coexist with a weak tip vortex that can be seen at the end of the wing at $Z/C \cong 0.75$. Both these vortices penetrate the separated flow that dominates the entire suction surface of the wing and periodically reach Plane D, which is placed downstream of the trailing edge, as shown in Fig. 9. Comparing these with Fig. 5a, where control has not been activated, the recirculation region is induced into a more compact one and closer to the wingtip.

6.5 Conclusions

There are two distinct modes of stall for wings with low sweep. The delta wing mode, whereby leading edge vortices break down but remain more or less in the same position over the wing and 2-D stall whereby vortices form, grow and then detach and shed in the wake. Both modes are possible over a planform with a 40^0 sweep, but our research indicates that the flow develops in the form of 2-D stall. This is consistent with the findings of Yaniktepe and Rockwell[6] who report on a plane similarly situated to our Plane D a broad area of cross-flow recirculation that contains weak and unorganized vorticity. For no-control flow, we presented evidence that in the inboard part of the wing, an attached vortex can be sustained, reminiscent of delta-wing type of a tip vortex, but further in the outboard region 2-D stall dominates. The flow is unsteady and vortices are shed periodically. The flow visualizations of Yaniktepe and Rockwell[6] and ours indicate that the leading edge vortex has the tendency to move inboard, but looses its coherence in the dead-air region of two-dimensional flow wake. We now present experimental evidence that leading edge activation with a C_μ=0.02 activates this vortex, which periodically penetrates the separated region and reaches beyond the trailing edge of the wing. This finding is consistent with the results we presented in Ref. 1, which indicate that in the pressure periodically drops in this region, resulting in increases of the lift in the average. Actuation on the inboard half of the leading edge has a strong effect on the outboard region as well. We find that the flow is much better organized, void of weak vortices that roll downstream. Instead the tip vortex is strengthen periodically. This must also contribute to the increase of lift in the average.

6.6 References

[1] Rullan, J.G., Vlachos, P.P. and Telionis, D.P., "The Aerodynamics of Low-Sweep Trapezoidal Wings" presented at the 43rd Aerospace Sciences Meeting and Exhibit, 10-13 January 2005, Reno, Nevada, Paper No AIAA-2005-0059.

[2] Ol, M. V. and Gharib, M., "Leading-Edge Vortex Structure of Nonslender Delta Wings at Low Reynolds Number," *AIAA Journal*, Vol. 41, No. 1, January 2003, pp. 16-26.

[3] Gursul, I., Taylor, G., and Wooding, C., "Vortex Flows over Fixed-Wing Micro Air Vehicles," *40th AIAA Aerospace Sciences Meeting & Exhibit*, Paper No. 2002-0698, AIAA, January 2003.

[4]Taylor, G. S., Schnorbus, T., and Gursul, I., "An Investigation of Vortex Flows over Low Sweep Delta Wings," *AIAA Fluid Dynamics Conference*, Paper No. AIAA-2003-4021, Orlando, FL, June 23-26, 2003.

[5]Gordnier, R. E. and Visbal, M. R., "Higher-Order Compact Difference Scheme Applied to the Simulation of a Low Sweep Delta Wing Flow," *41st AIAA Aerospace Sciences Meeting and Exhibit*, Paper No. AIAA-2003-0620, AIAA, Reno, NV, January 6-9, 2003.

[6]Yaniktepe, B. and Rockwell, D., "Flow Structure on a Delta Wing of Low Sweep Angle," *AIAA Journal*, Vol. 42, pp. 513-523.

[7]Rullan, J., Vlachos, P. P., Telionis, D. P. and Zeiger, M. D., "Flow Control of Unswept and Swept, Sharp-Edged Wings via Unsteady Blowing," *42nd Aerospace Sciences Meeting*, Paper No. AIAA-2004-0226, January 2004.

[8]Miranda, S., Vlachos, P. P., Telionis, D. P. and Zeiger, M. P., "Flow Control of a Sharp-Edged Airfoil," Paper No. AIAA-2001-0119, 2001, also *AIAA Journal*, vol. 43, pp 716-726, 2005.

[9]Guy, Yair, Morrow, Julie, A., McLaughlin, Thomas, E., "Velocity Measurements on a Delta Wing with Periodic Blowing and Suction," *38th Aerospace Sciences Meeting and Exhibit*, Paper No. AIAA-2000-0550, Reno, NV, January 10-13, 2000.

[10]Guy, Y., Morton, S. A. and Morrow, J. A., "Numerical Investigation of the Flow Field on a Delta Wing with Periodic Blowing and Suction," *AIAA Fluids 2000*, Paper No. AIAA-2000-2321, Denver, CO, June 19-22, 2000.

[11]Folk, C., and Ho, C.-M., "Micro-Actuators for Control of Delta Wing with Sharp Leading Edge," Paper No. AIAA-2001-0121.

[12]Washburn, A. E., and Amitay, M., "Active Flow Control on the Stingray UAV: Physical Mechanisms," *42nd Aerospace Sciences Meeting & Exhibit*," Paper No. AIAA-2004-0745, Reno, NV, January 5-8 2004.

[13]Westerweel, J., *Digital Particle Image Velocimetry, Theory and Application*, Delft University Press, 1993.

[14]Westerweel, J., *Optical Diagnostics in Fluid and Thermal Flow*, SPIE 2005, pp. 624-635.

[15]Vlachos, P. P., Donnelly, M. J. and Telionis, D. P., "On the Wake of a Circular Cylinder Piercing a Water Free Surface," *Proceedings of FEDS'98*, FEDS98-5177, 1998 ASME Fluids Engineering Division Summer Meeting.

[16]Vlachos, P. P. and Telionis, D. P., "Turbulence Characteristics in the Wake of a Circular Cylinder Near the Free Surface," FEDSM2000-11320, Boston, MA, 2000.

[17]Klute, S. M., Vlachos, P. P. and Telionis, D. P., "High-Speed DPIV Study of Vortex Breakdown," *Fluid Dynamics Symposium, Fluids 2000 Conference*, also *AIAA Journal* (in press).

[18]Asimopoulos, N., Vlachos, P. P., Telionis, D. P., "A High Speed, High Particle Density Particle Tracking Method for Turbulent Flows," ASME FEDSM'99-7139.

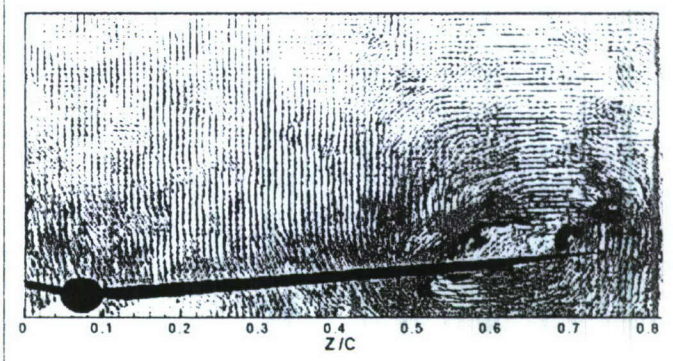

(a) no control

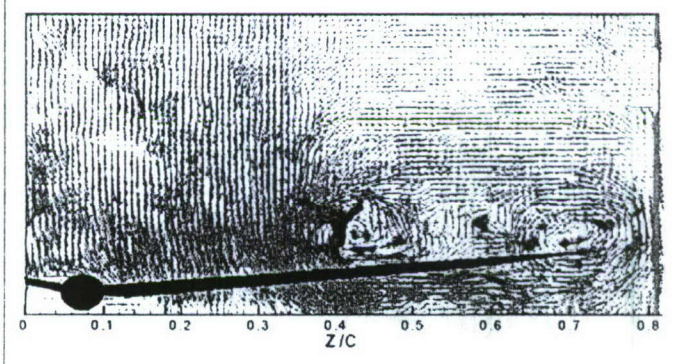

(b) control

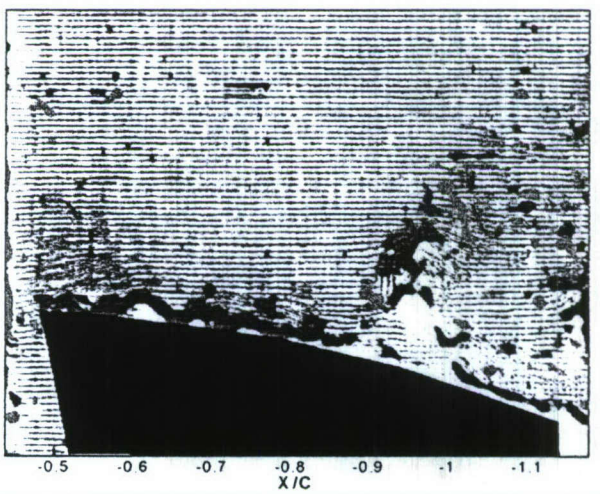

(c) control

Figure 5: Instantaneous frames at planes D, (a) & (b) and plane 5, (c).

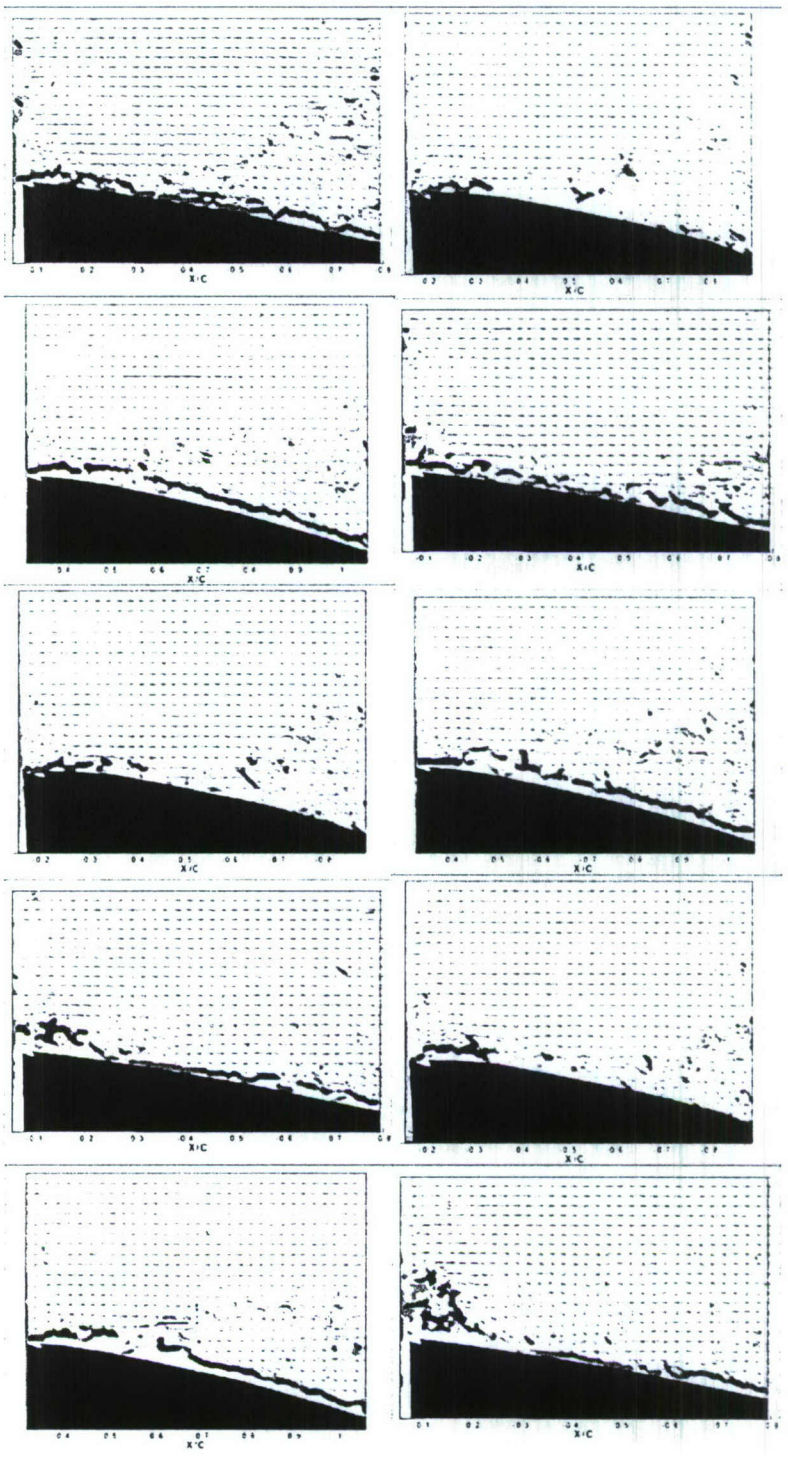

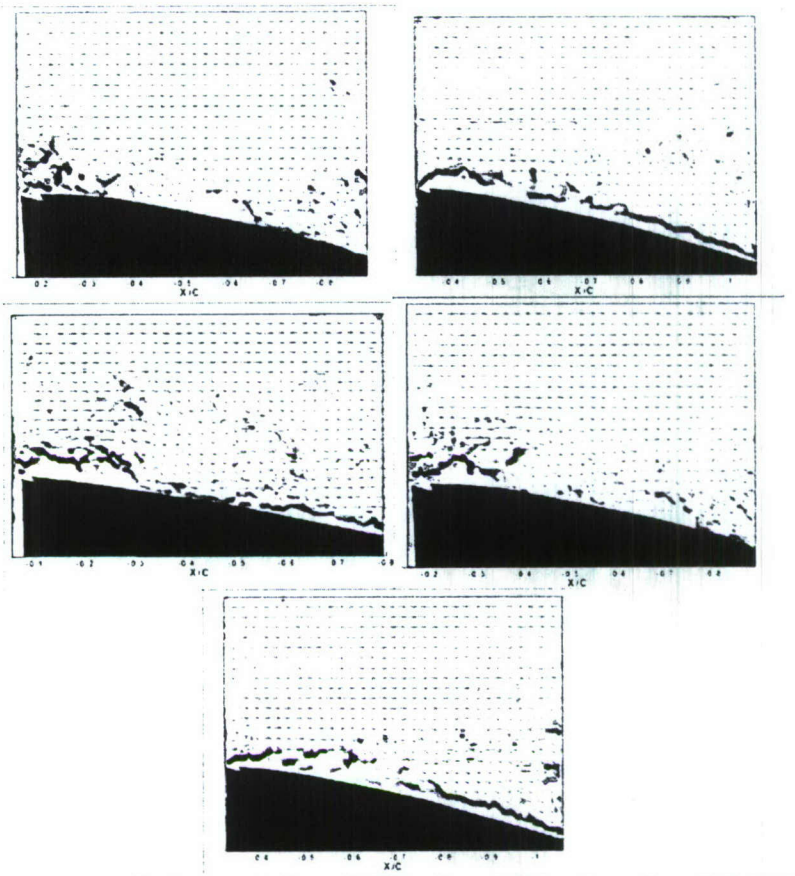

Figure 6: Instantaneous instances at planes 2 (left column), 3 (center column) & 4 (right column) with $\Delta t=T/8$.

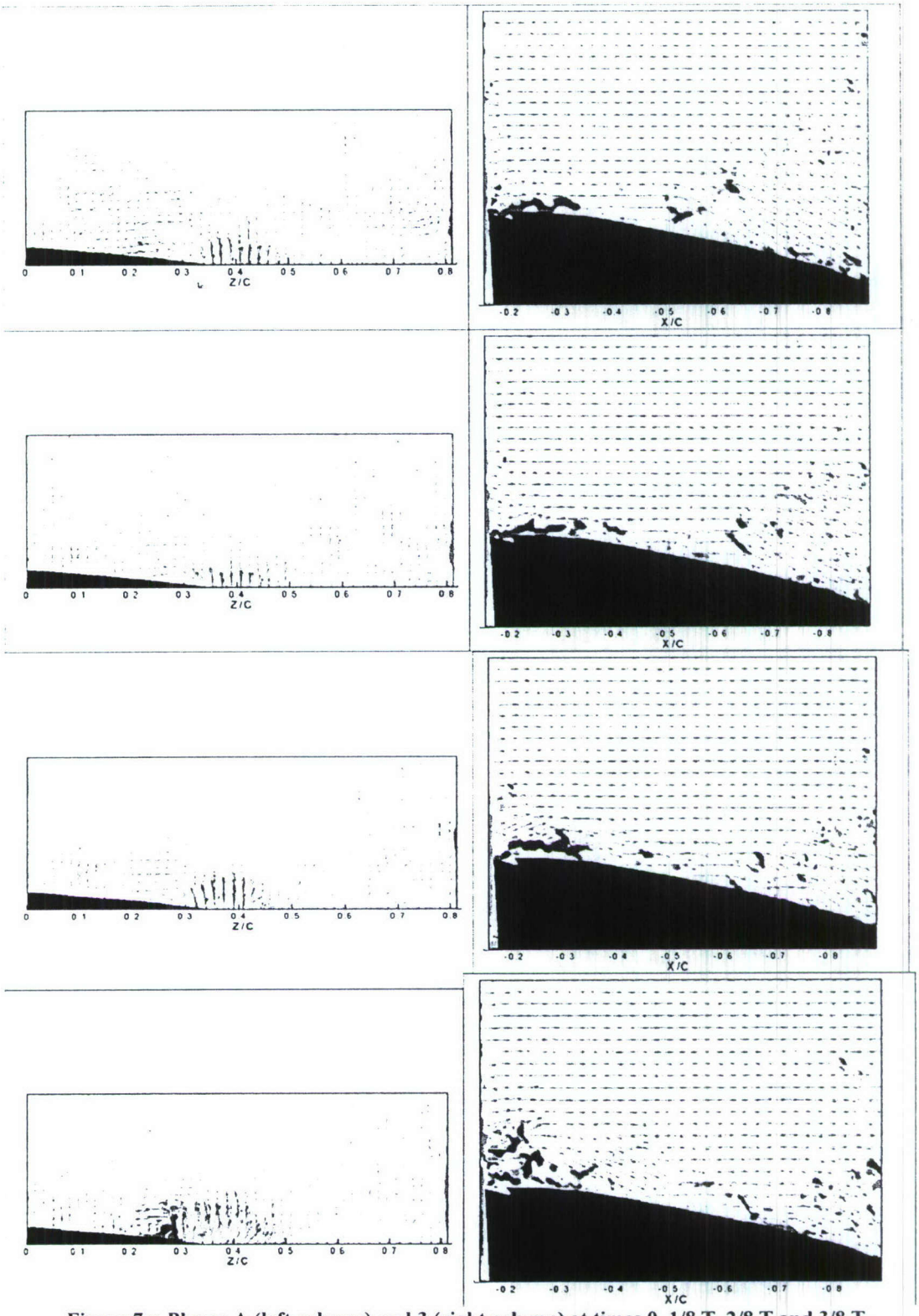

Figure 7a: Planes A (left column) and 3 (right column) at times 0, 1/8 T, 2/8 T and 3/8 T.

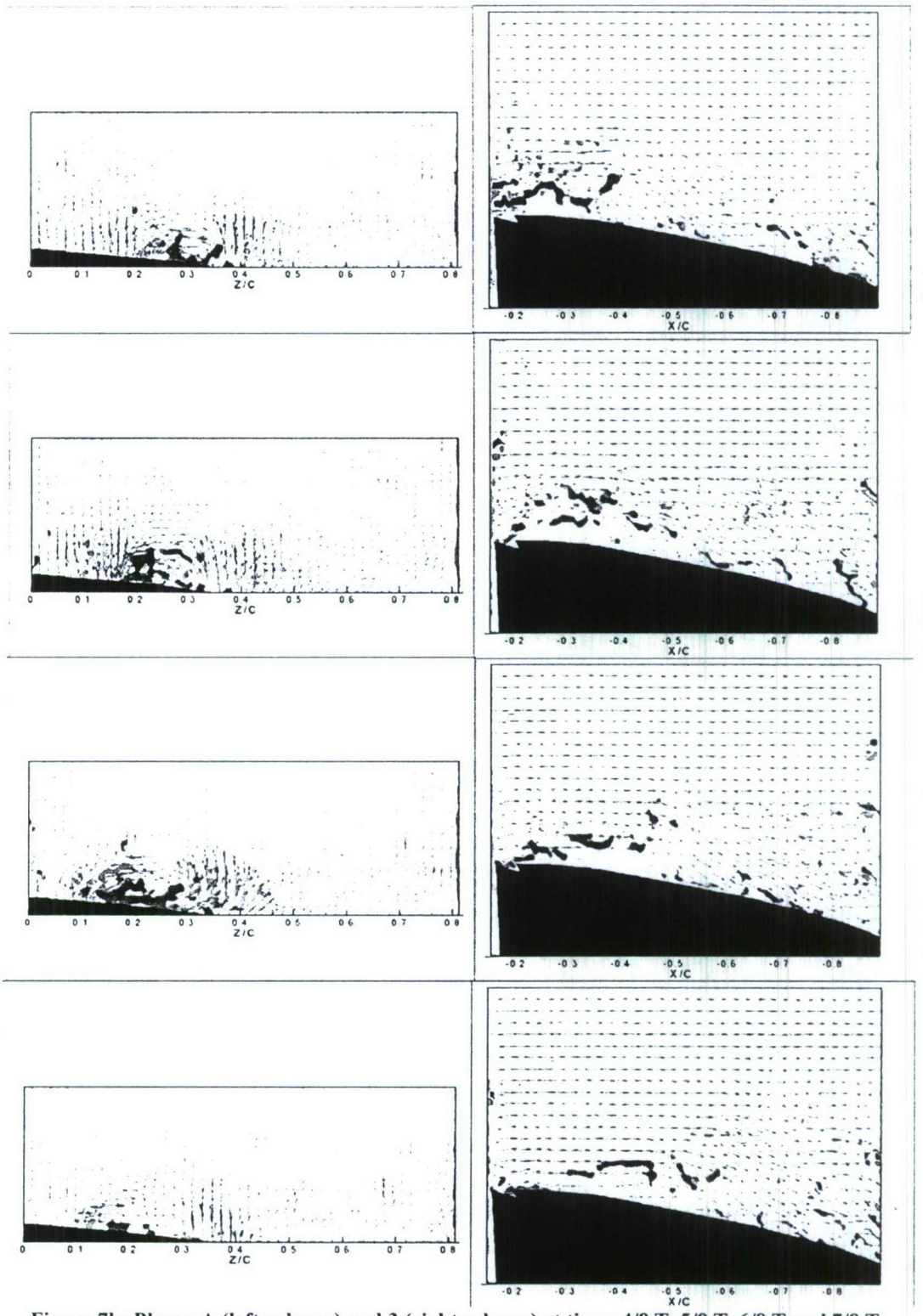

Figure 7b: Planes A (left column) and 3 (right column) at times 4/8 T, 5/8 T, 6/8 T and 7/8 T.

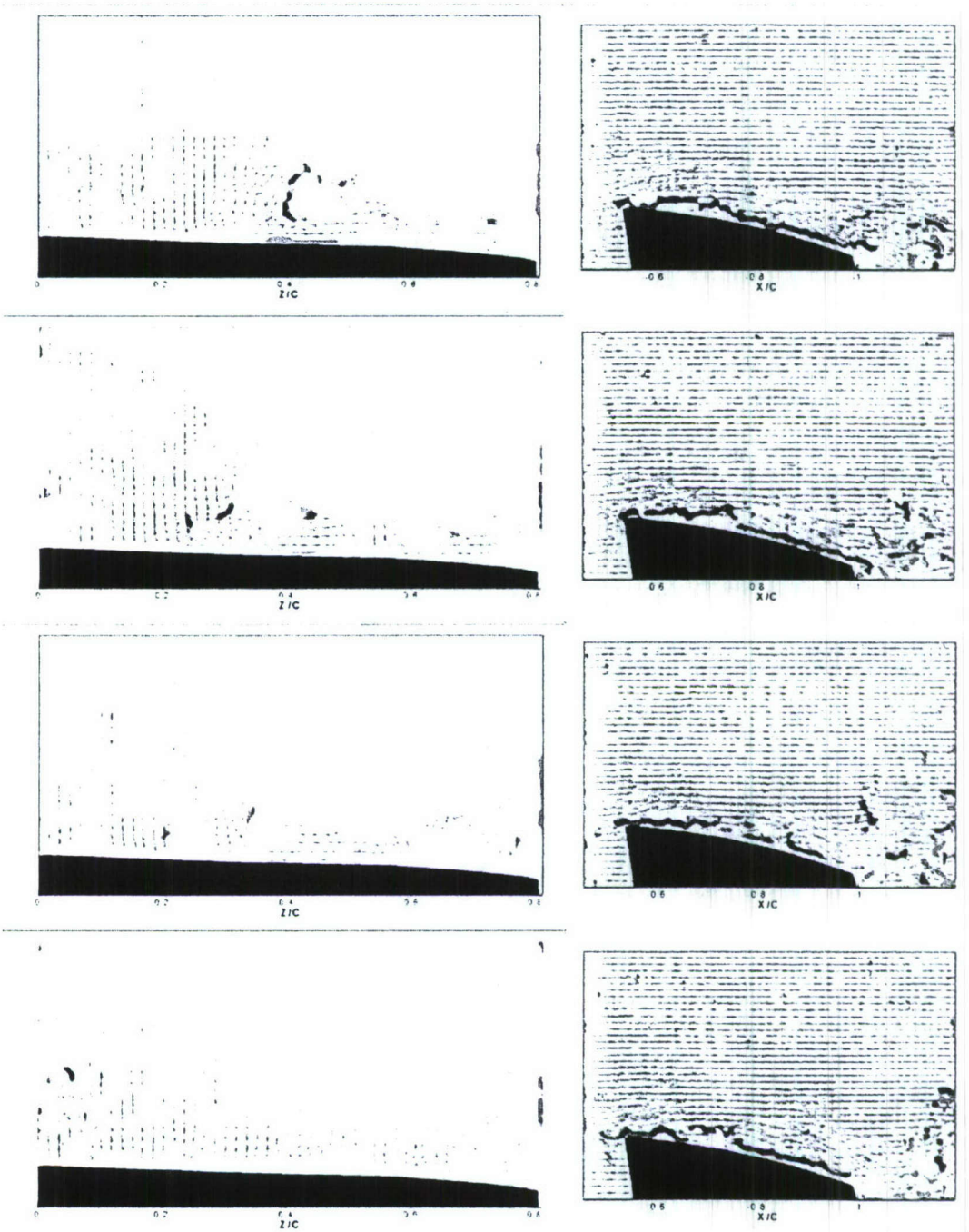

Figure 8a: Planes A (left column) and 3 (right column) at times 0, 1/8 T, 2/8 T and 3/8 T.

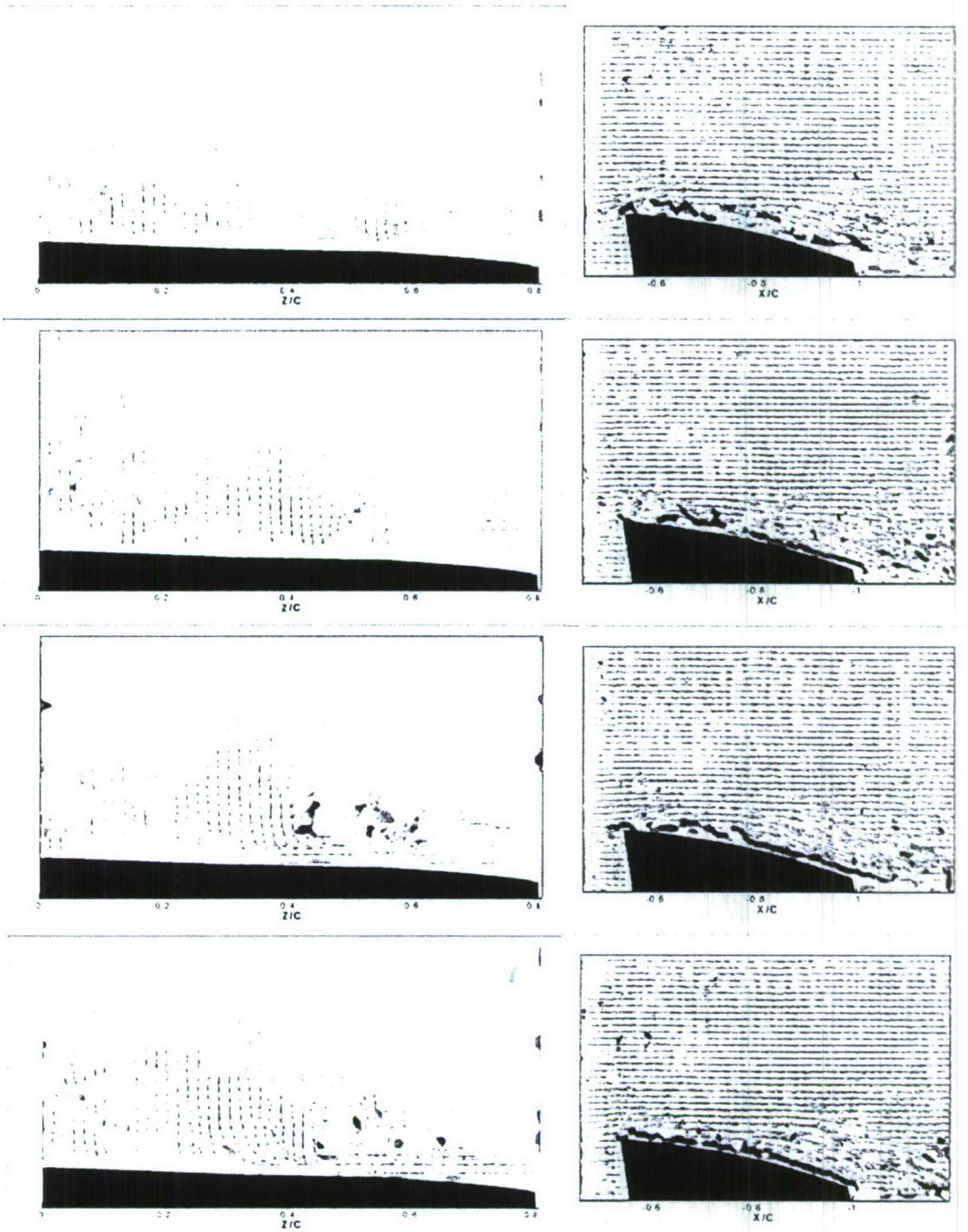

Figure 8b: Planes A (left column) and 3 (right column) at times 4/8 T, 5/8 T, 6/8 T and 7/8 T.

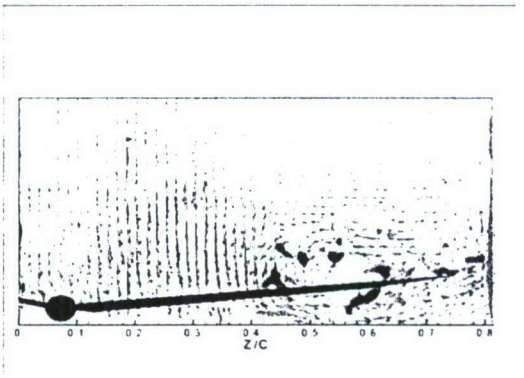
0 0.1 0.2 0.3 0.4 0.5 0.6 0.7 0.8
Z/C

(a)

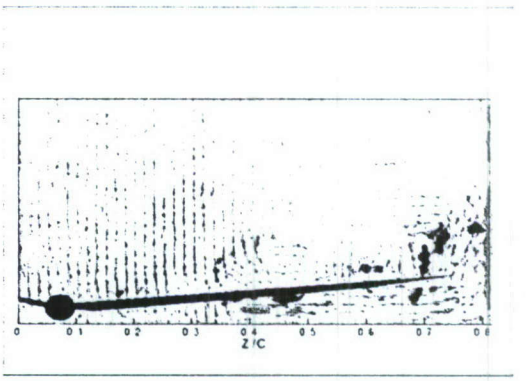
0 0.1 0.2 0.3 0.4 0.5 0.6 0.7 0.8
Z/C

(e)

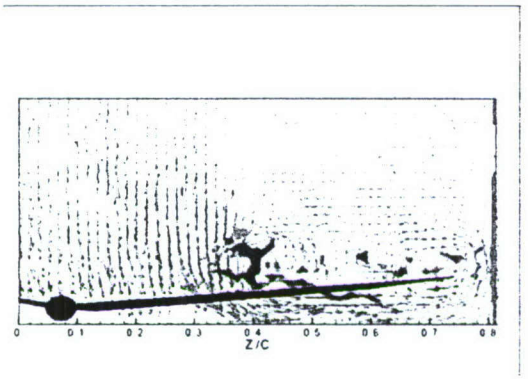
0 0.1 0.2 0.3 0.4 0.5 0.6 0.7 0.8
Z/C

(b)

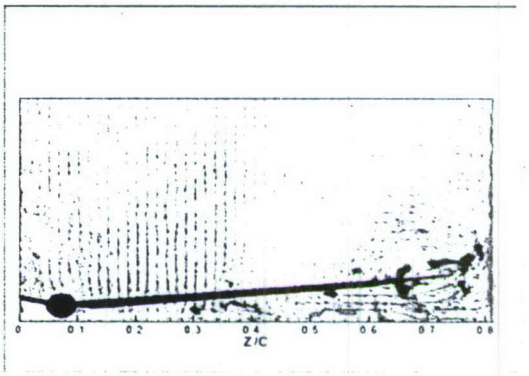
0 0.1 0.2 0.3 0.4 0.5 0.6 0.7 0.8
Z/C

(f)

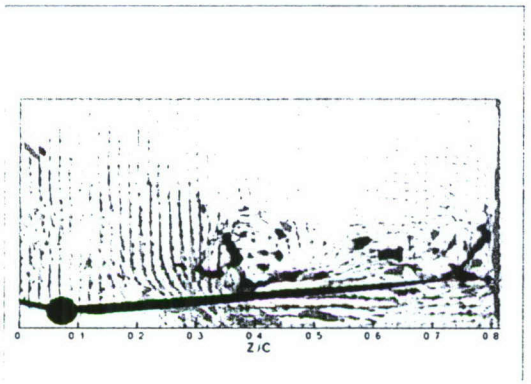
0 0.1 0.2 0.3 0.4 0.5 0.6 0.7 0.8
Z/C

(c)

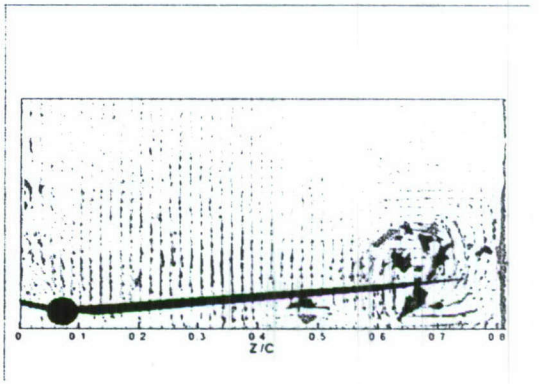
0 0.1 0.2 0.3 0.4 0.5 0.6 0.7 0.8
Z/C

(g)

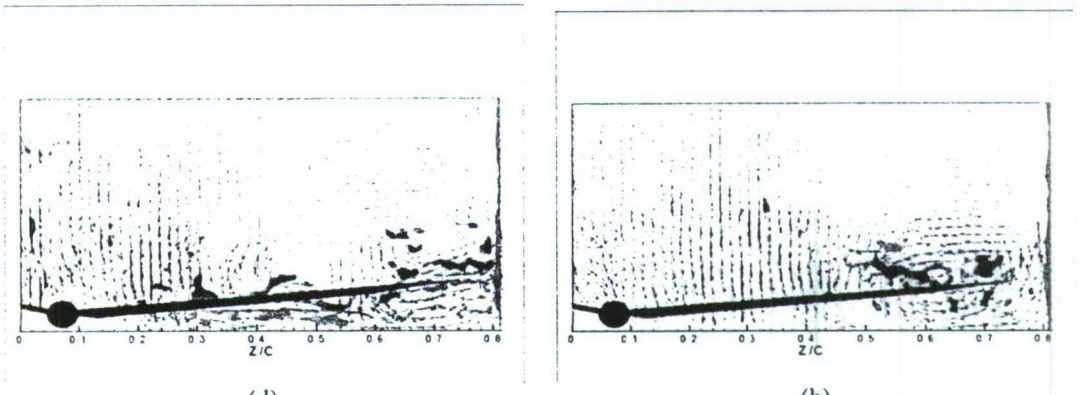

(d) (h)

Figure 9: Instantaneous data of Plane D at eight equally spaced instances of period.

7 FLOW CONTROL OF SWEPT WINGS – PRESSURE DISTRIBUTIONS

Wings swept by 30 to 40 degrees are today very common in fighter aircraft. And yet, there is very little work devoted to the understanding of the aerodynamics of such wings. In this report we study the aerodynamics and the flow control of two sharp-edged wing models. Two control mechanisms are employed, an oscillating mini-flap and a pulsed jet. Our Model A is a finite wing with parallel leading and trailing edges and a rectangular tip. This wing is swept by 0^0, 20^0, and 40^0. Our Model B is a wing with a diamond planform, with a leading edge sweep of 42^0. Surface pressure distributions are obtained and the control flow results are contrasted with the no-control cases. Our results indicate flow control is very effective at 20^0 sweep, but less so at 40^0 or 42^0. It was found that steady spanwise blowing is much more effective at the higher sweep angle.

Nomenclature

α= Angle of attack
b= semi-span
c = root chord
h= slot height
l= slot length
T= period of pulsing jet
x,y,z = coordinate system (see Fig. 3)
U_∞ = Characteristic velocity (free stream)
u_{jet} = Pulsating jet velocity
C_μ =momentum coefficient = $(\rho_{jet}\, u_{jet}^2\, h\, l) / (\rho_\infty\, U_\infty^2\, 2b\, c \sin\alpha)$
$f_{shedding}=0.21U_\infty/(c \sin\alpha)$
$f_{actuating}$=driving frequency
$F=f_{actuating}/f_{shedding}$

7.1 Introduction

Wings with sharp leading edges are most efficient at supersonic speeds. They also significantly reduce radar signature. But at low speeds, sharp-edged wings have notoriously poor aerodynamic performance, and require large leading-edge flaps for take-off and landing, or for low-speed maneuvering. Flow control can generate extra lift over

sharp-edged wings at low speeds, and has proven to have an effect equivalent to the deployment of a large leading-edge flap[1-5].

There is a considerable volume of literature for steady flow over sharp edged wings swept by over 40°, and the vast majority of these contributions deal with delta wings. But for a wing with sharp leading and trailing edges, at zero sweep angle, the authors were able to find only a NACA report published about fifty years ago[6]. The first authors to report efforts to control the flow over wings with sharp leading edges are Zhou et al.[1] Since then, the present team has published a sequence of papers[3-5,7,8] on the flow control of sharp-edged wings at low to moderate angles of attack and sweep angles varying between zero and 40°.

Research on delta wing flows for sweep angles as low as 50^0 indicate that delta wing vortices are present, but break down very close to the leading edge[9-13]. In fact, even before break down, these vortices display wake-like flow where the velocity is very low in the core of the vortex. In some cases[4] it was found that the low aspect ratio wing at medium angles of attack does not behave like a delta wing but rather like an unswept wing. A sweep angle of 50^0 is not low enough to demonstrate the transition from the vortex breakdown stall to the two-dimensional unsteady stall. More recently, Yaniktepe and Rockwell[13] studied the flow over a wing with a sweep angle of 38.7^0. They provided evidence that up to an angle of attack of 25^0, the flow appears to be dominated by delta wing tip vortices. At the highest angle of attack, the vortices seem to be displaced inboard. But more detailed measurements along planes parallel to the free stream[7] indicate the presence of multiple axial vortices, as well as separated flow patterns similar to those observed over unswept wings. The most common sharp-edged airfoil section studied is the circular-arc airfoil which has been employed both in laboratory studies[6] as well as aeronautical applications. The flow over airfoils with sharp leading and trailing edges separates at angles of attack as low as 6°.

Zhou et al.[1] and Miranda et al[3] placed a min-flap at the leading edge of the pressure side of sharp-edged wings, and demonstrated that oscillating this mini-flap could lead in the average to lift increases of up to 70%. The present authors designed a pulsed-jet actuator, in order to demonstrate that similar effects with those of oscillating mini-

flaps could be achieved pneumatically[4]. But the sections of Zhou et al.[1] and Rullan et al.[5] had a thickness ratio over 10%. As it turned out, the flow over thick sharp-edged airfoils does not separate massively, even at angles of attack as high as 9°.

We should emphasize here that we control fully separated flow. In earlier contributions on airfoil flow control the aim was to delay separation and stall altogether. The control of fully-separated flow has received so far little attention, even though it has a greater potential in defense applications. Such flows are encountered over sharp-edged wings at low to moderate angles of attack or over wings in deep stall. The idea is to accept the fact that in some situations, the flow is fully separated, and periodic shedding of vortices is established. The aim then becomes to control the dynamic development of vortical structures in order to improve the performance of the lifting surface. These are the type of flows that develop over wings moderately swept and the focus of the present research.

The present team has undertaken an exhaustive study of flow control over swept and unswept edges at low and intermediate angles of attack using both oscillating mini-flaps and a pulsed jet actuator. Experiments were carried out at Reynolds numbers ranging 10^4 to 10^6. We reported earlier[7] results obtained in a water tunnel for a wing with a leading edge swept by 40°. For this case we presented exhaustive PIV time-averaged and time resolved, data for steady flow. In the present paper we present pressure data obtained over two models, tested in two wind tunnels, at Reynolds numbers of 5×10^4 and 10^6. The VA Tech Stability Tunnel is shown in Fig. 1. The first model, Model A is a circular-arc airfoil, with parallel sharp leading and trailing edges. This was mounted at its root, and thus allowed the examination of tip effects, at sweep angles of 0°, 20° and 40°. The second model, Model B, is a trapezoidal wing with a sweep angle of 42°, and a planform typical of modern fighter aircraft. Model A was equipped with the pulsed-jet actuator

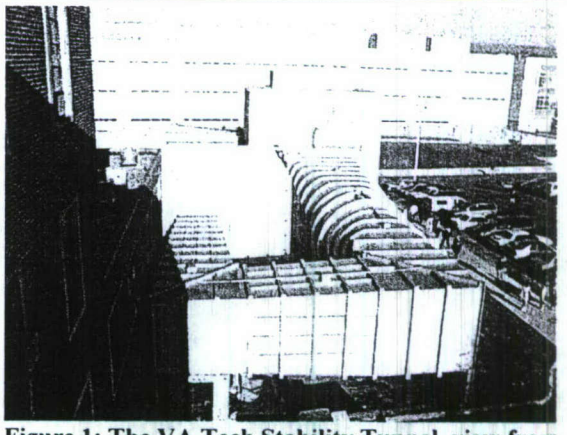

Figure 1: The VA Tech Stability Tunnel, view from Randolph Hall

developed by the present team[4,8]. Model B was equipped with oscillating min-flaps and spanwise blowing nozzles.

7.2 Facilities, Models and Equipment

Facilities and Models

Two wind tunnel facilities were used, the ESM Wind Tunnel and the VA Tech Stability Tunnel. The first is a low-speed tunnel with a 20"x20" test section. Basic ideas and instrumentation are tested there before moving on to the other tunnel. The second facility, the VA Tech six-foot subsonic wind tunnel (Fig. 1), originally the NACA Stability Tunnel is classified as a continuous, closed-jet, single return, subsonic wind tunnel. One of our models mounted on the tunnel sting is shown in Fig. 2. The tunnel is equipped with 25-foot interchangeable, round and square test sections of six foot cross section. The tunnel is powered by a 600 hp DC motor driving a 14 foot propeller that provides a maximum speed of 230 ft/sec and a Reynolds number per foot up to $1.4X10^6$ in a normal 6'x6' configuration. The settling chamber has a contraction ratio of 9 to 1, and is equipped with seven anti-turbulence screens. This combination provides an extremely smooth flow in the test section. The turbulence levels vary from 0.018% to 0.045% depending on the free-stream velocity. The average velocity

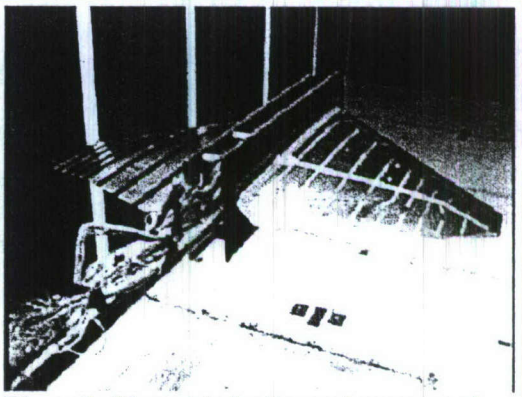

Figure 2: Diamond planform wing mounted on the Stability Tunnel sting

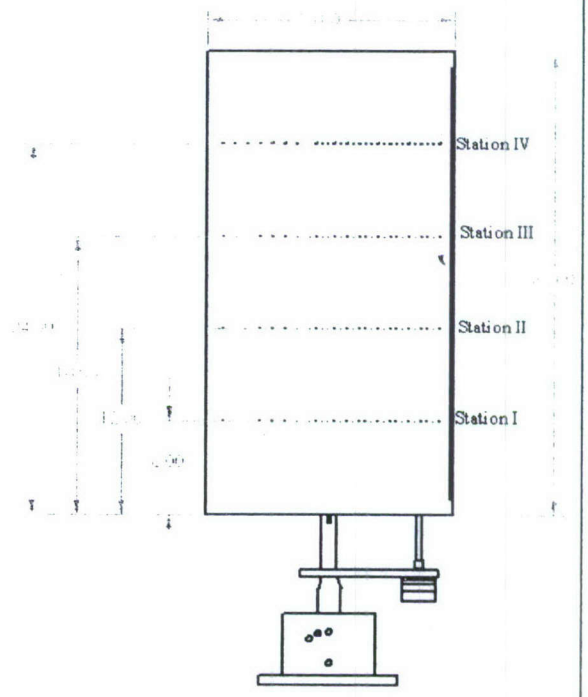

Figure 3: Model A showing the pressure tap strips. Also shown is the motor that drives the pulse-jet actuator

fluctuation across the test section is about 0.5%, and flow angularities are limited to 2° maximum. The settling chamber is 9 feet long and the diffuser has an angle of 3°. The ambient temperature and pressure in the test section are nearly equal to the ambient outdoor conditions due to the presence of an air exchanger. During testing, the control room is maintained at the same static pressure as the test section.

We carried out experiments with two basic models. Model A (Fig. 3) is a rectangular circular-arc wing that can be mounted at different sweep angles, and angles of attack. We have tested two such wings in the past at low and high Reynolds numbers, with both oscillating mini-flaps and unsteady leading-edge blowing (Miranda et al.[3], Rullan et al.[8]). The present model, Model A has a smaller thickness ratio (10%) and a larger aspect ratio that improves the delivery of pulsed jets. This model was mounted on the floor of the tunnel via a mechanism that allowed the setting of the angle of attack at any desired value and the sweep angle at the values of 0^0, 20^0 and 40^0. The model tip reached very close to the middle of the tunnel, and thus the mounting allowed the study of three-dimensional effects. This model is equipped with an unsteady jet actuator, which is described later. Pressure taps were placed along four chordwise lines on both the pressure and the suction side, as indicated in Fig. 3. The spacing of the taps was smaller on the front part of the model. The four stations are labeled with Roman numerals as shown in the Figure.

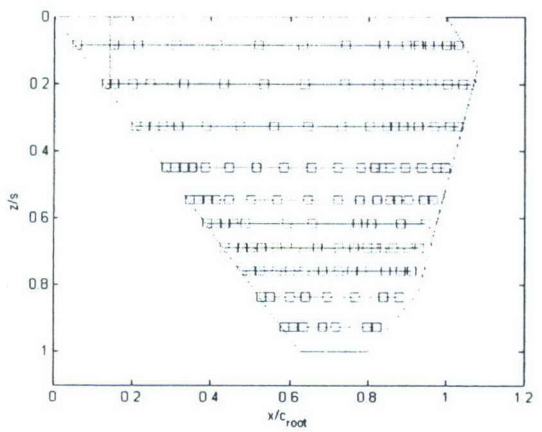

Figure 4: Model B, showing pressure tap locations and spanwise blowing nozzles. Ten chordwise stations are shown, referred to in the text as Stations 1 through 10, starting from the root side.

Our second model, Model B (Fig.4) is a diamond-planform wing with a leading-edge sweep of 42°. This model is a stainless-steel model on loan by Lockheed Martin, equipped with pressure taps. The flow over this model is controlled by an oscillating mini-flap device, similar to the one already tested on circular-arc wing sections[3]. The spanwise stations are numbered with

numerals starting from the root side of the wing. We have also designed, constructed and tested two similar but smaller diamond-planform wings that were tested in our water tunnel and in our low-speed wind tunnel at low Reynolds numbers.

Pressure scanners were employed to monitor the pressure distributions over wind tunnel models. Two 32-channel ESPs by Pressure Systems Inc. monitor the pressure distribution along spanwise stations over both models. Data were obtained along ten stations over the suction side of Model B and seven stations over its pressure side.

Equipment

Pressure scanners by Pressure Systems Inc. have been extensively used in our laboratory. These scanners are small, high-density packages containing multiple differential sensors. ESP packages contain 8, 16, 32 or 64 channels. Each pressure sensor is a miniature piezoresistive pressure transducer, and all of the pressure transducers in a module share a common silicon substrate. The output of each transducer is internally amplified to ±5 V full-scale, and these analog outputs are multiplexed within the scanner. The settling time inherent in the multiplexer corresponds to a maximum sampling rate of 20 kHz. This allows near-simultaneous sampling of the ESP. For instance, thirty-two ports can be sampled in 1.6 ms. However, the pressure port geometry limits the frequency response of the ESP to 50 Hz at the pressure inputs. Since the transducers are differential, a reference pressure must be chosen. In all cases in the present work, the reference pressure was the tunnel free-stream static pressure. The static accuracy of the ESP's, including nonlinearity, hysteresis and non-repeatability effects, is 0.10% of the full scale at constant temperature after a full calibration.

On many occasions, we have placed miniature ESP scanners inside the wind tunnel models, thus minimizing the length of the Tygon tubing. This allows the monitoring of dynamic phenomena with frequencies up to about 50 Hz, with less than 2% error in the peak values. Data over the 16-inch-chord model (Model A) discussed in the previous section were obtained with the pressure scanner located at the supporting base. To obtain pressures over Model B, we mounted the pressure scanners near the root of the wing.

Flow Control Mechanisms

The actuation mechanism on Model A consists of a pressurized plenum, essentially the inside of the entire wing, and a valve that allows a jet to issue out of the plenum. This valve consists of two concentric cylinders shown in Figure 5. This is essentially the leading sharp edge of the airfoil. The inner cylinder, a 7/16"-inch diameter brass tube has two 1/16" wide slots, which span its length. This cylinder is mounted on five bushings and rotates about a fixed axis inside a fixed outer cylinder created in the machined wedge. Tube was fixed to a motor drive shaft so that it can be driven by a small DC motor as shown in Fig. 3. The last two bushings are used to stabilize the tube in the machined leading edge but allowing rotation at the same time. All the bushings were press-fit to insure that the inner and outer cylinders are sealed tightly in order to maintain sufficient pressure in the inner cylinder.

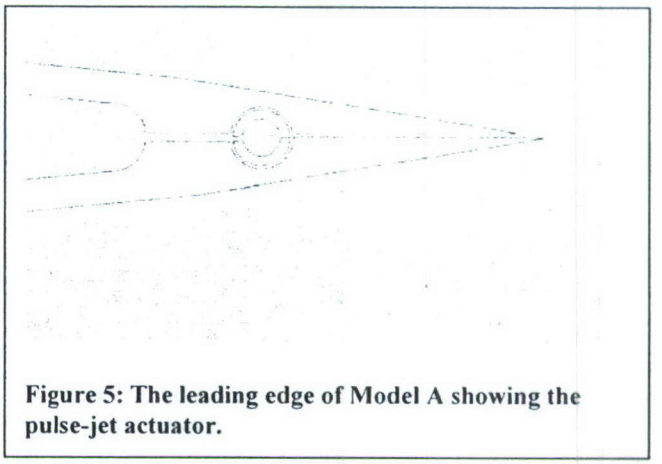

Figure 5: The leading edge of Model A showing the pulse-jet actuator.

This device operates as follows. The plenum is continuously supplied with high-pressure air and is driven in rotation at a fixed frequency. When the slots of the inner rotating tube and the fixed outer tube match as shown in the Fig. 5, the pressurized cavity releases air in the form of a jet. The flow is guided by the 1/16-width duct and released very close to the apex of the wedge. When the slots of the inner and the outer cylinder do not match, the passage is closed but some air leaks between the two cylinders and finds its way through the duct. The jet therefore has a non-zero mean component with an unsteady flow superimposed. Our earlier experimental data[8] indicate that the efficiency of this actuator is practically independent of the frequency. In Fig. 6 we display the jet velocity time record and the corresponding power spectrum for one of the cases tested. This Figure indicates that if the cylinder is not rotating, leaking through the passage between the cylinders generates a steady jet, but when the inner cylinder rotates, a puling jet issues. And there wave form is clean, in the sense that most of the energy resides in a narrow frequency band around the driving frequency. The modified design that includes a

larger plenum proved that uniform and more powerful pulsing jets could be generated along the span of the airfoil. This means that the device is an excellent candidate for a robust flight actuator, where the required frequency is changing with aircraft speed and the angle of attack.

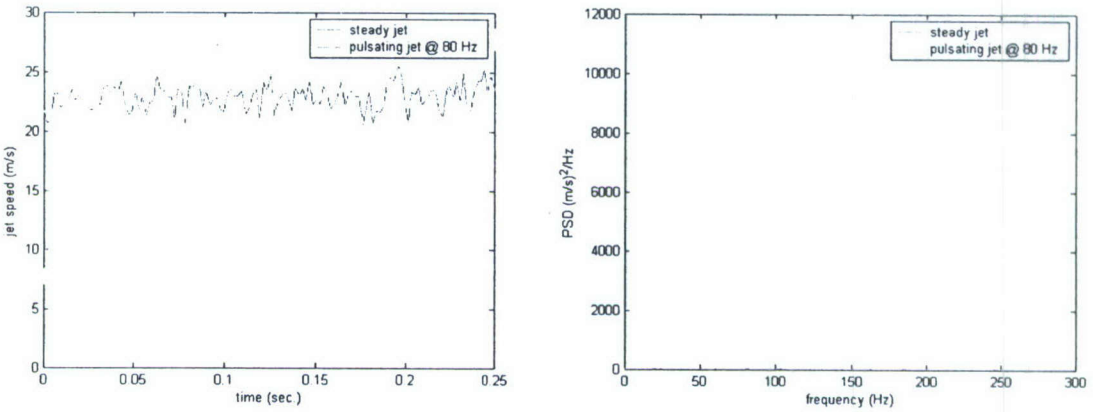

Figure 6: Jet velocity time series and power spectrum generated by the pulsed-jet actuator

A pulsed-jet actuation mechanism does not fit near the leading edge of Model B. Instead we employed an oscillating mini-flap that has proven to be equally effective with unsteady blowing[4,7,8]. Miniflaps we employed earlier were hinged downstream of the leading edge and were flushed with the wing section when not deployed. The flap mounted on Model B was hinged right along the leading edge and thus protruded forward. Two flap configurations were tested; one that spanned half of the length of the wing, starting from the root and another that spanned the entire length of the leading edge. These miniflaps were oscillated by a brushless DC motor connected to a flywheel which is equipped with an eccentric shaft. The flywheel is balanced statically to work with minimum vibrations at speeds in the order of 100 Hertz. The amplitude of oscillation could be adjusted with an accuracy of $\pm 1°$.

The DC motor employed for both mechanisms is a Pittman brushless DC servo motor that operates at 24 VDC. It features 3 Hall sensors for feedback control so as to obtain linear torque. It is operated with an Allmotion EZSV23 servo motor controller which in turn is connected to a PC by a serial port. This provides a direct frequency control of the

motor. A wire was connected from the output of one of the Hall sensors to obtain a read-out and to record the actual driving frequency.

7.3 Results and Discussion

A. Model A; Pulsed-Jet Actuation

Experiments were carried out with Model A, at a Reynolds number of one million, for three different angles of sweep, namely 0, 20 and 40 and several angles of attack. The pulsed-jet mechanism was activated at two different momentum coefficients. Data were also obtained with no actuation to provide comparison for the no-control case. The results are presented in Figs. 7-11 for a sweep angle of zero, Figs. 12-16 for an angle of 20^0 and Figs. 17-21 for an angle of 40^0. In all these figures an underline feature of flow control must be observed. Regions of fully separated flow can be recognized by a relatively horizontal and flat pressure distribution. And regions of strong suction that appear like local humps of the pressure distribution may indicate a large vortex that is captured in this area of the wing. It is in these regions that the control mechanism is most effective. It should also be emphasized that for the angles of attack larger than 15^0, the flow cannot reattach. Our control mechanism therefore is modifying the development of vortices in the separated region. In all the figures of this section, we present pairs of frames, with the left frame corresponding to Stations I and II, which following the notation of Fig. 3 are close to the root of the wing and the right frame corresponding to Stations III and IV, which are in the outboard part of the wing.

The case of zero sweep tested here does not correspond to two-dimensional flow, because the wing spans about half of the width of the tunnel. The tip effect is therefore significant. We are testing a finite wing, and thus we are exposing the effects of flow control to the aerodynamics of the wing tip. Figure 7 indicates that a vortex is captured near the leading edge of the wing. Evidence to this effect was reported earlier by the present authors[8]. Further downstream, the flow in the inboard section may be attached. Here actuation has little effect, confined mostly to the leading-edge region. For higher angles of attach (Figs. 8-11), actuation is more effective. It is intriguing to note that

actuation results in pressure distributions reminiscent of attached flow over airfoils, namely strong suction on the front that decreases sharply towards the aft region of the wing. What is surprising is that flow control is very effective in the outboard region as well. A possible explanation of this phenomenon is the following. Reduction of local circulation and of pressure suction near the tip is due to the tip vortex, clearly a three-dimensional effect. Our actuation on the other hand activates and energizes vortices that are normal to the free stream, and thus parallel to the wing axis. It is the pressure imprints of these vortices that when averaged, they produce the increased suction over the wing surface. Apparently energizing such vortices allows them to penetrate further in the outboard region and thus suppress that tip effects. This phenomenon is more pronounced at higher angles of attack (Figs. 10 and 11), where we observe that the increase in suction due to flow control is even stronger in the outboard region than in the inboard region. A surprising finding here is that actuation seems to be effective at much higher angles than those we have tested on other models. Working at lower Reynolds numbers and a model with oscillating flaps, we found that actuation effect was barely discernible at angles of attack higher than 15^0.

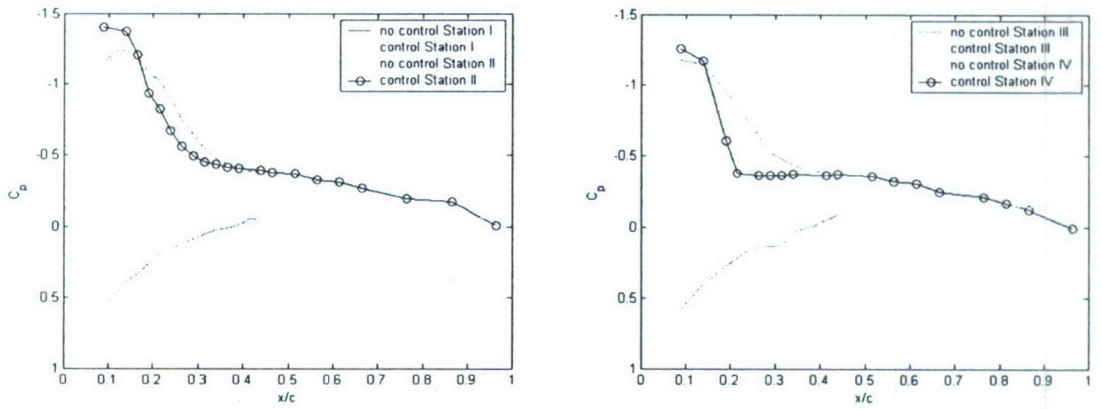

Figure 7: Pressure distributions for zero sweep at $\alpha=9^0$. Stations I and II (left); III and IV (right)

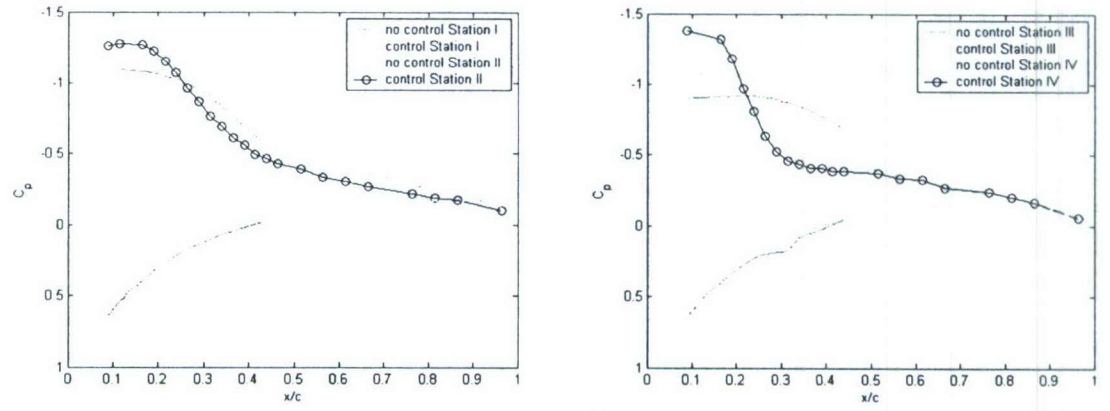

Figure 8: Pressure distributions for zero sweep at $\alpha=12^0$. Stations I and II (left); III and IV (right)

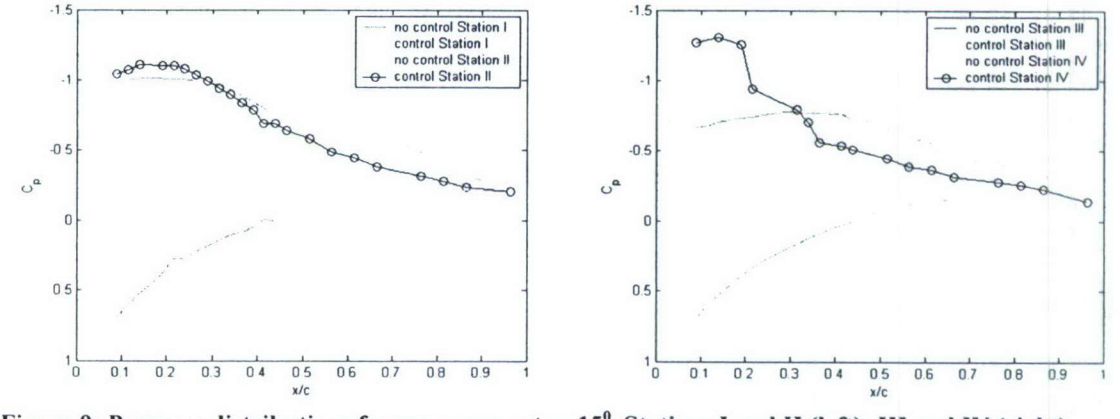

Figure 9: Pressure distributions for zero sweep at $\alpha=15^0$. Stations I and II (left); III and IV (right)

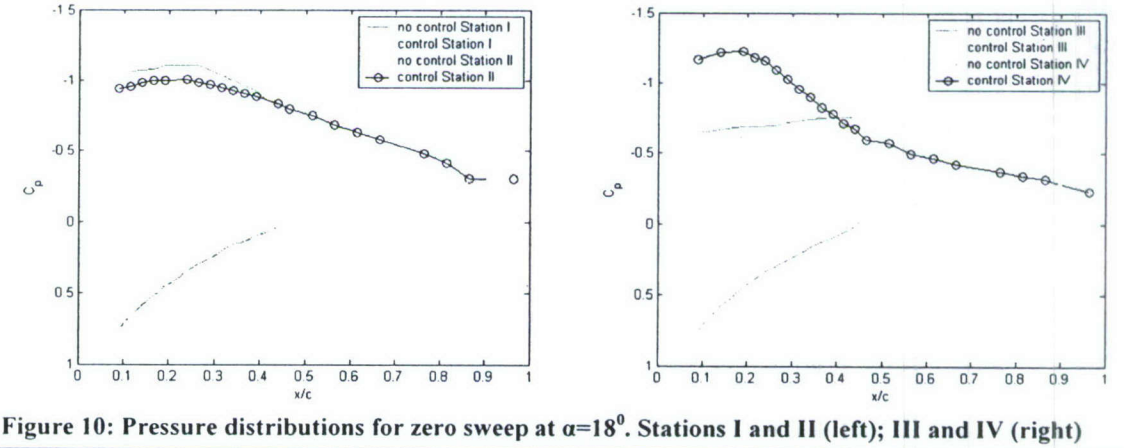

Figure 10: Pressure distributions for zero sweep at $\alpha=18^0$. Stations I and II (left); III and IV (right)

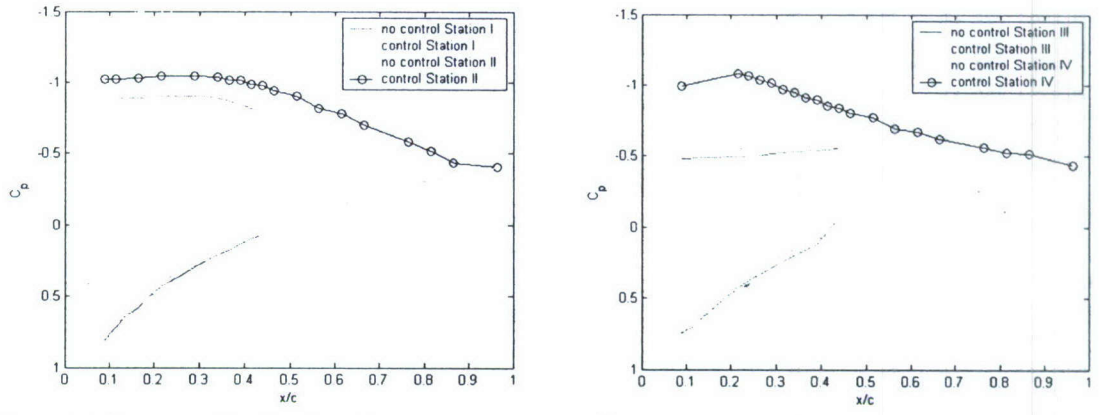

Figure 11: Pressure distributions for zero sweep at $\alpha=21^0$. Stations I and II (left); III and IV (right)

For a sweep angle of 20^0 (Figs. 12-16) the qualitative behavior is almost the same. We find that the curves are "drawn" to the right, and thus pressure patterns are stretched towards the aft of the wing. But the effect of the control is equal and perhaps even stronger. However, for a sweep angle of 40^0, the effect of our flow control mechanism is reduced as shown in Figs. 17 to 21. This phenomenon of reduction in the effectiveness of actuation along the leading edge at high-sweep-angle wings has been observed earlier by the present authors[4] in experiments conducted at lower Reynolds numbers. The results for a sweep angle of 40^0 (Figs. 17-21) show considerable reduction in the effect of flow control. It may be necessary to increase the momentum coefficient beyond the value of 0.03 that was employed in all the tests discussed here. For angles of attack of 12^0 and 15^0 there is some increase in suction in the middle sections of the wing. We did not have the resources to test the case of a sweep angle of 30^0.

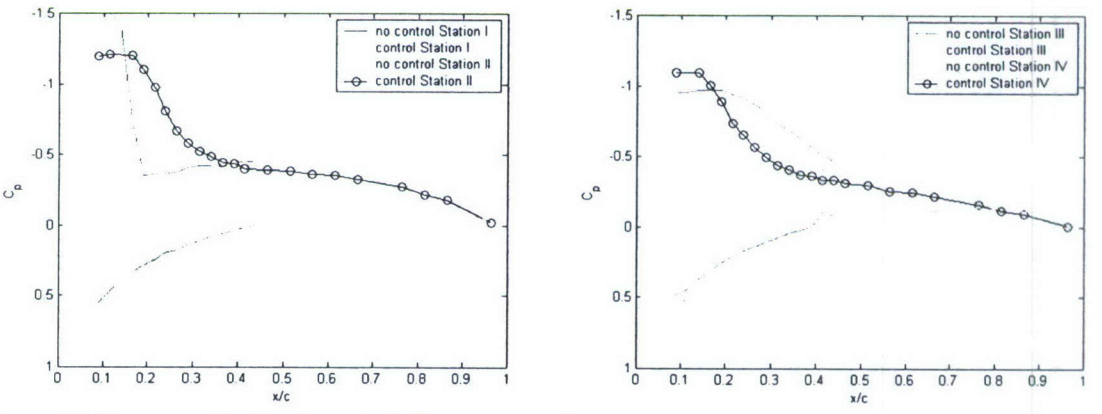

Figure 12: Pressure distributions for 20^0 sweep at $\alpha=9^0$. Stations I and II (left); III and IV (right)

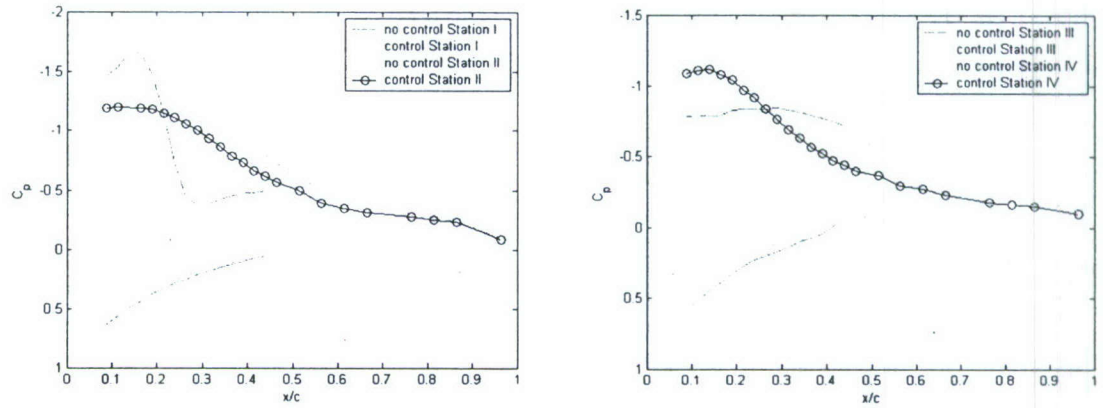

Figure 13: Pressure distributions for 20^0 sweep at $\alpha=12^0$. Stations I and II (left); III and IV (right)

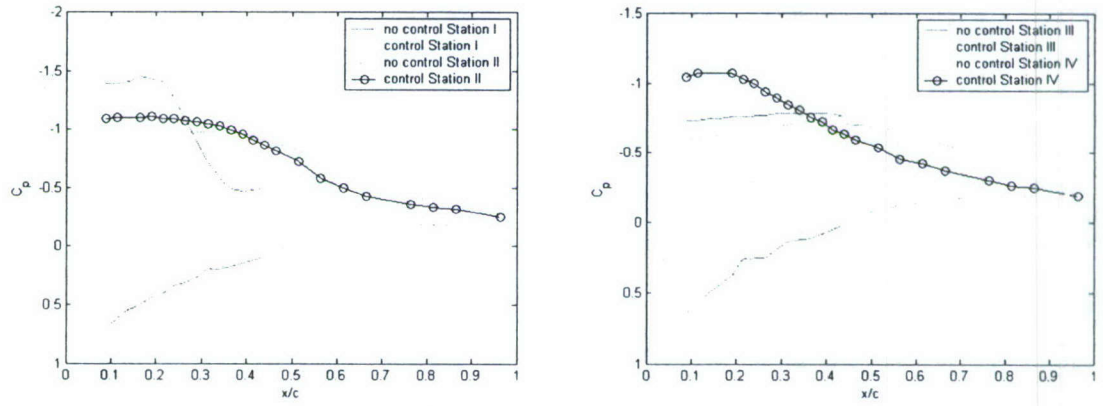

Figure 14: Pressure distributions for 20^0 sweep at $\alpha=15^0$. Stations I and II (left); III and IV (right)

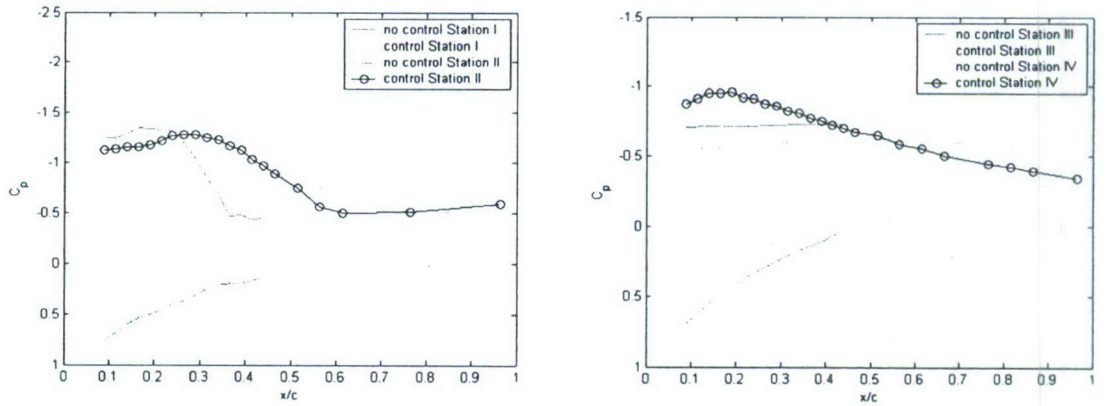

Figure 15: Pressure distributions for 20^0 sweep at $\alpha=18^0$. Stations I and II (left); III and IV (right)8

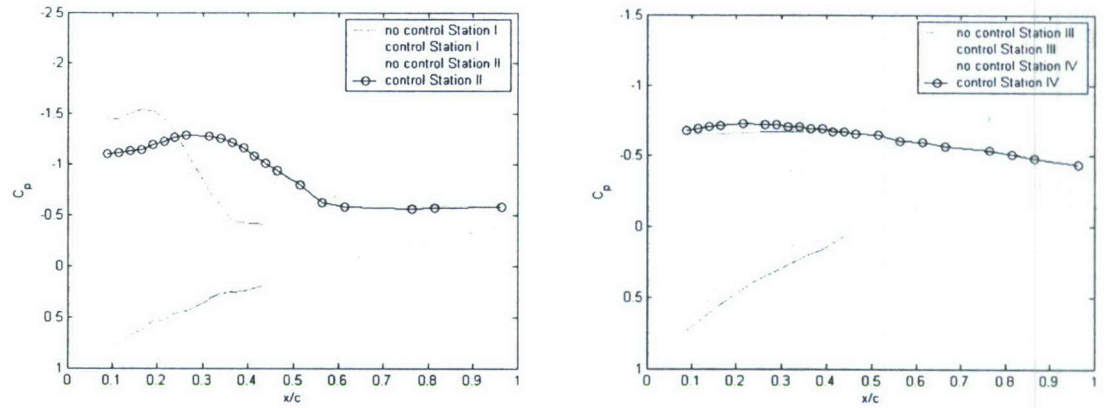

Figure 16: Pressure distributions for 20^0 sweep at $\alpha=21^0$. Stations I and II (left); III and IV (right)

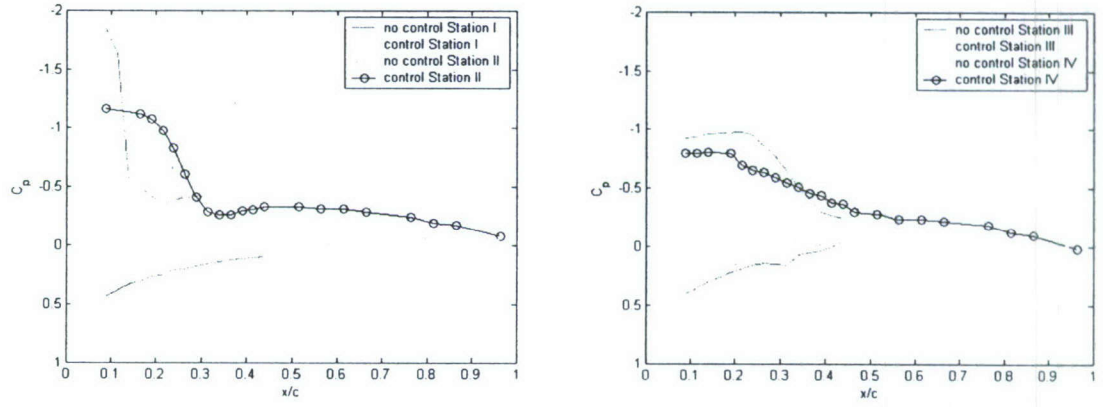

Figure 17: Pressure distributions for 40^0 sweep at $\alpha=09^0$. Stations I and II (left); III and IV (right)

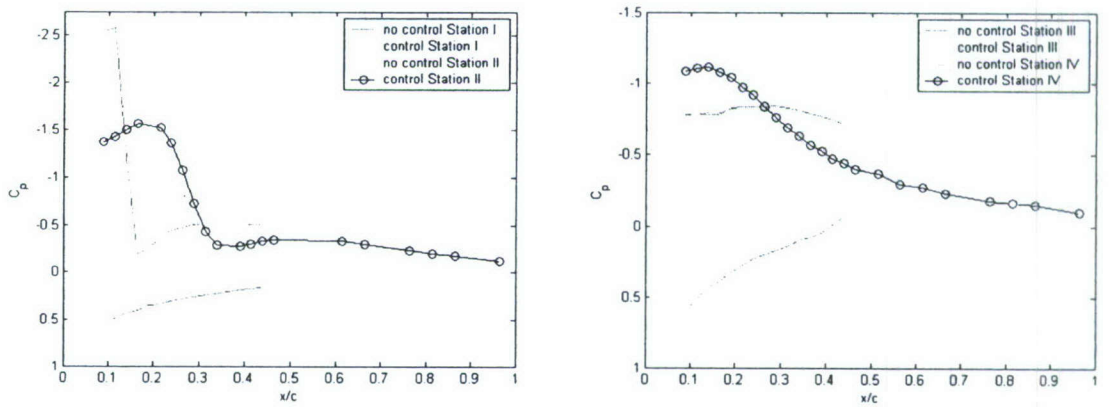

Figure 18: Pressure distributions for 40^0 sweep at $\alpha=12^0$. Stations I and II (left); III and IV (right)

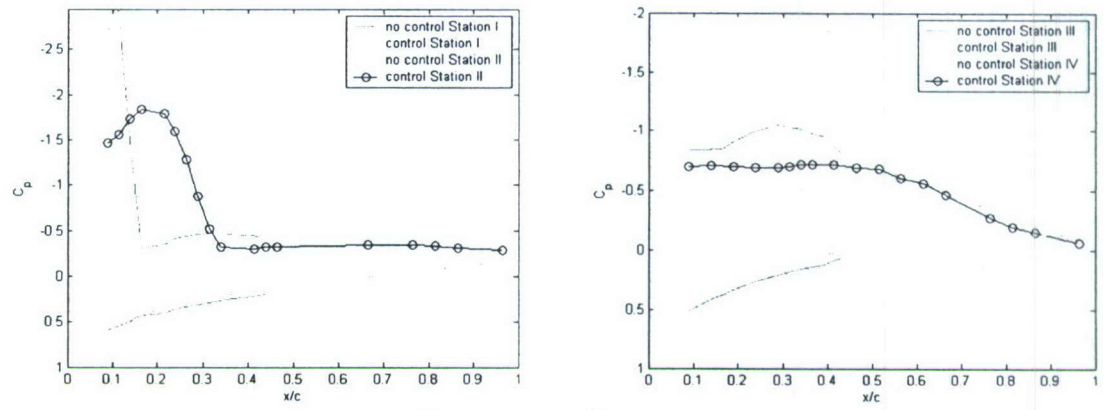

Figure 19: Pressure distributions for 40^0 sweep at $\alpha=15^0$. Stations I and II (left); III and IV (right)

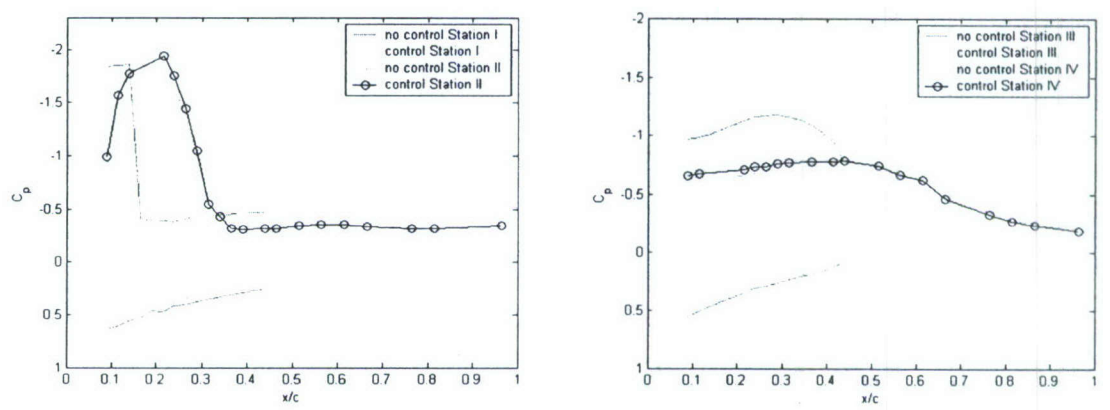

Figure 20: Pressure distributions for 40^0 sweep at $\alpha=18^0$. Stations I and II (left); III and IV (right)

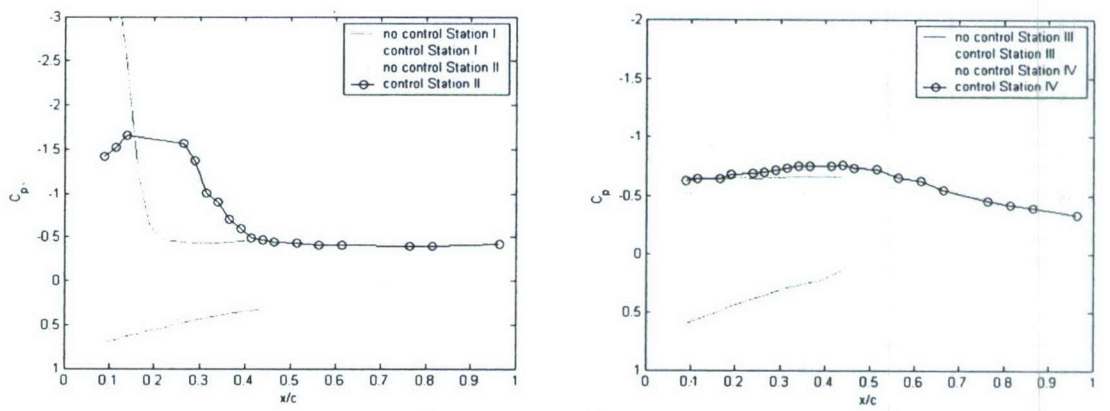

Figure 21: Pressure distributions for 40^0 sweep at $\alpha=21^0$. Stations I and II (left); III and IV (right)

B. Model B; Oscillating-Flap Actuation

The leading edge of Model B is swept by 42^0. It is therefore expected that the distributions would be similar to those obtained with Model A swept by 40^0. The differences between the two cases are that the planform of the two wings and the actuation mechanisms are different. Model B has a diamond-shaped planform, and thus its trailing edge may not affect events near the leading edge in the inboard region. Moreover, oscillating flaps probably offer a more robust influence to the flow, unaffected by the local aerodynamic conditions. The results are presented in Figs 22-33 for three angles of attack, namely $\alpha=13^0$, 17^0 and 21^0. Results are displayed for eight of the ten stations, because the data for Stations 5 and 6 were corrupted. As expected and discussed above, the results indicate very small effect of control for low angles of attack (Figs. 22-29), yet somewhat more pronounced than in the case of Model A. The leading edge vortex, appearing as a large localized suction near the front of the wing and mostly in the inboard region indicates some increase in suction with flow control. And further in the outboard region where the flow is separated there is some mild influence of flow control. But for a sweep angle of 21^0 we observe a considerable influence of flow control resulting in increase of suction by up to about 50%. We can explain this behavior as follows. We know from our previous work[7], that even at angles of attack as high as 20^0, the flow is attach in the inboard region. This is typical behavior for delta wings, for which the vicinity of the apex is where the tip vortices originate, but are very small. In fact for delta wings with leading edges swept by more than 45^0, this behavior is sustained at angles of attack as high as 40^0, or even 50^0. But in the present case, the flow is separated in the inboard region at $\alpha=21^0$. This is indicated by pressure coefficients that take the very low values of -1.6 to -1.8 for $\alpha=13^0$ and $\alpha=17^0$ at the root of the wing, but this strong suction is decreased to about -1 at $\alpha=21^0$. Here is where the flow control mechanism is most effective. It brings the strength of suction back to the unseparated values, as indicated in Figs. 20 and 21. In fact, for $\alpha=21^0$, flow control is effective further outboard as well, where the flow is fully separated, as detected by a flat horizontal pressure distribution. But as we approach the tip, the influence of flow control is somewhat diminished.

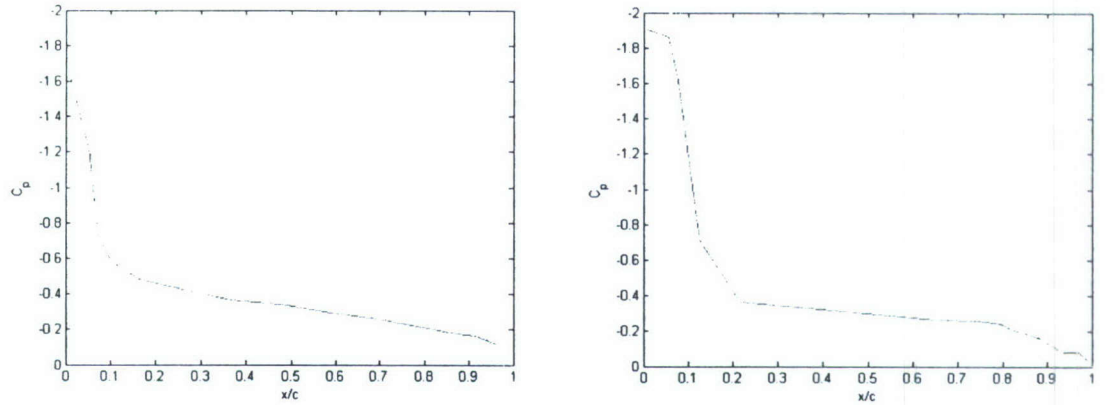

Figure 22: Pressure distributions for Model B at $\alpha=13^0$. Stations 1 (left); 2 (right)

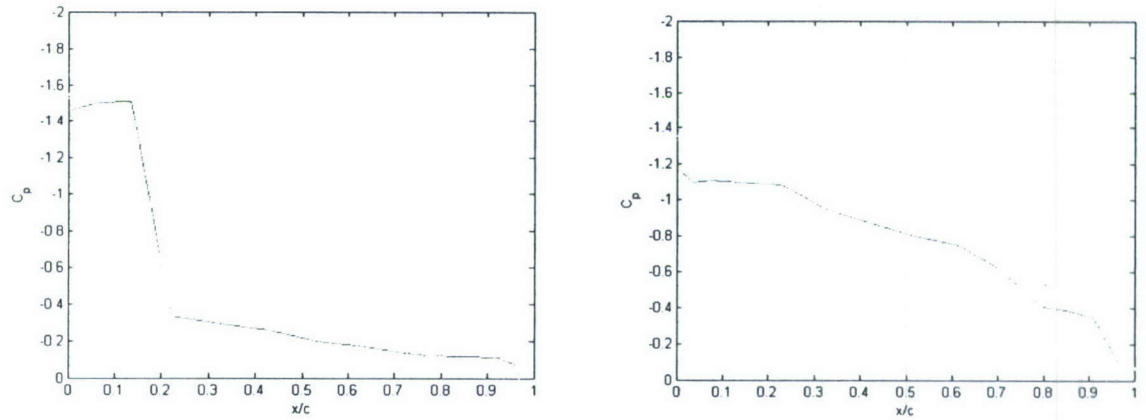

Figure 23: Pressure distributions for Model B at $\alpha=13^0$. Stations 3 (left); 4 (right)

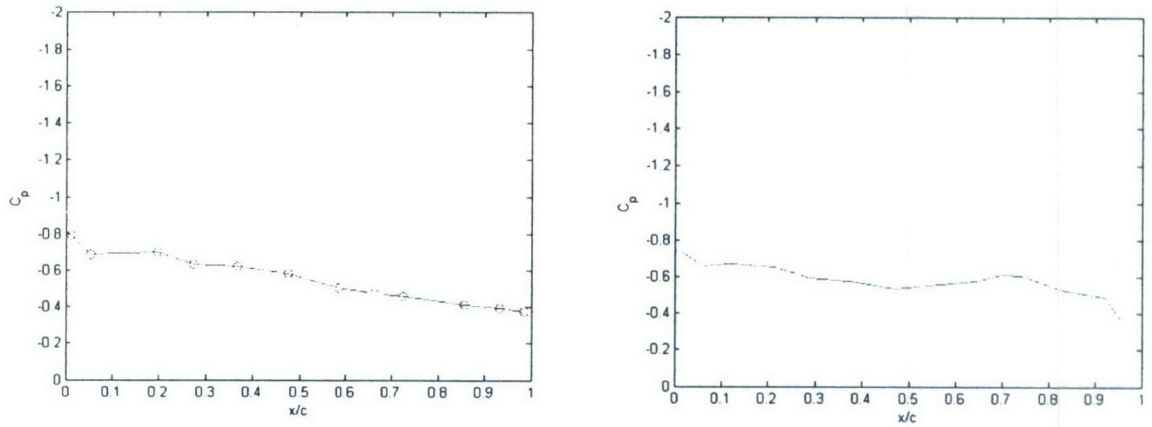

Figure 24: Pressure distributions for Model B at $\alpha=13^0$. Stations 7 (left); 8 (right)

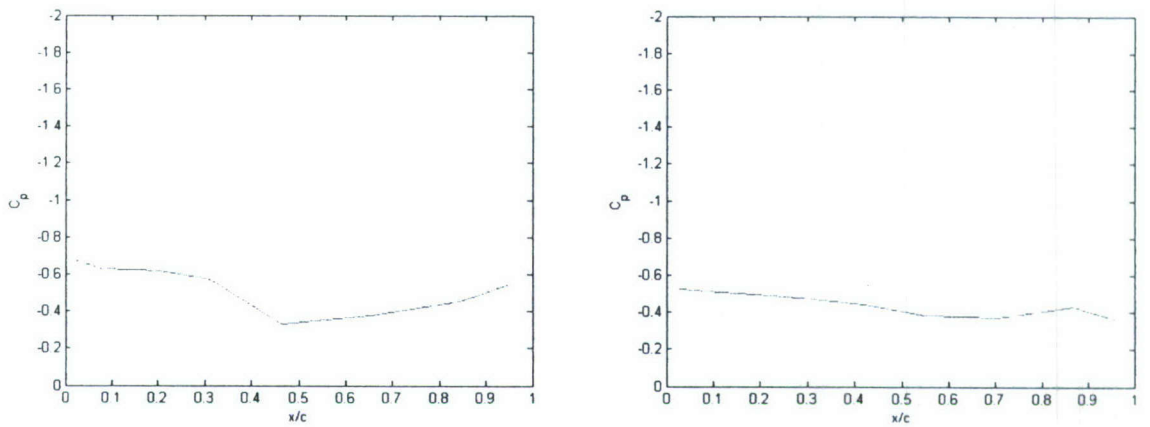

Figure 25: Pressure distributions for Model B at $\alpha=13^0$. Stations 9 (left); 10 (right)

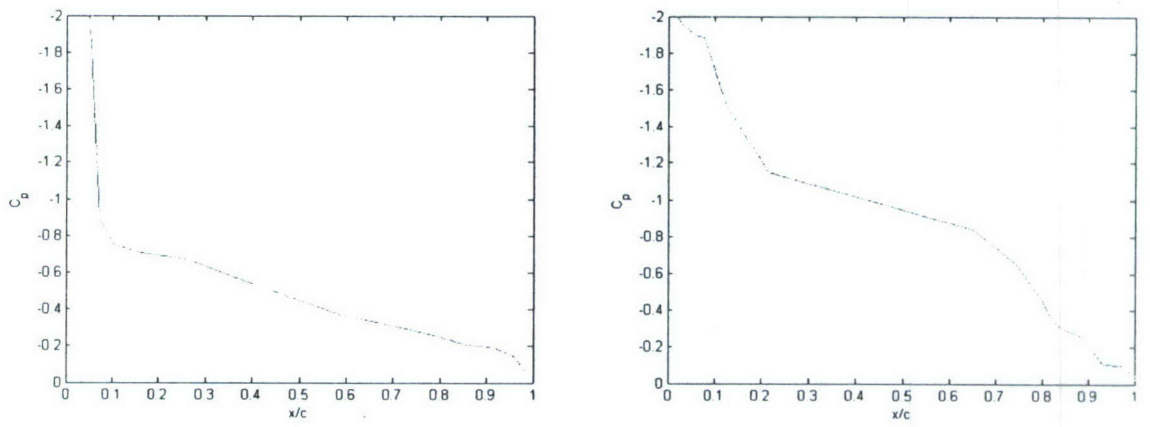

Figure 26: Pressure distributions for Model B at $\alpha=17^0$. Stations 1 (left); 2 (right)

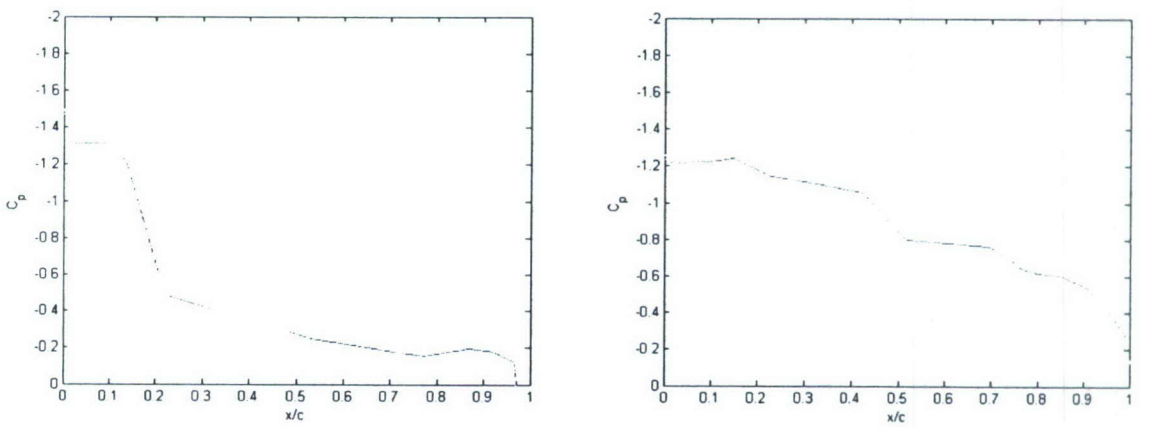

Figure 27: Pressure distributions for Model B at $\alpha=17^0$. Stations 3 (left); 4 (right)

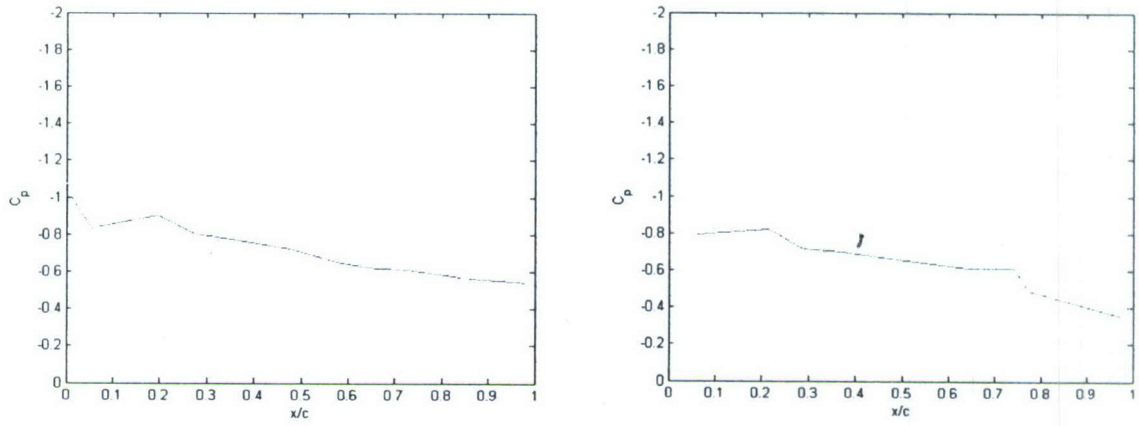

Figure 28: Pressure distributions for Model B at $\alpha=17^0$. Stations 7 (left); 8 (right)

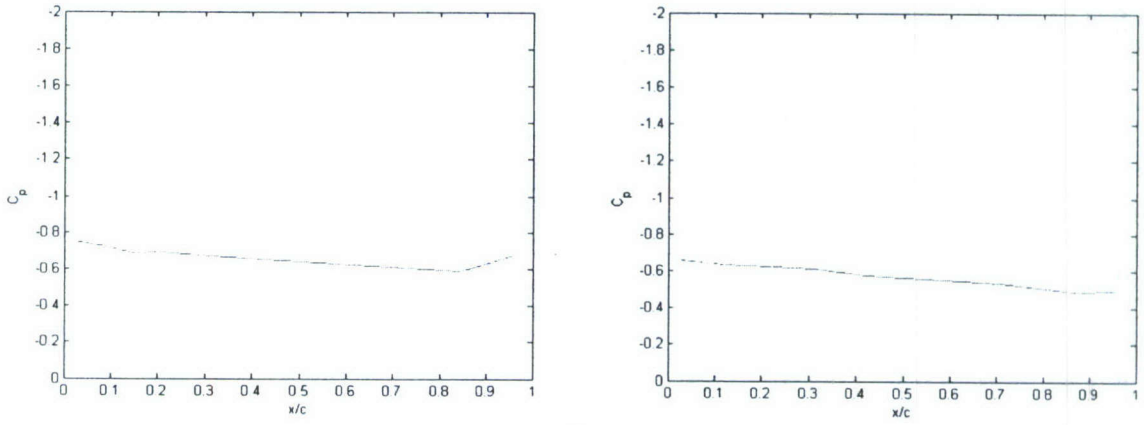

Figure 29: Pressure distributions for Model B at $\alpha=17^0$. Stations 9 (left); 10 (right)

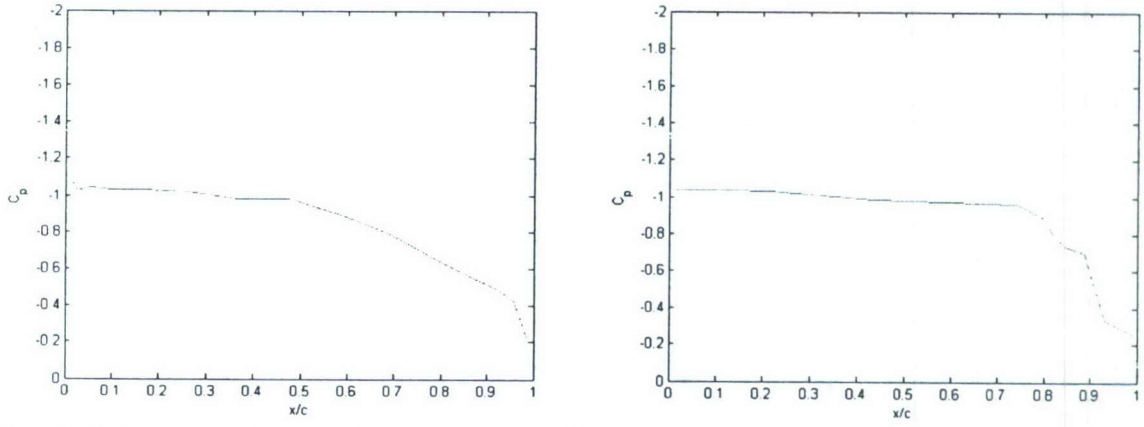

Figure 30: Pressure distributions for Model B at $\alpha=21^0$. Stations 1 (left); 2 (right)

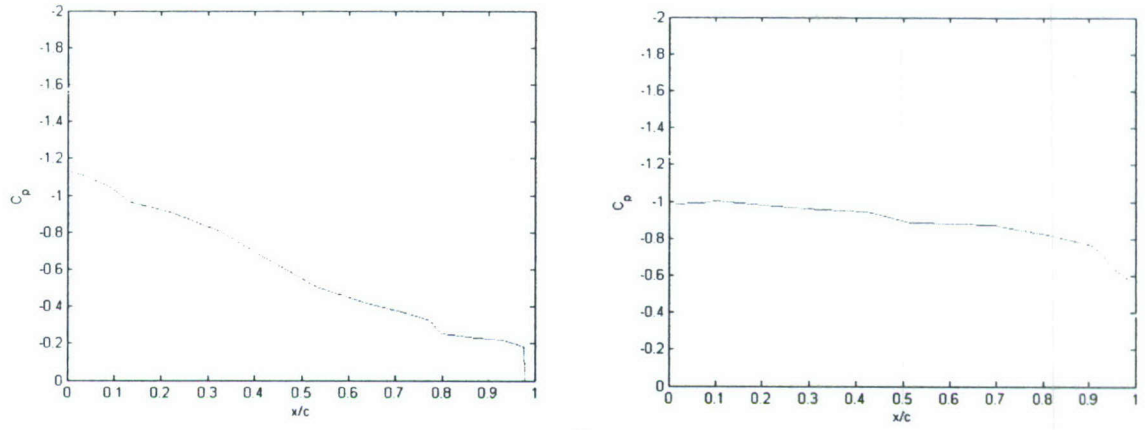

Figure 31: Pressure distributions for Model B at $\alpha=21^0$. Stations 3 (left); 4 (right)

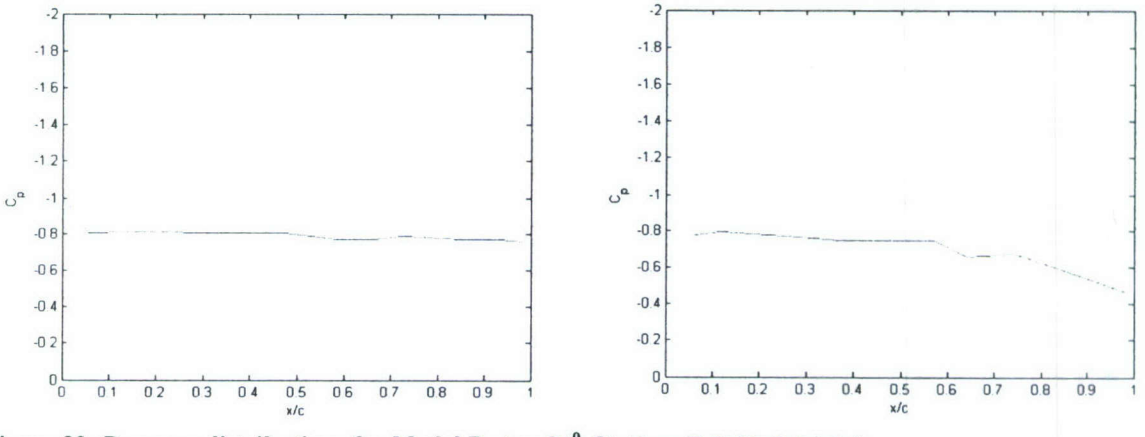

Figure 32: Pressure distributions for Model B at $\alpha=21^0$. Stations 7 (left); 8 (right)

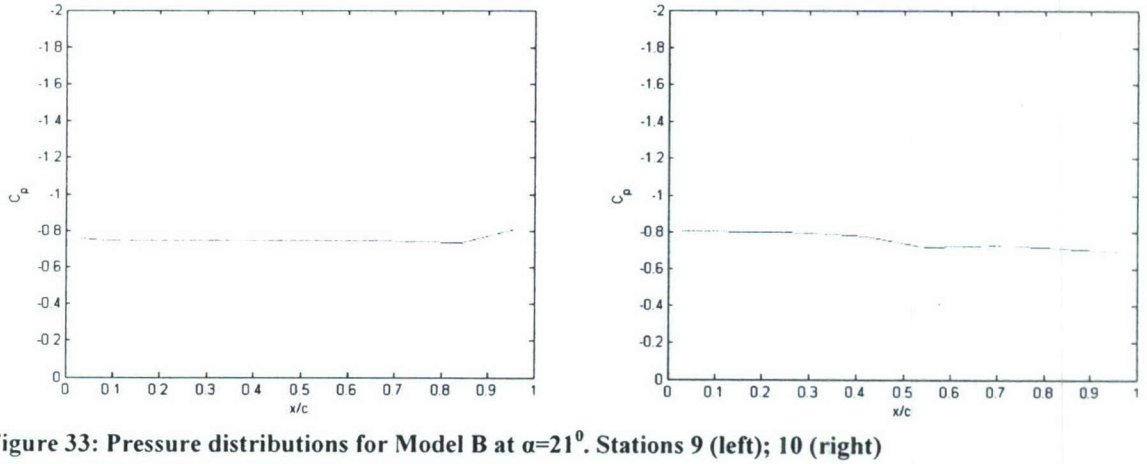

Figure 33: Pressure distributions for Model B at $\alpha=21^0$. Stations 9 (left); 10 (right)

In an effort to find ways to increase the effect of flow control at the angles of attack of $\alpha=13^0$ and 17^0, where the oscillating flap was ineffective, we studied the results of our earlier work. In Ref. 7 we presented PIV evidence that local actuation excites a peculiar underline feature of the flow over mildly swept wings. Axial vortices emerge in the inboard region, with their axis in the streamwise direction and parallel to the tip vortices. To excite such vortices, we decided to blow at a point near the leading edge, but in the spanwise direction. The spanwise nozzle locations are marked in Fig. 4. This method proved to be much more efficient in controlling the flow as shown in Figs. 34 and 35. They show that spanwise blowing produces a strong suction similar to pressure profile induced by attached flow. From previous as well as current data it has been documented that stations 5 through 10 present pressure profiles that belong to separated flow. With the use of steady blowing the effect is felt very strong up to station 10 even though the two nozzles are located at about 20% and 40% of the span as seen in Fig. 4. It is noticeable that the effect is the strongest for a momentum coefficient of 0.42%. Compare to others this is a very small use of energy. This idea deserves further attention. The data presented are preliminary, but are included here to provide evidence that flow control could be very effective over diamond planforms, even at moderate angles of attack.

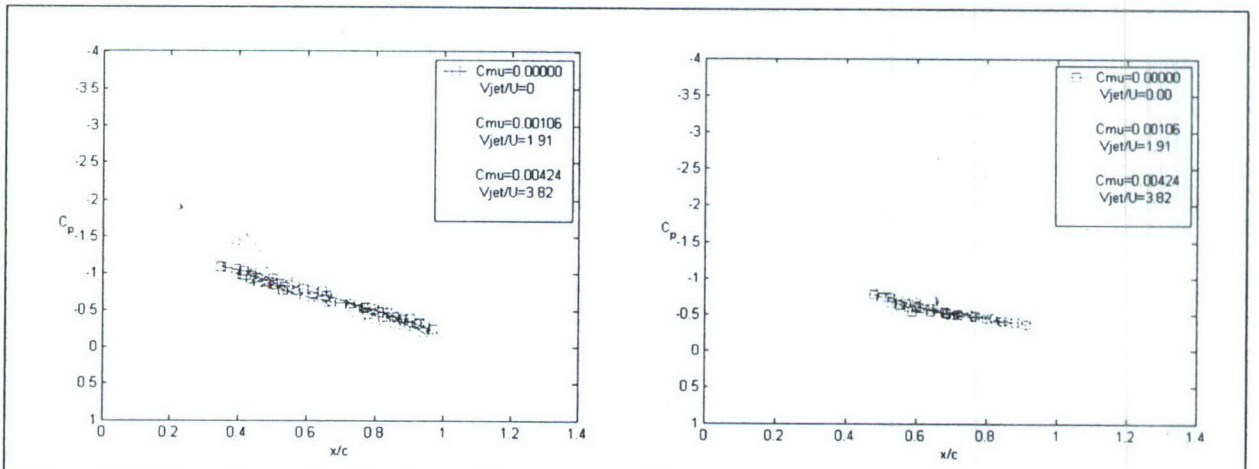

Figure 34: Effect of spanwise blowing on Model B at $\alpha=13^0$. Stations 5-7 (left) and 8-10 (right)

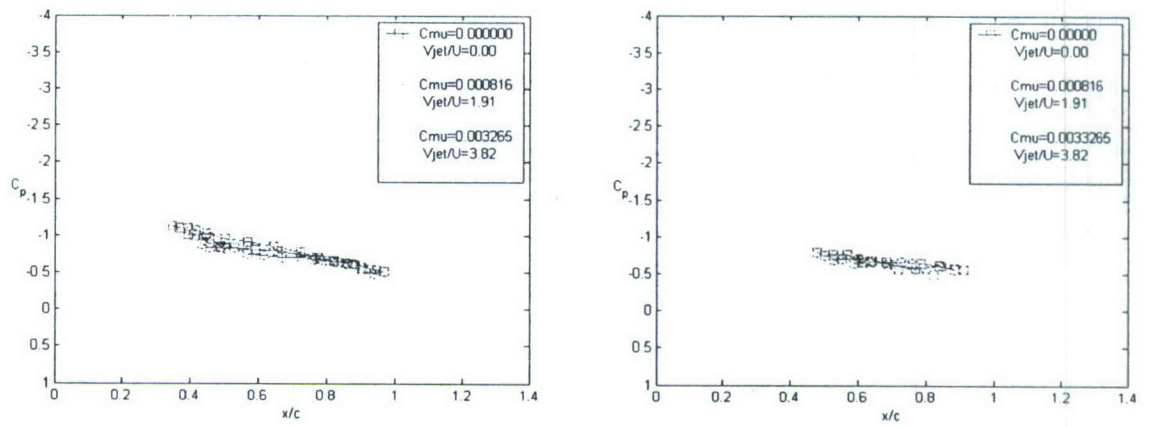

Figure 35: Effect of spanwise blowing on Model B at $\alpha=17^0$. Stations 5-7 (left) and 8-10 (right)

7.4 Conclusions

We tested two models with swept wings employing two actuation mechanisms along the leading edges. We found that when the flow is fully separated, it is still possible for flow control to generate significantly lower suction in the average. This means that the controlled flow is still separated, but the vortical structures in the separated region can be managed so that if averaged over time, they can lead to increases in lift. We experimented with two flow control actuators, a pulsed jet and an oscillating mini-flap, both placed along the entire span of the leading edge. We present evidence that these mechanisms are effective at higher angles of attack, namely up to 21 degrees, than indicated previously. Moreover, we demonstrated that the flow over swept edges can also be controlled, but when the leading edge is swept by 40 degrees, the flow control effect is minimal at moderate angles of attack, namely up to 17 degrees. Surprising for an angle of attack of 21 degrees, actuation generates a very strong suction even at a sweep of 42 degrees. We have also tested an alternative actuation mechanism, steady spanwise blowing from two round nozzles. This proved to be very effective in the range of angles that the other methods were inefficient. This was for a sweep of 40 degrees and angles of attack 13 and 17 degrees.

7.5 References

[1] Zhou, M. D., Fernholz, H. H., Ma, H. Y., Wu, J. Z., Wu, J. M., 1993, "Vortex Capture by a Two-Dimensional Airfoil with a Small Oscillating Leading-Edge Flap", AIAA 93-3266.

[2]Wu, J. Z., Lu, X. Y., Denny, A. G., Fan, M., Wu, J. M., 1998, "Post-stall flow control on an airfoil by local unsteady forcing", *Journal of Fluid Mechanics* 371, pp. 21-58.

[3]Miranda, S., Vlachos, P. P., Telionis, D. P. and Zeiger, M. P., "Flow Control of a Sharp-Edged Airfoil," Paper No. AIAA-2001-0119, 2001, also *AIAA Journal*, vol. 43, pp 716-726, 2005.

[4]Rullan, J., Vlachos, P. P., Telionis, D. P. and Zeiger, M. D., "Flow Control of Unswept and Swept, Sharp-Edged Wings via Unsteady Blowing," *42nd Aerospace Sciences Meeting*, Paper No. AIAA-2004-0226, January 2004

[5] Rullan, J.G., Vlachos, P.P. and Telionis, D.P., "The Aerodynamics of Low-Sweep Trapezoidal Wings" *43rd Aerospace Sciences Meeting and Exhibit, 10-13 January 2005, Reno, Nevada,* Paper No AIAA-2005-0059.

[6]Cahil F, Underwood, W. J., Nuber R. J., and Cheesman G. A., (1953) :"Aerodynamics forces on symmetrical circular-arc airfoils with plain leading-edge and plain trailing-edge flaps", NACA Report 1146.

[7] Rullan, J.G., Vlachos, P.P. and Telionis, D.P., "Flow Control over Trapezoidal-Wing Planforms with Sharp Edges." *44rth Aerospace Sciences Meeting and Exhibit, 9-12 January 2006*, Reno, Nevada, Paper No AIAA-2006-0857.

[8]Rullan, J.G., Vlachos, P.P. and Telionis, D.P., "Post-Stall Flow Control of Sharp-Edged Wings via Unsteady Blowing" *41st Aerospace Sciences Meeting and Exhibit, 6-9 January 2003, Reno, Nevada,* Paper No AIAA-2003-0062, also Journal of Aircraft, Vol. 43, No 6, November 2006, pp. 1738-1746.

[9]Ol, M. V. and Gharib, M., "Leading-Edge Vortex Structure of Nonslender Delta Wings at Low Reynolds Number," *AIAA Journal*, Vol. 41, No. 1, January 2003, pp. 16-26.

[10]Gursul, I., Taylor, G., and Wooding, C., "Vortex Flows over Fixed-Wing Micro Air Vehicles," *40th AIAA Aerospace Sciences Meeting & Exhibit*, Paper No. 2002-0698, AIAA, January 2003.

[11]Taylor, G. S., Schnorbus, T., and Gursul, I., "An Investigation of Vortex Flows over Low Sweep Delta Wings," *AIAA Fluid Dynamics Conference*, Paper No. AIAA-2003-4021, Orlando, FL, June 23-26, 2003.

[12]Gordnier, R. E. and Visbal, M. R., "Higher-Order Compact Difference Scheme Applied to the Simulation of a Low Sweep Delta Wing Flow," *41st AIAA Aerospace Sciences Meeting and Exhibit*, Paper No. AIAA-2003-0620, AIAA, Reno, NV, January 6-9, 2003.

[13]Yaniktepe, B. and Rockwell, D., "Flow Structure on a Delta Wing of Low Sweep Angle," *AIAA Journal*, Vol. 42, pp. 513-523.

8 SUMMARY AND CONCLUSIONS

The basic aim of this research has been to develop actuation mechanisms for the control of the flow over sharp leading-edge wings, unswept or moderately swept. The fundamental aerodynamics has also been explored. Pulsed-jet actuators were designed and tested, but oscillating mini-flaps were also designed and mounted along the leading edge of the wings. The effect of actuation was then explored for different angles of attack and Reynolds numbers.

Perhaps the most significant contribution of this effort is the identification of a new underlying feature of the aerodynamics of moderately swept wings and the fact that the corresponding flow pattern can be excited with proper actuation. In a nutshell here is what we discovered. It is well known that on unswept wings, vorticity along the spanwise direction is generated. We called vortices that are generated by the roll-up of such vorticity "rollers". This vorticity is "turned" in the streamwise direction along the tip of the wing, and becomes an axial vortex, namely a "streamer" in our terminology. For swept wings, the vorticity is generated nearly parallel to the leading edge, but it is again turned along the tip of the wing to become again a streamer. We discovered that for moderately-swept wings, there is a tendency for vorticity to turn in the streamwise direction along the midspan of the wing. This underline feature of the flow can be excited by appropriate actuation. A strong streamer can then be directed along the midspan of the wing, and induce very low pressures and therefore increases of lift.

A novel pulsing jet actuator was designed and constructed. One of the features of this device is that it can generate oscillating disturbances without any oscillating mechanical parts like a flap, which could be detrimental to the radar signature of an airplane. Another feature is that the efficiency of this actuator is practically independent of the driving frequency. This means that the device is an excellent candidate for a robust flight actuator, where the required frequency and mass flow are changing with aircraft speed and the angle of attack. The design proved that uniform and more powerful pulsing jets could be generated along the span of the airfoil. In addition, this actuator did not generate nonlinear interactions and therefore any secondary frequencies as synthetic jets tend to

do. This means that the device is an excellent candidate for a robust flight actuator, where the required frequency is changing with aircraft speed and angle of attack.

Testing our pulsed-jet actuator on a sharp-edged airfoil demonstrated for the first time that unsteady blowing right at the leading edge of a sharp-edged circular arc wing section allows the management of the separated flow, leading to averaged pressure distributions that correspond to higher lift. This was shown to be due to convecting vortices, as detected in the form of a low pressure traveling wave. Significant improvement was obtained in the lift coefficient for moderate to high angles of attack. But the effect decreased as the angle of attack was further increased, possibly due to less effective interaction between the disturbance and the shear layer. The data obtained with unsteady blowing indicate that there is a minimum of energy needed in order to exert a proper disturbance to the shear layer. In addition, the research suggests that the harmonics of the natural shedding frequency can have even greater impact than the natural frequency. Finally, the actuating frequency did not have to match the natural frequency, since resonance was still achieved when locked to higher actuating frequencies.

We tested two models with swept wings employing two actuation mechanisms along the leading edges. We found that when the flow is fully separated, it is still possible for flow control to generate significantly lower suction in the average. This means that the controlled flow is still separated, but the vortical structures in the separated region can be managed so that if averaged over time, they can lead to increases in lift. We experimented with two flow control actuators, the pulsed jet discussed earlier and an oscillating mini-flap, both placed along the entire span of the leading edge. We present evidence that these mechanisms are effective at higher angles of attack, namely up to 21 degrees, than indicated previously. Moreover, we demonstrated that the flow over swept edges can also be controlled, but when the leading edge is swept by 40 degrees, the flow control effect is minimal at moderate angles of attack, namely up to 17 degrees. Surprising for an angle of attack of 21 degrees, actuation generates a very strong suction even at a sweep of 42 degrees. We have also tested an alternative actuation mechanism, steady spanwise blowing from two round nozzles. This proved to be very effective in the

range of angles that the other methods were inefficient. This was for a sweep of 40 degrees and angles of attack 13 and 17 degrees.

APPENDIX

Error propagation from the pressure coefficients to the force coefficient for the sharp-edge airfoil:

In the case of the sharp edge airfoil, $\Delta\theta$ is very nearly equal to 1, so that (d/2) $d\theta$ is essentially in our case dx or Δx. For N pressure ports, I then estimated by reducing Eq. (2.4) that the error in the force coefficient is $[(\delta C_P)^2/N]^{1/2}$. This is what I expected all along and argued with some of you. So, integration smoothes the result and the larger the number of points of measurement, the smaller the error.

Once all of the modifications to the original pressure coefficients are finished, other pertinent quantities may be calculated. The dimensionless sectional vertical and horizontal forces are calculated from

$$C_V = \frac{1}{c}\oint C_p dx \qquad (2.1)$$

and

$$C_H = \frac{1}{c}\oint C_p dy \qquad (2.2)$$

respectively. c is the airfoil chord (the characteristic length. Since the pressure coefficients are known only at discrete points, the integrals are calculated by using the trapezoidal rule and averaging the pressure coefficients between adjacent points. For N discrete circumferential pressure ports, this results in the following equations for the sectional yaw and normal force, respectively:

$$C_V = \frac{1}{2\cdot c}\sum_{i=1}^{N}\left[(C_{p,i} + C_{p,i+1})\cdot(x_{i+1} - x_i)\right] \qquad 2.3$$

$$C_H = \frac{1}{2\cdot c}\sum_{i=1}^{N}\left[(C_{p,i} + C_{p,i+1})\cdot(y_{i+1} - y_i)\right] \qquad 2.4$$

x_i and $C_{p,i}$ are the angular position and ensemble-averaged pressure coefficient of the i^{th} port, respectively. .

The uncertainty in C_V and C_H may be determined by the application of the method of Kline and McKlintock [1953] (equation 2.1???) to equations 2.??? and 2.???. Assuming that the uncertainty in d, D and are negligible (all being due to machining accuracy), and realizing that the uncertainty in angular position $\delta\theta$ will be the same for all ports, the uncertainty in the sectional vertical force may be expressed as

$$\delta C_V = \left\{ \left[\left(\frac{\partial C_V}{\partial C_{p,i}} \right) \cdot \delta C_{p,i} \right]^2 + \left[\left(\frac{\partial C_V}{\partial C_{p,i+1}} \right) \cdot \delta C_{p,i+1} \right]^2 + \left[\left(\frac{\partial C_V}{\partial x_i} \right) \cdot \delta x_i \right]^2 + \left[\left(\frac{\partial C_V}{\partial x_{i+1}} \right) \cdot \delta x_{i+1} \right]^2 \right\}^{\frac{1}{2}}$$

$$= \frac{1}{2 \cdot c} \left\{ \left[\sum_{i=1}^{N} (x_{i+1} - x_i) \cdot \delta C_{p,i} \right]^2 + \left[\sum_{i=1}^{N} (x_{i+1} - x_i) \cdot \delta C_{p,i+1} \right]^2 + \left[\sum_{i=1}^{N} (C_{p,i} + C_{p,i+1}) \delta x_i \right]^2 + \left[\sum_{i=1}^{N} (C_{p,i} + C_{p,i+1}) \delta x_{i+1} \right]^2 \right\}^{\frac{1}{2}}$$

(2.5)

The calculation for the uncertainty in the sectional horizontal force coefficient is similar:

$$\delta C_H = \frac{1}{2 \cdot c} \left\{ \left[\sum_{i=1}^{N} (y_{i+1} - y_i) \cdot \delta C_{p,i} \right]^2 + \left[\sum_{i=1}^{N} (y_{i+1} - y_i) \cdot \delta C_{p,i+1} \right]^2 + \left[\sum_{i=1}^{N} (C_{p,i} + C_{p,i+1}) \delta y_i \right]^2 + \left[\sum_{i=1}^{N} (C_{p,i} + C_{p,i+1}) \delta y_{i+1} \right]^2 \right\}$$

(2.6)

For actual calculations, all of the geometric data are known a priori, $\delta\theta_i$ is estimated at 0.75° worst-case based on the accuracy with which the models can be placed in the facilities, and $\delta C_{p,i}$ is determined during ensemble averaging. If the standard deviation associated with the ensemble-averaged $C_{p,i}$ is σ, then $\delta C_{p,i} = \frac{\sigma}{\sqrt{N}}$, where N is the number of usable ensembles after application of Chauvenet's criterion.

Applying the method of Kline and McKlintock to the definition of the pressure coefficient in equation 2.3, we find

$$\delta C_P = \left\{ \left[\left(\frac{\partial C_P}{\partial (\Delta P)} \right) \delta (\Delta P) \right]^2 + \left[\left(\frac{\partial C_P}{\partial q} \right) \delta q \right]^2 \right\}^{\frac{1}{2}} = \left\{ \left[\frac{\delta (\Delta P)}{q} \right]^2 + \left[- \frac{\delta q \cdot \Delta P}{q^2} \right]^2 \right\}^{\frac{1}{2}}$$

(2.85)

But since the measurement of q and P are made by the same instrument and in the same manner, they are subject to the same uncertainties, so $\delta q = \delta(\Delta P) = \delta P$. Substituting for the error quantities, expanding and rearranging equation 2.85 results in

$$\delta C_P = \left\{ \frac{([\delta P]^2 [q^2 + (\Delta P)^2]}{q^4} \right\}^{\frac{1}{2}}$$

We observe that the largest value of δC_P for a given q would result when ΔP is a maximum. The relation of q and ΔP is such that from the experimental data of the sharp

edge airfoil, $(\Delta P)_{Max}$ is no greater than –1.5q (i.e. the highest observed pressure coefficient is not greater than 1.5 in magnitude). Using $\Delta P = -1.5q$ as a worst-case scenario, equation 2.96 becomes

$$\delta C_P = \left\{ \frac{([\delta P]^2 \cdot 3.25q^2}{q^4} \right\}^{\frac{1}{2}} = \left\{ \frac{(3.25[\delta P]^2}{q^2} \right\}^{\frac{1}{2}} = \frac{\sqrt{3.25} \cdot \delta P}{q} \tag{2.107}$$

which gives the uncertainty in the measured pressure coeffcient as a function of the uncertainty in the measured pressures and the dynamic pressure of the test.

$\delta P = 0.001 * 4981.8 = 4.981 Pa$

$q = 58.96 Pa$

$\delta C_P = 0.1548$

Reference: Kline, S.J., and McClintok, F.A., Describing Uncertainties in Single-Sample Experiments, The American Society of Mechanical Engineers, Vol. 75, Number 1, Easton, PA, January 1953